AD603152

$ 4.00

A GOVERNMENT RESEARCH REPORT

U.S. DEPARTMENT OF COMMERCE

OFFICE OF TECHNICAL SERVICES

distributes this and thousands of similar reports in the interest of science, industry, and the public—for which research and new products mean better health, better living, and a stronger economy.

HOW TO GET OTHER REPORTS

The Office of Technical Services is the Nation's clearinghouse for reports of research supported by the Army, Navy, Air Force, Atomic Energy Commission, and other Government agencies.

Abstracts of new reports available are published twice a month in U. S. GOVERNMENT RESEARCH REPORTS ($15 a year domestic).

Selected Reports of particular interest to small business are described monthly in TECHNICAL REPORTS NEWSLETTER ($1 a year domestic).

Translations of foreign technical material are also available from the Office of Technical Services and other sources. These are listed or abstracted semimonthly in TECHNICAL TRANSLATIONS ($12 a year domestic).

The above periodicals may be ordered from Superintendent of Documents, U. S. Government Printing Office, Washington, D. C., 20402, or through a U. S. Department of Commerce Field Office.

Inquiries about the availability of reports and translations on any particular subject may be directed to Office of Technical Services, U. S. Department of Commerce, Washington, D.C., 20230, or to any Commerce field office.

Reports and translations are published by the Office of Technical Services for use by the public. Thus, you may use the know-how or reprint the information therein except that where patent questions appear to be involved the usual preliminary search is advised, and where copyrighted material is used permission should be obtained for its further publication.

These documents are reprinted by OTS from the best available copy.

603152

123 p #4.00 hc
#0.75 mf

Eclipse Fractions for Sun-Synchronous Orbits

10 JUNE 1964

Prepared by H. K. KARRENBERG

Astrodynamics Department

Guidance and Control Subdivision

Electronics Division

Prepared for COMMANDER SPACE SYSTEMS DIVISION

AIR FORCE SYSTEMS COMMAND

LOS ANGELES AIR FORCE STATION

Los Angeles, California

EL SEGUNDO TECHNICAL OPERATIONS • AEROSPACE CORPORATION

CONTRACT NO. AF 04(695)-269

ECLIPSE FRACTIONS FOR SUN-SYNCHRONOUS ORBITS

Prepared by

H. K. Karrenberg
Astrodynamics Department
Guidance and Control Subdivision
Electronics Division

El Segundo Technical Operations
AEROSPACE CORPORATION
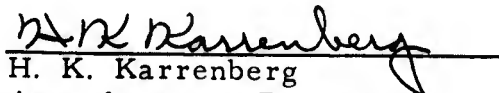El Segundo, California

10 June 1964

Prepared for

ECLIPSE FRACTIONS FOR SUN-SYNCHRONOUS ORBITS

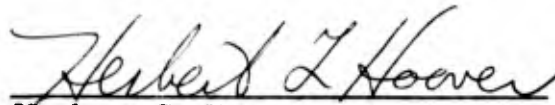Prepared by:

H. K. Karrenberg
Astrodynamics Department

Approved by:

C. M. Price, Head
Astrodynamics Department

E. Levin, Director
Guidance and Control Subdivision

This technical documentary report has been reviewed and is approved for publication and dissemination. The conclusions and findings contained herein do not necessarily represent an official Air Force position.

For Space Systems Division
Air Force Systems Command:

Herbert G. Hoover
Lt Colonel, USAF
Chief, Studies and Analysis

ABSTRACT

Eclipse fraction is defined as the fraction of the orbital period that a satellite spends in the earth's shadow. This fraction is of great importance to any satellite which depends on a sun energizing unit (e.g., solar cell) for its electrical power.

Sun-synchronous orbits possess unusual eclipsing properties because of the unique orbital characteristic which defines them. The purpose of this study is to determine the characteristics of non-eclipsed sun-synchronous orbits (providing they exist) and the time history and average value of the eclipse fraction for those orbits which are eclipsed. Comparisons with non-sun-synchronous orbits are made. The effects of atmospheric drag, lunar and solar gravitational fields, injection errors, oblate earth geometry, atmospheric refraction of the sun's rays and the eccentricity of the earth's orbit are examined. Comparisons with the investigations of other authors are made.

CONTENTS

FIGURES

TABLE

1. INTRODUCTION

Eclipse fraction is defined as the fraction of the orbital period that a satellite spends in the earth's shadow. This fraction is of great importance to any satellite which depends on a sun energizing unit (e.g., solar cell) for its electrical power. If this fraction is small, the weight of auxiliary batteries required during eclipsed periods may be held to a reasonable figure. If the eclipse fraction could be reduced to zero, no auxiliary batteries would be required; this elimination would result in a further weight reduction making it possible for the satellite to carry a larger payload and/or to require less booster capability.

Sun-synchronous orbits possess unusual eclipsing properties because of the unique orbital characteristic which defines them: $\dot{\Omega}$ (the nodal regression rate of the orbit) equals $\dot{\lambda}$ (the earth's mean rate of revolution about the sun); therefore, $\Omega = \lambda + K$ (a constant which may be selected). Depending on the value of K and the altitude, the eclipse fraction as a function of the time of year may be large, or small, or even zero.

One of the goals of the following analysis is to determine the characteristics of noneclipsed satellite orbits, providing such orbits exist. It is conceivable that such orbits exist because the oblateness of the earth causes a nodal regression effect on satellite orbits. The nodal regression effect is a secular rotation of the satellite orbit about the polar axis of the earth. Thus, the inertial orientation of the satellite orbit is continually changing as the earth revolves around the sun. Therefore, a phasing relationship between nodal regression and earth revolution will be sought.

The analysis in this report is restricted to circular orbits, and spherical earth geometry is assumed even though an oblate potential is required for nodal regression. The effects of elliptical orbits and oblate earth geometry are examined in Section 8.

2. DETERMINATION OF ECLIPSE FRACTION

The geometry relating the earth, sun, and a satellite may be visualized best by referring to Figure 1. This figure depicts a geocentric coordinate system in which the X-axis is directed toward the vernal equinox, the Z-axis is directed toward the north celestial pole, and the Y-axis, in the equatorial plane, forms a right-handed coordinate system with the X and Z axes. The orientation of the orbit plane is described by:

a. The node (Ω) in the equatorial plane measured eastward from the vernal equinox to the ascending node of the orbit plane.

b. The inclination (i) measured in a counterclockwise direction at the ascending node from the equatorial plane to the orbit plane.

The obliquity of the ecliptic (ϵ) is the angle between the ecliptic (the plane of motion of the sun as seen from the center of the earth), and the equatorial plane. The celestial longitude of the sun (λ) in the ecliptic is measured eastward from the vernal equinox to the sun. The angle ϕ, where $0° \leq \phi \leq 180°$, is the geocentric angle between the sun and the satellite, at any specified time. The significance of ϕ in the determination of the eclipse fraction (f) is indicated in Figure 2. (Figure 2 shows R as the radius of the spherical earth and h as the circular orbit altitude.) The sun's rays are assumed to be parallel (i.e., sun at infinity) so that the earth's shadow is cylindrical in shape. The angle ϕ' given by Equation (1) is the geocentric angle between the sun and the satellite at the time of entrance into or exit from the earth's shadow.

$$\phi' = 180° - \sin^{-1}\left(\frac{R}{R+h}\right) \tag{1}$$

When $\phi > \phi'$ the satellite is eclipsed.

The derivation of the eclipse fraction will be further facilitated by referring to Figure 3 where δ_1 and δ_2 are the declinations of the sun and satellite,
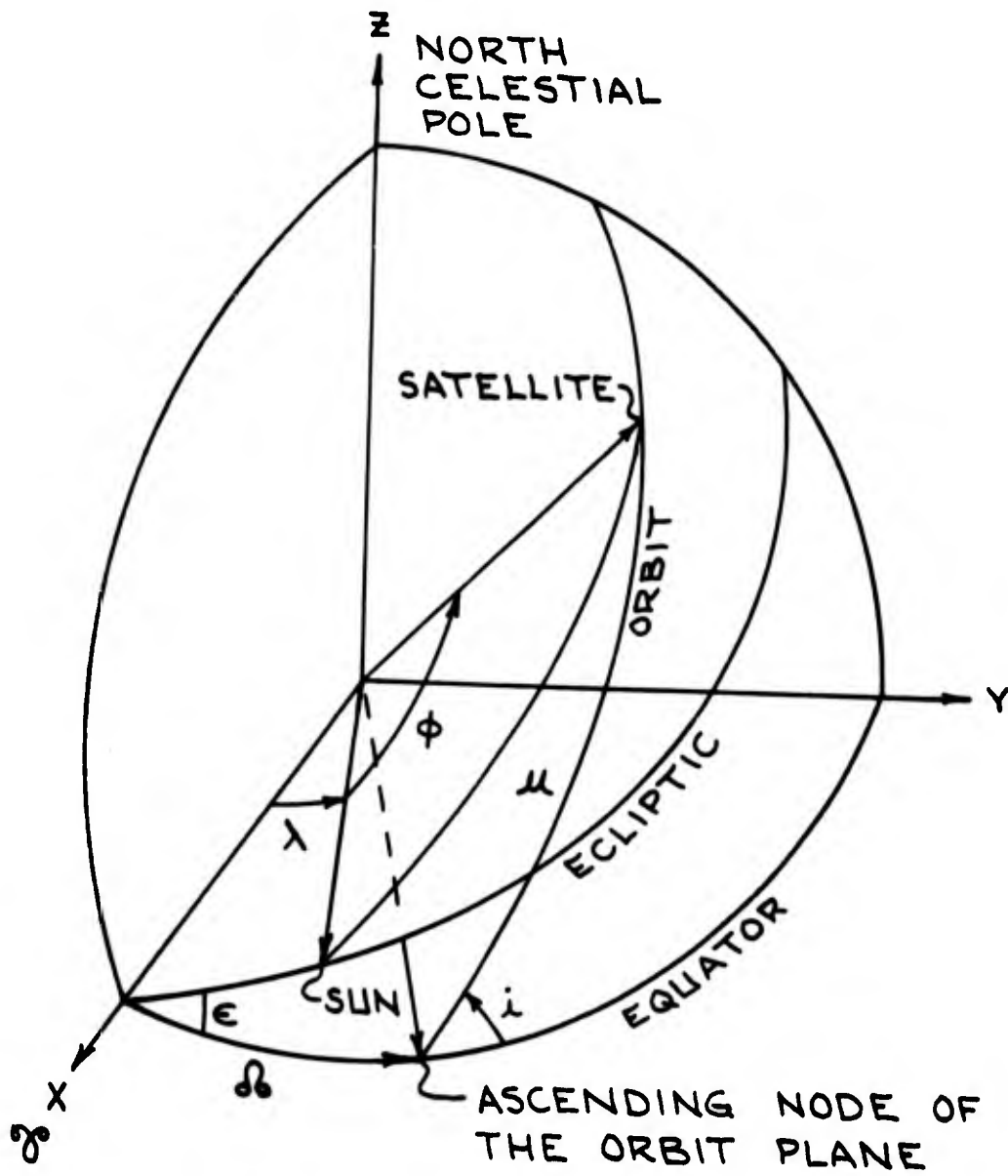
Figure 1.   Earth, Sun, Satellite Geometry

$$\phi' = 180° - \sin^{-1}\left(\frac{R}{R+h}\right)$$
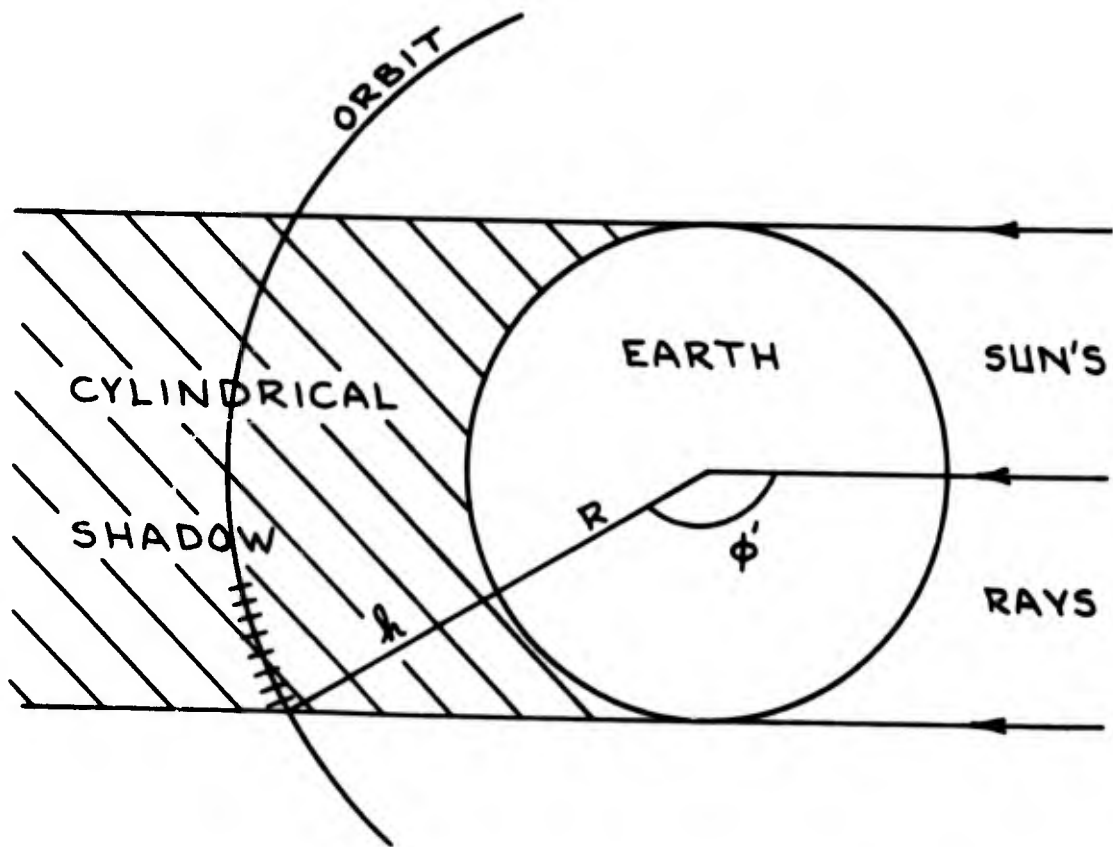
WHEN $\phi > \phi'$ THE SATELLITE IS ECLIPSED

Figure 2. Configuration at Shadow Entrance or Exit
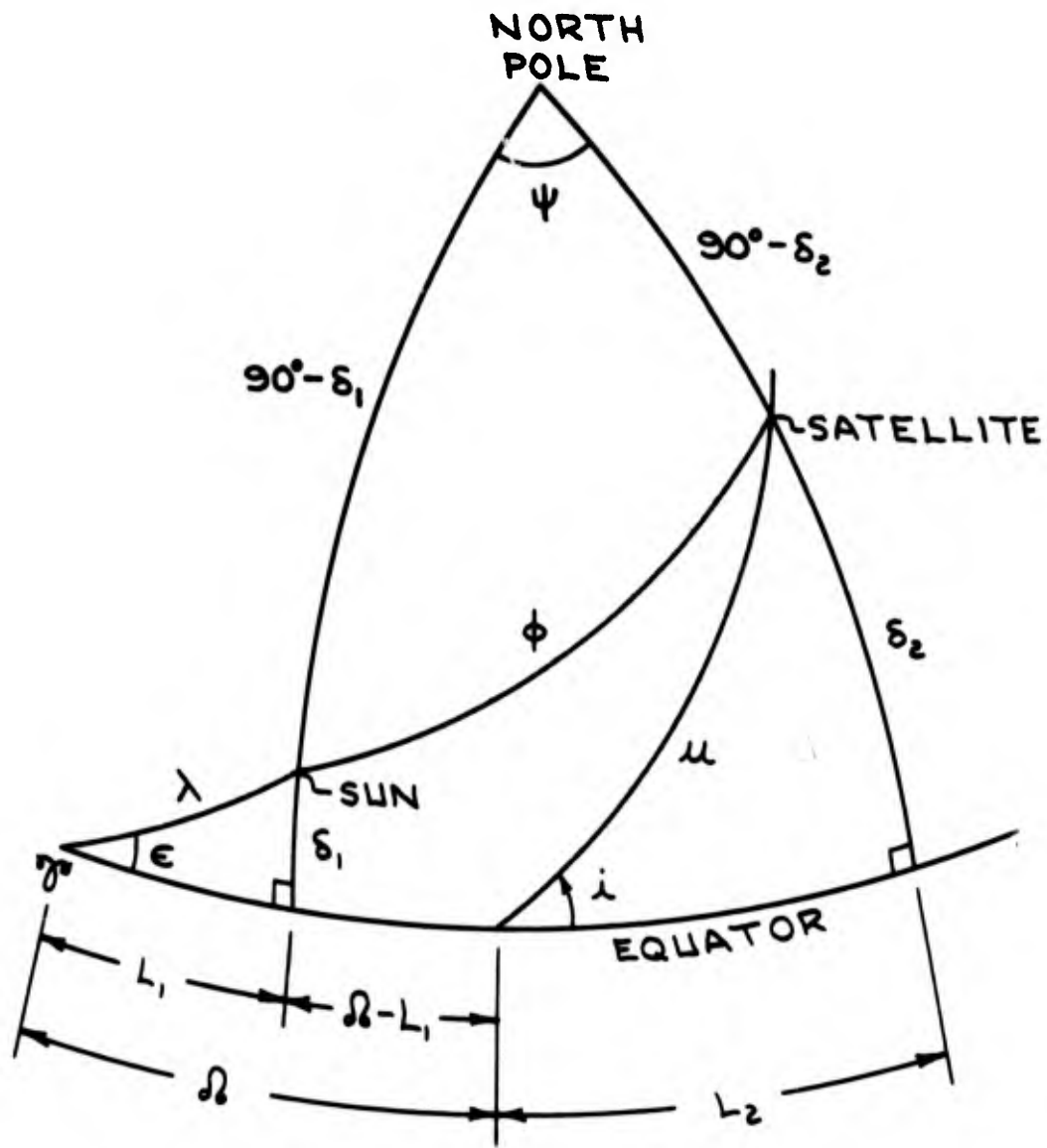
Figure 3. Geometry for Derivation of Eclipse Fraction

respectively, at any specified time. The longitudinal positions of the sun and satellite (L_1 and L_2) are measured from the vernal equinox and ascending node, respectively. The argument of latitude (u) is measured from the ascending node to the satellite. (The angle ψ is an auxiliary angle of no special significance.)

Spherical trigonometry provides the following relations:

$$\sin \delta_1 = \sin \epsilon \, \sin \lambda \tag{2}$$

$$\sin \delta_2 = \sin i \, \sin u \tag{3}$$

$$\sin L_1 = \tan \delta_1 / \tan \epsilon \tag{4}$$

$$\sin L_2 = \tan \delta_2 / \tan i \tag{5}$$

$$\cos L_1 = \cos \lambda / \cos \delta_1 \tag{6}$$

$$\cos L_2 = \cos u / \cos \delta_2 \tag{7}$$

and

$$\cos \phi = \sin \delta_1 \sin \delta_2 + \cos \delta_1 \cos \delta_2 \cos \psi \tag{8}$$

Since $\psi = \Omega + (L_2 - L_1)$, $\cos \psi = \cos \left[\Omega + \left(L_2 - L_1 \right) \right]$ and trigonometric functions of the sums of the angles yield

$$\cos \psi = \cos \Omega \left(\cos L_2 \cos L_1 + \sin L_2 \sin L_1 \right)$$

$$- \sin \Omega \left(\sin L_2 \cos L_1 - \cos L_2 \sin L_1 \right) \tag{9}$$

With suitable reduction, substitution of Equations (2) through (7) and Equation (9) into Equation (8) yields

$$\cos \phi = \sin u \left[\sin \lambda \left(\sin \epsilon \sin i + \cos \epsilon \cos i \cos \Omega \right) \right.$$
$$\left. - \cos \lambda \left(\cos i \sin \Omega \right) \right]$$
$$+ \cos u \left[\sin \lambda \left(\cos \epsilon \sin \Omega \right) + \cos \lambda \left(\cos \Omega \right) \right] \qquad (10)$$

If ϕ' and then Equation (1) are substituted into Equation (10),

$$\cos \phi' = \cos \left[180^\circ - \sin^{-1} \left(\frac{R}{R+h} \right) \right] = -\cos \sin^{-1} \left(\frac{R}{R+h} \right) = -\frac{\sqrt{h(2R+h)}}{R+h}$$

$$= \sin u \left[\sin \lambda \left(\sin \epsilon \sin i + \cos \epsilon \cos i \cos \Omega \right) \right.$$
$$\left. - \cos \lambda \left(\cos i \sin \Omega \right) \right]$$
$$+ \cos u \left[\sin \lambda \left(\cos \epsilon \sin \Omega \right) + \cos \lambda \left(\cos \Omega \right) \right] \qquad (11)$$

Given the orientation of an orbit (i and Ω), its altitude (h), and the date (in terms of λ), two solutions for u may be obtained from Equation (11). One solution corresponds to entrance into the shadow; the other to exit from the shadow. Because we are only concerned with circular orbits, the eclipse fraction (f) is

$$f = \frac{u_{exit} - u_{entrance}}{360^\circ} \qquad (12)$$

In order to facilitate determinations of f, the appropriate equations were programmed for a large digital computer, the IBM 7090. As might be expected the program is relatively simple and very rapid. For single values of h and i and 360 values of Ω and λ, 360 values of f and an average ($\bar{f}$) taken over all values of f are calculated in approximately 0.2 minute. This run corresponds to almost daily samplings of f for a year for a given orbit.

-8-

3. SUN-SYNCHRONOUS ORBITS

The nodal regression rate ($\dot{\Omega}$) due to oblateness is also programmed into the computer and is given by

$$\dot{\Omega}\left(\frac{\text{deg}}{\text{day}}\right) = -9.960\ 795\left(\frac{R}{R+h}\right)^{3.5} \cos i \tag{13}$$

Figure 4 shows h vs i for various positive values of $\dot{\Omega}$. Although only retrograde inclinations, $90° \leq i \leq 180°$, are shown, the figure is symmetrical about $i = 90°$ so that values for direct inclinations, $0° \leq i \leq 90°$, may be read along the abscissa by replacing i by $(180° - i)$. As Equation (13) indicates, $\dot{\Omega}$ is negative for direct orbits.

A sun-synchronous orbit is defined as an orbit which has a nodal regression rate equal in magnitude and sense to the earth's mean rate of revolution about the sun. Thus, $\dot{\Omega} = \dot{\lambda} = 0.985\ 647$ deg/day and $\Omega = \lambda + K$ (a constant which may be selected). The locus of sun-synchronous orbits is presented as a broken line on Figure 4. These orbits are all retrograde and lie between h = 0 n mi, $i = 95°.679$ and h = 3225.3 n mi, $i = 180°$. Sun-synchronous orbits about the earth do not exist above 3225.3 n mi. If the ecliptic and equatorial planes were coincident and if the earth's orbit were circular, the nodes of a sun-synchronous orbit would maintain forever, neglecting perturbations, their initial orientation relative to the sun. Noon-midnight $(\Omega - \lambda = 0°)$ and twilight $(\Omega - \lambda = 90°)$ orbits are depicted in Figure 5. Because good illumination is required for photography a noon-midnight sun-synchronous orbit has been selected (Reference 1) for the Nimbus meteorological satellites. Almost one-half of every revolution will be available for photography. On the other hand the twilight orbits seem ideally suited for our purposes because their lines of nodes are always perpendicular to the sun line. Although the ecliptic and equatorial planes are not coincident ($\epsilon = 23°.4441$) and the earth's

-9-
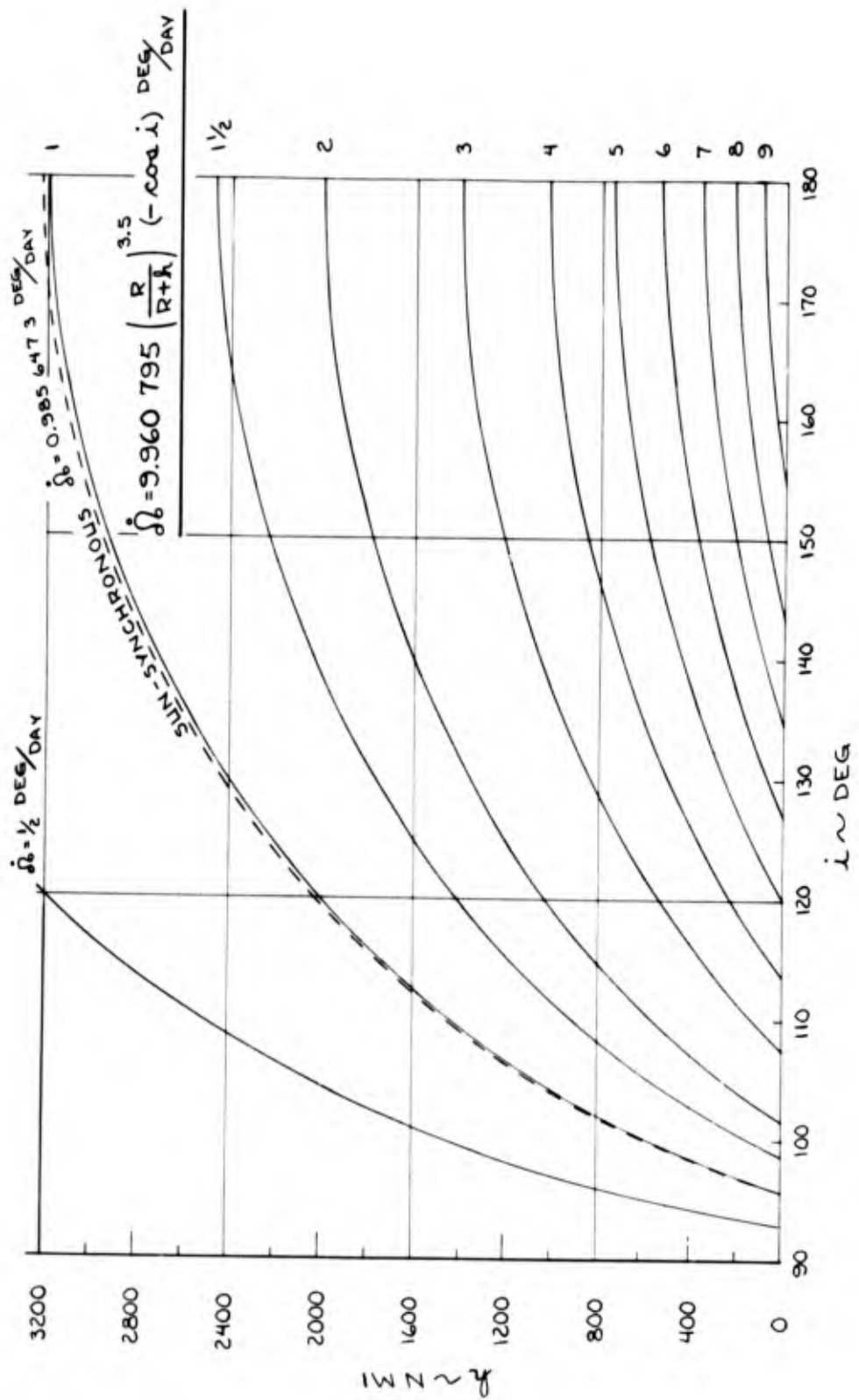
Figure 4. Altitude versus Inclination for Various Values of the Nodal Regression Rate
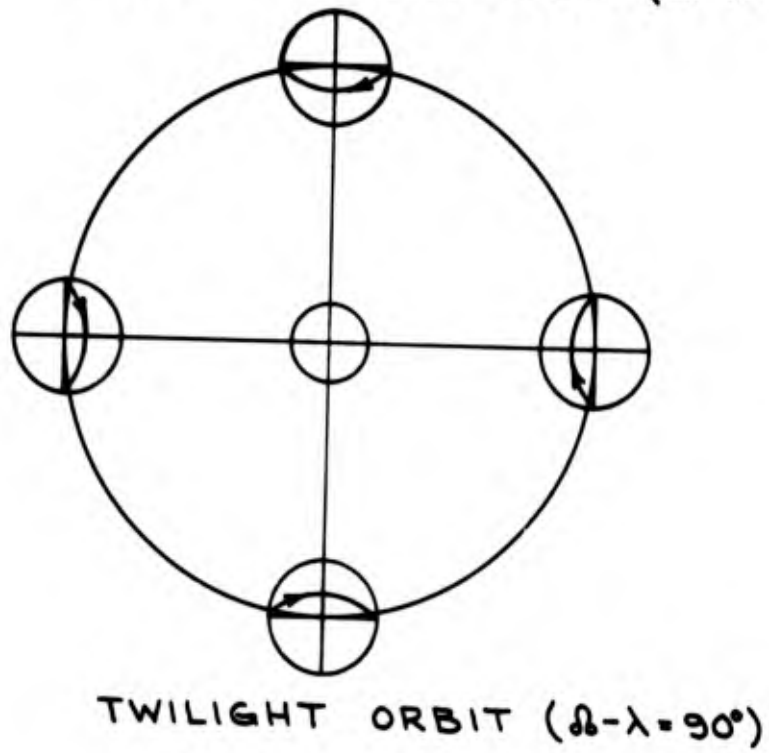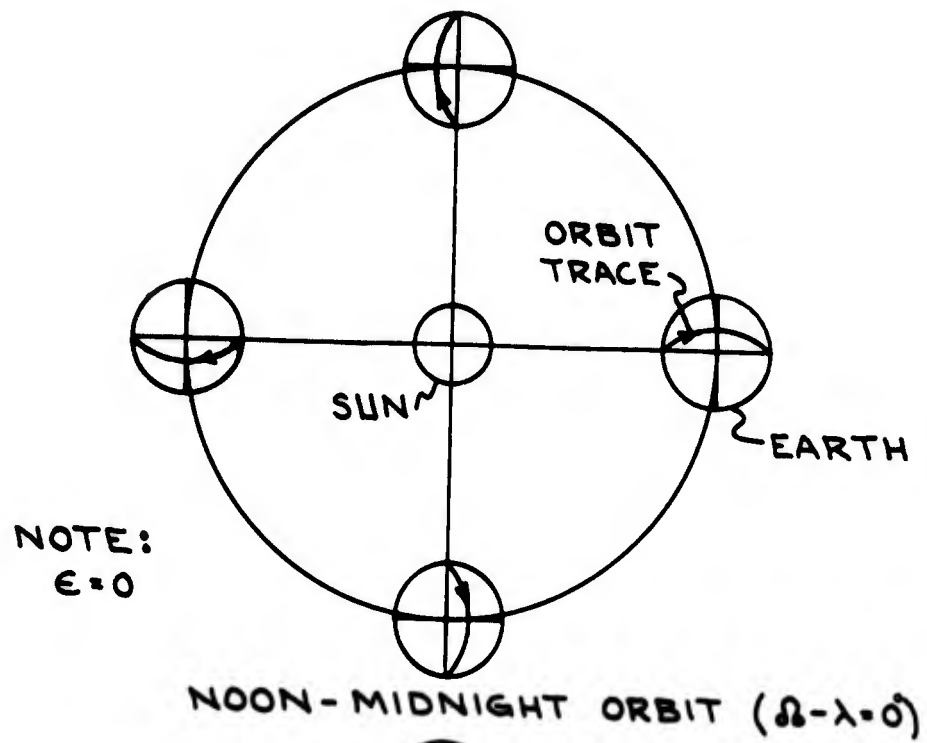
Figure 5.   Noon-Midnight and Twilight
Sun-Synchronous Orbits

orbit is not circular (eccentricity = 0. 0167), these effects do not substan-
tially alter the nodal-sun orientations just described. The actual sun-earth-
orbit-shadow geometry for a twilight orbit is depicted in Figure 6 which shows
three positions (summer solstice, autumnal equinox and an intermediate date)
of the earth in its orbit.
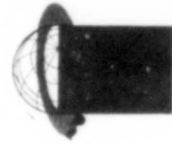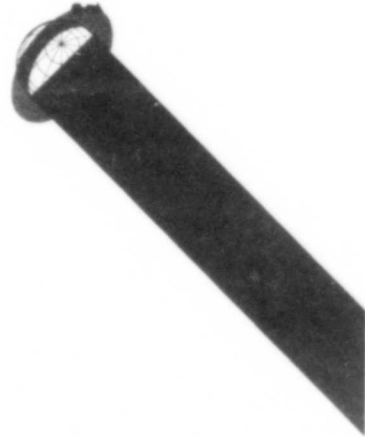
Figure 6. Actual Sun-Earth-Orbit-Shadow Geometry for Three Dates

-13-

4. A PREFERRED ORIENTATION, $\Omega - \lambda = 90°$

The search for orbits that are never eclipsed has led to the class of sun-synchronous orbits with a $\Omega - \lambda = 90°$ orientation. However, all combinations of h and i of this class are not expected to be noneclipsing.

When an orbit is seen edgewise, it appears as a line segment with definite end points. The locus of sun-synchronous orbit end points is presented in Figure 7. The earth and straight lines delimiting the cylindrical shadow at those times of the year that correspond to the vernal equinox ($\lambda = 0°$), summer solstice ($\lambda = 90°$), autumnal equinox ($\lambda = 180°$), and winter solstice ($\lambda = 270°$) are also shown. Note that for each time of year a portion of the locus lies outside the shadow. For the times of year between those previously mentioned, the noneclipsed portion of the locus may be geometrically described (Figure 7) by rotating the shadow boundaries through an angle δ_1. The declination of the sun, δ_1, measured from the vernal equinox, may be determined from λ by the relation $\sin \delta_1 = \sin \epsilon \sin \lambda$. At the equinoxes $\delta_1 = 0°$, at the summer solstice $\delta_1 = \epsilon = 23.°44$ and at the winter solstice $\delta_1 = -\epsilon = -23.°44$. The smallest of these noneclipsed regions corresponds to the summer solstice ($\lambda = 90°$) which is the most restrictive time of year. Computer runs of orbits in this smallest region were made and they verified the fact that this region is noneclipsing.

The geometry which defines this region is presented in Figure 8. The trigonometric relation which defines the sun-synchronous orbit that is tangent to the shadow is $\cos(i + \epsilon - 90°) = \sin(i + \epsilon) = R/(R + h)$. This relation may also be obtained from Equation (11) in the following manner. If $\Omega - \lambda = 90°$, Ω may be eliminated from Equation (11) and

$$-\cos \sin^{-1}\left(\frac{R}{R + h}\right) = \sin u \left\{ \sin \lambda \left[\sin \epsilon \sin i + \sin \lambda \cos i \left(1 - \cos \epsilon\right) \right] - \cos i \right\} - \cos u \left\{ \sin \lambda \cos \lambda \left(1 - \cos \epsilon\right) \right\} \qquad (14)$$

-15-
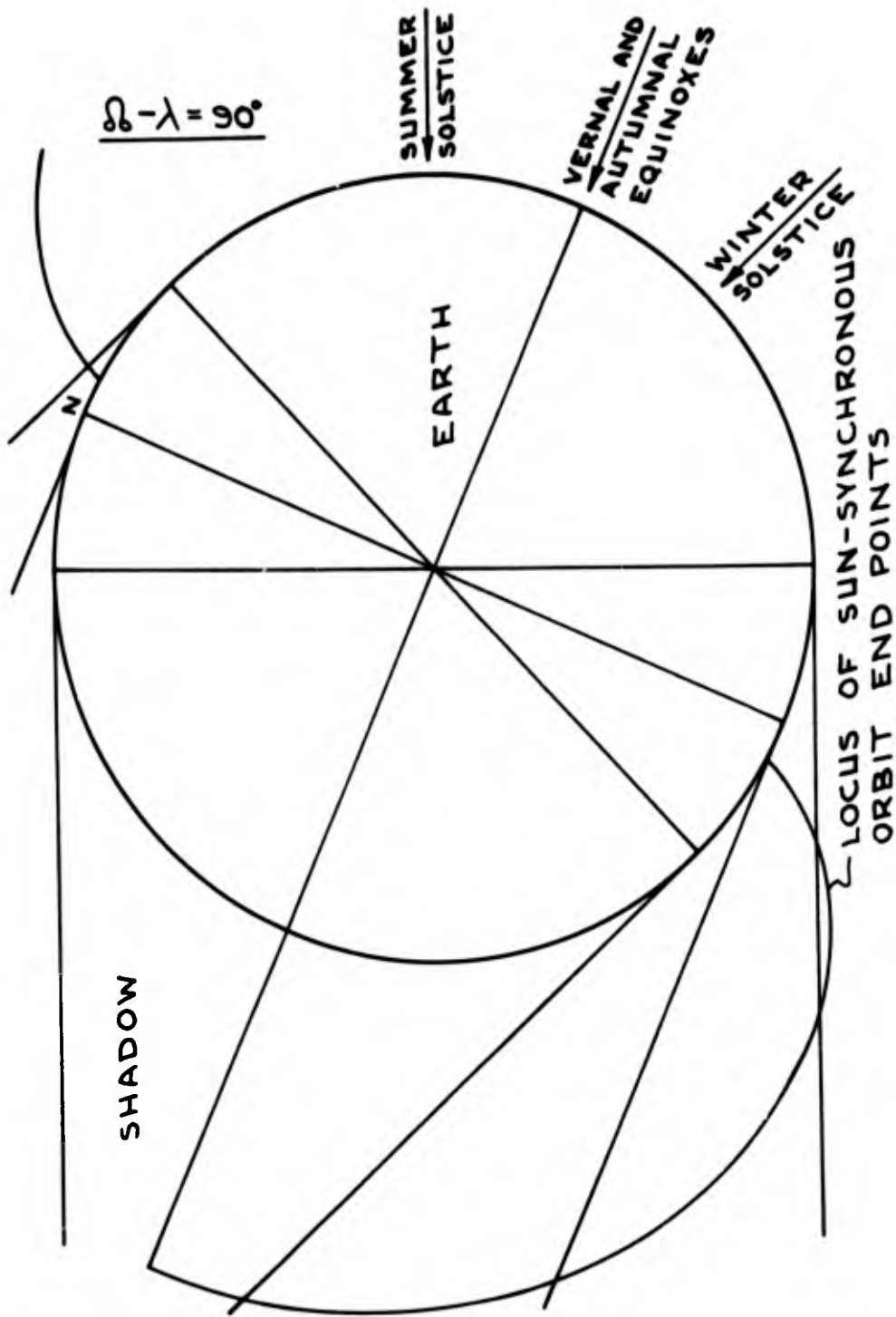
Figure 7. Orbit, Earth and Shadow Geometry for Sun-Synchronous Orbits

$$\mathcal{B} - \lambda = 90°$$

SUMMER SOLSTICE

$$\lambda = 90°$$
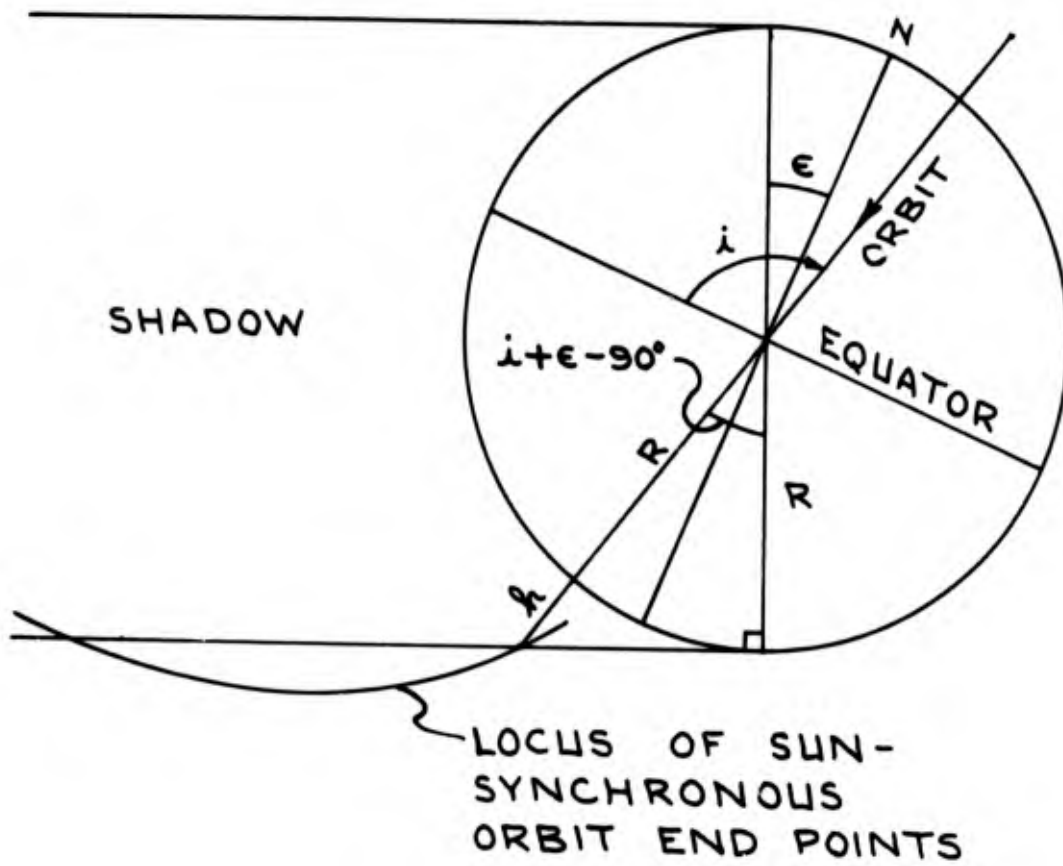
$$\cos(i + \epsilon - 90°) = \sin(i + \epsilon) = \frac{R}{R+h}$$

Figure 8. Criterion for Noneclipsing

At the summer solstice, $\lambda = 90°$, and at the point of tangency, $u = 270°$, therefore Equation (14) becomes

$$-\cos \sin^{-1}\left(\frac{R}{R+h}\right) = -\left(\sin \epsilon \sin i + \cos i - \cos \epsilon \cos i - \cos i\right)$$

$$-\cos \sin^{-1}\left(\frac{R}{R+h}\right) = \cos(i + \epsilon)$$

$$\frac{R}{R+h} = \sin(i + \epsilon) \qquad (15)$$

This corroborates the relation obtained from Figure 8. If $\dot{\Omega} = \dot{\lambda} = 0.985\ 647$ deg/day and Equation (15) are substituted into Equation (13),

$$\sin^{3.5}(i + \epsilon)\cos i = -0.098\ 952\ 7 \qquad (16)$$

An iteration procedure was used to solve for the double roots $i = 101°39$ and $i = 115°47$. The altitudes associated with these inclinations are $h = 751.9$ n mi and $h = 1796.6$ n mi, respectively. Thus, any sun-synchronous orbit with a $\Omega - \lambda = 90°$ orientation that lies between altitudes of 751.9 n mi and 1796.6 n mi is never eclipsed by the earth.

It is interesting to determine the orbit whose end point is farthest from the shadow at its closest point (see Figure 8); it is desired to maximize the distance $(R + h)\cos(i + \epsilon - 90°)$. The procedure will be to take the partial derivative of this distance with respect to the inclination, set this derivative equal to zero, and solve for the optimum inclination.

$$\left(\frac{R + h}{R}\right)\sin(i + \epsilon) = K \cos^{\frac{1}{3.5}} i \, \sin(i + \epsilon)$$

-18-

where

$$K = \left(\frac{9.960795}{\dot{\Omega}}\right)^{\frac{1}{3.5}} = \text{constant}$$

$$\frac{\partial\left[\left(\frac{R+h}{R}\right)\sin(i+\epsilon)\right]}{\partial i} = K\cos^{\frac{1}{3.5}}i\cos(i+\epsilon) - \frac{K}{3.5}\sin(i+\epsilon)\cos^{\frac{1}{3.5}-1}i\sin i = 0$$

This equation yields a solution for $i = 107^\circ.96$. The corresponding altitude is 1321.4 n mi. The distance from the shadow at the closest point is 130.4 n mi.

Eclipse fraction (f) as a function of celestial longitude (λ) for various altitudes (h) outside the noneclipsed region is displayed in Figures 9 and 10. These orbits are of interest because their eclipse fractions may be less, in an average sense, than the fractions for all other orbits at the same altitude. The other orbits would differ in inclination and/or initial orientation. (An examination of this hypothesis will be made in a later section.) For each altitude noted, Figures 9 and 10 also present the corresponding $\bar{f}$, the average value of f during a yearly cycle.

Figure 9 presents altitudes in the region $0 \leq h \leq 751.9$ n mi whereas Figure 10 presents altitudes in the region $1796.6 \leq h \leq 3225.3$ n mi. The curves of both figures were machine computed but many interesting special cases were determined analytically. Because the curves are mirror images about $\lambda = 90^\circ$ (summer solstice) and $\lambda = 270^\circ$ (winter solstice), the region $90^\circ \leq \lambda \leq 270^\circ$ is not displayed. Maxima occur at $\lambda = 90^\circ$ and 270° except for $h = 0$ n mi and for altitudes between approximately 3000 and 3225.3 n mi. For $h = 0$ n mi, $f = 0.5$ for all values of λ. Half the earth's surface is always in darkness, therefore half of every great circle on that surface is in darkness. For $h = 3225.3$ n mi maxima of equal magnitude occur at $\lambda = 0^\circ$ and 180°. Minima occur at $\lambda = 90^\circ$ and 270° in the region $3207.9 \leq h \leq 3225.3$ n mi.

-19-
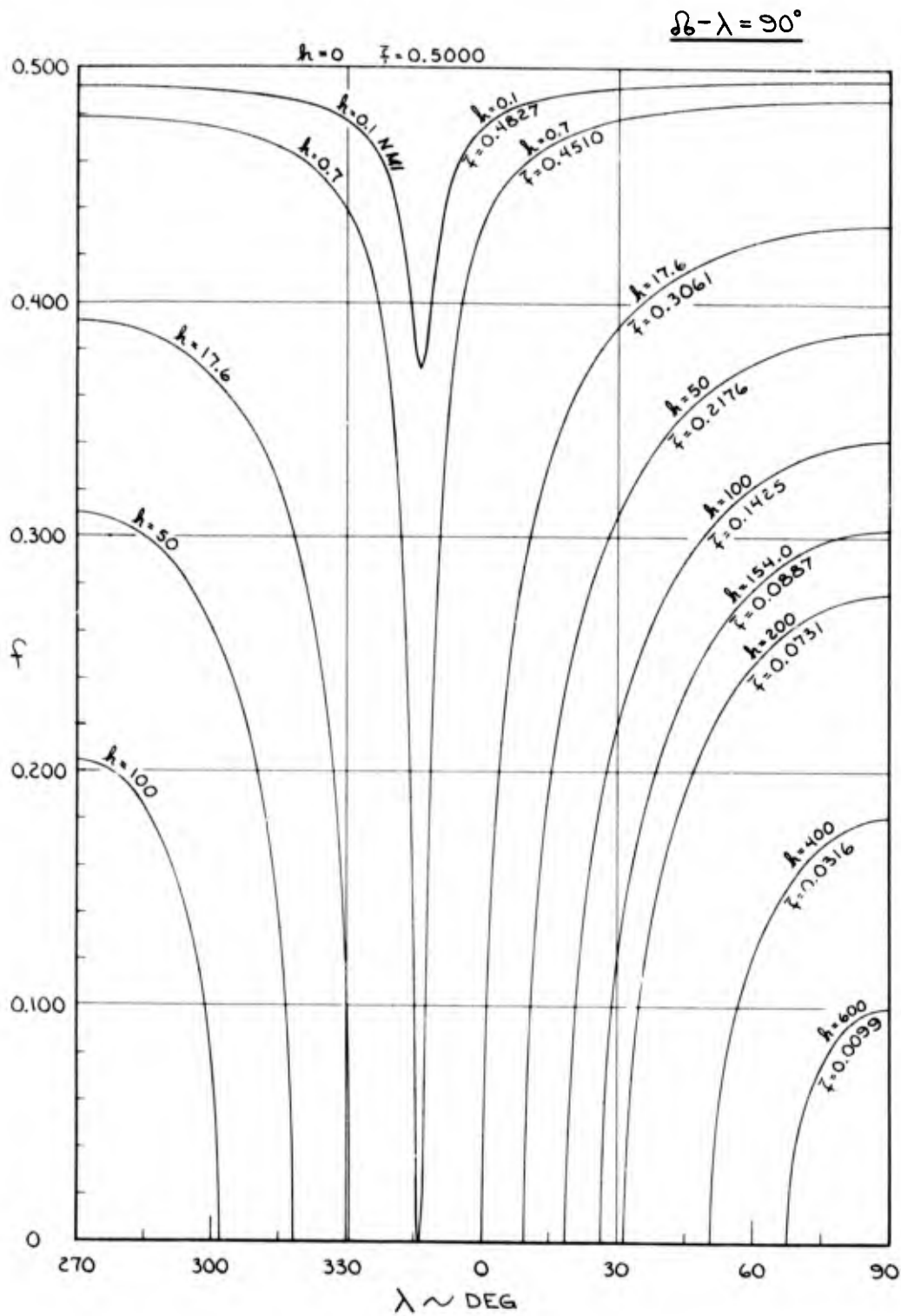
Figure 9.   Eclipse Fraction versus Celestial
Longitude for Various Altitudes
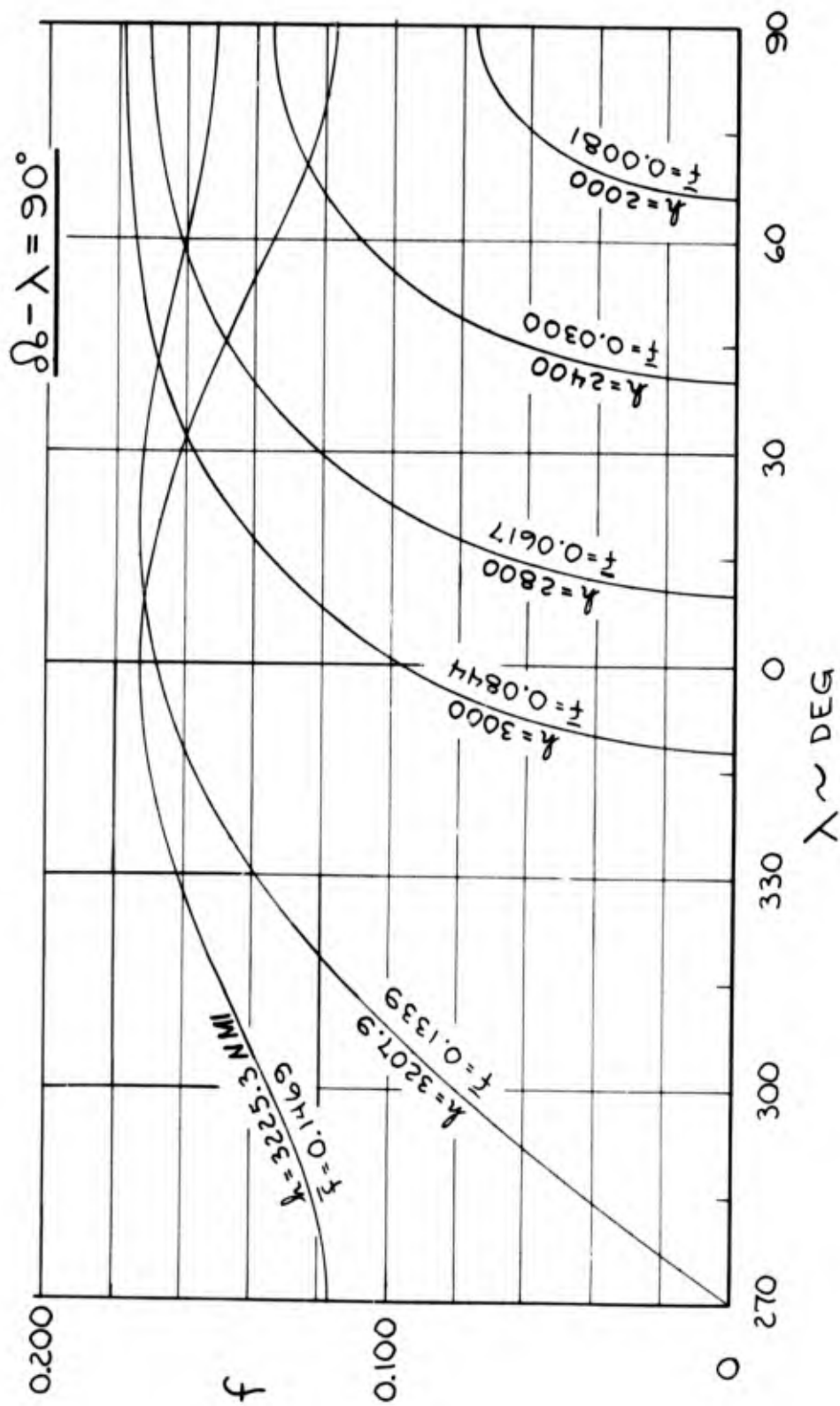
Figure 10. Eclipse Fraction versus Celestial Longitude
for Various Altitudes

Values of f at $\lambda = 90°$, $270°$, $0°$ and $180°$ may be determined analytically from Equation (14). For $\lambda = 90°$ Equation (14) becomes

$$-\cos \sin^{-1}\left(\frac{R}{R+h}\right) = \sin u\left(\sin \epsilon \, \sin i + \cos i - \cos i \, \cos \epsilon - \cos i\right)$$

which reduces to

$$\sin u = \frac{\cos \sin^{-1}\left(\frac{R}{R+h}\right)}{\cos(i + \epsilon)} \qquad (17)$$

The two solutions for u may then be substituted into Equation (12) to obtain f. For $\lambda = 270°$, Equation (14) becomes

$$\sin u = \frac{\cos \sin^{-1}\left(\frac{R}{R+h}\right)}{\cos(i - \epsilon)} \qquad (18)$$

and for both $\lambda = 0°$ and $\lambda = 180°$, Equation (14) becomes

$$\sin u = \frac{\cos \sin^{-1}\left(\frac{R}{R+h}\right)}{\cos i} \qquad (19)$$

Many machine computed points on the curves of Figures 9 and 10 were checked by means of Equations (17), (18) and (19).

Values of λ where $f = 0$ are of special interest. These values define the intervals during the year when noneclipsing occurs. The bounds on these intervals are described by a tangency condition. The orbit is tangent to the cylindrical shadow at these points. These points may be derived analytically as follows: Equation (14) may be rewritten as

$$\cos \phi' = A \sin u - B \cos u \qquad (20)$$

where

$$A = \left\{ \sin \lambda \left[\sin \epsilon \, \sin i + \sin \lambda \, \cos i \left(1 - \cos \epsilon \right) \right] - \cos i \right\}$$

$$B = \left\{ \sin \lambda \, \cos \lambda \left(1 - \cos \epsilon \right) \right\}$$

Squaring Equation (20) and solving for sin u by the quadratic formula,

$$\sin u = \frac{2A \cos \phi' \pm \sqrt{(2A \cos \phi')^2 - 4(A^2 + B^2)(\cos^2 \phi' - B^2)}}{2(A^2 + B^2)} \qquad (21)$$

Because of the tangency condition only a single solution for u exists. This requires that the quantity under the radical equals zero which reduces to,

$$\cos^2 \phi' = A^2 + B^2 \qquad (22)$$

Equation (22) may be solved for the desired values of λ. Various points on Figures 9 and 10 were determined from Equation (22). A special case exists when $f = 0$ at $\lambda = 0°$. In this situation Equation (22) reduces to $i = \phi'$ or equivalently $\sin i = R/(R + h)$. When this condition is combined with Equation (13) for $\dot{\Omega} = \dot{\lambda} = 0.985\,647$ deg/day the following equation results:

$$\sin^{3.5} i \, \cos i = -0.098\,952\,7 \qquad (23)$$

Equation (23) yields $i = 95°.78$. The corresponding altitude is 17.6 n mi which is displayed in Figure 9.

Another special case occurs when $f = 0$ at $\lambda = 270°$. In this case Equation (22) becomes $\cos \phi' = A = -\sin \epsilon \, \sin i + \cos i - \cos \epsilon \, \cos i - \cos i$ which reduces to,

$$\frac{R}{R + h} = \sin(i - \epsilon) \qquad (24)$$

If $\dot{\Omega} = \dot{\lambda} = 0.985\ 647$ deg/day and Equation (24) are substituted into Equation (13),

$$\sin^{3.5}(i - \epsilon)\cos i = -0.098\ 952\ 7 \tag{25}$$

Equation (25) yields double roots, $i = 172\overset{\circ}{.}26$ and $i = 96\overset{\circ}{.}62$. The associated altitudes are $h = 3207.9$ n mi and $h = 154.0$ n mi, respectively. The curve for $h = 3207.9$ n mi is displayed in Figure 10. It has a maximum $f = 0.173$ at $\lambda = 20°$ and a local minimum $f = 0.152$ at $\lambda = 90°$. All orbits with altitudes in the region $3207.9 \leq h \leq 3225.3$ n mi are eclipsed a portion of every day of the year (all values of λ). The curve for $h = 154.0$ n mi is displayed in Figure 9. It has a maximum $f = 0.304$ at $\lambda = 90°$ and $f = 0$ for all λ except the region $26\overset{\circ}{.}3 \leq \lambda \leq 153\overset{\circ}{.}7$. This is also the threshold altitude at which a blip begins to appear at $\lambda = 270°$. As the altitude decreases from $h = 154.0$ n mi, the blip grows rapidly until $f = 0.392$ at $\lambda = 270°$ for $h = 17.6$ n mi. But even at this altitude there is a gap between $\lambda = 330\overset{\circ}{.}8$ and $\lambda = 0$ for which $f = 0$. This gap must close for some altitude between 17.6 n mi and zero because $f = 0.500 =$ constant for $h = 0$ n mi.

The altitude for which the gap closes can be found analytically as follows. Equation (22) may be expanded and rearranged to obtain a quartic equation in $\sin \lambda$:

$$\cos^2\phi' = \left[-\sin^2 i\left(1 - \cos \epsilon\right)^2\right]\sin^4\lambda$$

$$+ \left[2 \sin i \cos i \sin \epsilon \left(1 - \cos \epsilon\right)\right] \sin^3\lambda$$

$$+ \left[\left(1 - \cos \epsilon\right)^2 - 2 \cos^2 i\left(1 - \cos \epsilon\right) + \sin^2 \epsilon \sin^2 i\right]\sin^2\lambda$$

$$+ \left[-2 \sin i \cos i \sin \epsilon\right]\sin \lambda + \cos^2 i \tag{26}$$

Since the altitude for which the gap closes is known to be very low, the approximation that $h/R \ll 1$ yields the following expression for $\cos^2\phi'$:

$$\cos^2\phi' = \cos^2\left[\sin^{-1}\left(\frac{R}{R+h}\right)\right] \approx \cos^2\left[\sin^{-1}\left(1 - \frac{h}{R}\right)\right] \approx 2\frac{h}{R} \qquad (27)$$

Combining Equations (26) and (27) and using $i = 95°.68$ which corresponds to $h = 0$ n mi,

$$\frac{h}{R} = -0.00338 \sin^4\lambda - 0.00324 \sin^3\lambda + 0.0810 \sin^2\lambda + 0.0392 \sin\lambda + 0.00490$$

$$(28)$$

For solution, an additional relation involving h or λ, or both, was needed. Such a relation was found by determining the geocentric angle between the line to the sun and the normal to the orbit plane. The hypothesis is that this angle is a minimum for the λ at which the gap closes. Eclipsing is least likely at this point because the orbit plane is most nearly perpendicular to the sun line. The desired angle may be obtained by first specifying two new rectangular coordinate systems (see Figure 1). The first geocentric system has an X-axis, X_{sun}, which passes through the sun; Y_{sun} is in the ecliptic plane, $90°$ east of X_{sun}, and Z_{sun} is in the direction of the north ecliptic pole. The second geocentric system has an X-axis, X_{orb}, which passes through the ascending node of the orbit plane; Y_{orb} is in the orbit plane $90°$ from X_{orb} in the direction of satellite motion, and Z_{orb} is normal to the orbit plane forming a right handed system with X_{orb} and Y_{orb}. The transformation between X_{sun}, Y_{sun}, Z_{sun} and X_{orb}, Y_{orb}, Z_{orb} is given by the following matrix expression.

$$\begin{pmatrix} X_{sun} \\ Y_{sun} \\ Z_{sun} \end{pmatrix} = \begin{pmatrix} \cos\lambda & \sin\lambda & 0 \\ -\sin\lambda & \cos\lambda & 0 \\ 0 & 0 & 1 \end{pmatrix} \begin{pmatrix} 1 & 0 & 0 \\ 0 & \cos\epsilon & \sin\epsilon \\ 0 & -\sin\epsilon & \cos\epsilon \end{pmatrix} \begin{pmatrix} \cos\Omega & -\sin\Omega & 0 \\ \sin\Omega & \cos\Omega & 0 \\ 0 & 0 & 1 \end{pmatrix} \begin{pmatrix} 1 & 0 & 0 \\ 0 & \cos i & -\sin i \\ 0 & \sin i & \cos i \end{pmatrix} \begin{pmatrix} X_{orb} \\ Y_{orb} \\ Z_{orb} \end{pmatrix}$$

$$(29)$$

Equation (29) was obtained by successively rotating the orb system through the angles i, Ω, ϵ and λ in order to bring the orb and sun systems into coincidence. The angle between the sun line and the normal to the orbit plane is the angle between X_{sun} and Z_{orb}. When the rotation matrices of Equation (29) are expanded into one matrix, the cos of (X_{sun}, Z_{orb}) is the component in the upper right-hand corner.

$$\cos(X_{sun}, Z_{orb}) = \cos \lambda \sin \Omega \sin i - \sin \lambda \cos \Omega \sin i \cos \epsilon + \sin \lambda \cos i \sin \epsilon$$

(30)

When $\Omega - \lambda = 90°$, Ω may be eliminated from Equation (30),

$$\cos(X_{sun}, Z_{orb}) = \sin i - \sin^2 \lambda \sin i(1 - \cos \epsilon) + \sin \lambda \cos i \sin \epsilon \qquad (31)$$

In order to find a minimum value for (X_{sun}, Z_{orb}) the partial derivative of (X_{sun}, Z_{orb}) with respect to λ will be set equal to zero and solved for the optimum value of λ,

$$\frac{\partial(X_{sun}, Z_{orb})}{\partial \lambda} = \frac{2 \sin \lambda \cos \lambda \sin i(1 - \cos \epsilon) - \cos \lambda \cos i \sin \epsilon}{\sin(X_{sun}, Z_{orb})} = 0 \qquad (32)$$

One solution of Equation (32) is given by $\cos \lambda = 0°$ for which $\lambda_{opt} = 90°$ and $\lambda_{opt} = 270°$. However, these are not the desired solutions because they yield <u>maximum</u> values for (X_{sun}, Z_{orb}). Another solution is given by

$$2 \sin \lambda \sin i(1 - \cos \epsilon) - \cos i \sin \epsilon = 0$$

or

$$\sin \lambda = \frac{\cos i \sin \epsilon}{2 \sin i(1 - \cos \epsilon)} \qquad (33)$$

For $i = 95°.68$, $\lambda_{opt} = 346°.1$ and $\lambda_{opt} = 193°.9$. These are the desired solutions because they yield a minimum value for X_{sun}, $Z_{orb} = 1°.07$. Figure 11 presents (X_{sun}, Z_{orb}) vs λ for $i = 95°.68$. When $\lambda_{opt} = 346°.1$ is substituted into Equation (28), $h/R = 0.000\ 192$ and $h = 0.66$ n mi. This is the altitude for which the gap closes. Machine computation results shown in Figure 9 for $h = 0.7$ n mi verified the above analysis. Results for $h = 0.1$ n mi are also shown in Figure 9 in order to emphasize the rapid changes occurring in the low altitude curves. In the low altitude region, $0 < h \leq 0.66$ n mi, f is a minimum at $\lambda = 346°.1$ and $193°.9$ whereas Figure 10 shows that f is a minimum at $\lambda = 270°$ in the high altitude region, $3207.9 \leq h \leq 3225.3$ n mi.
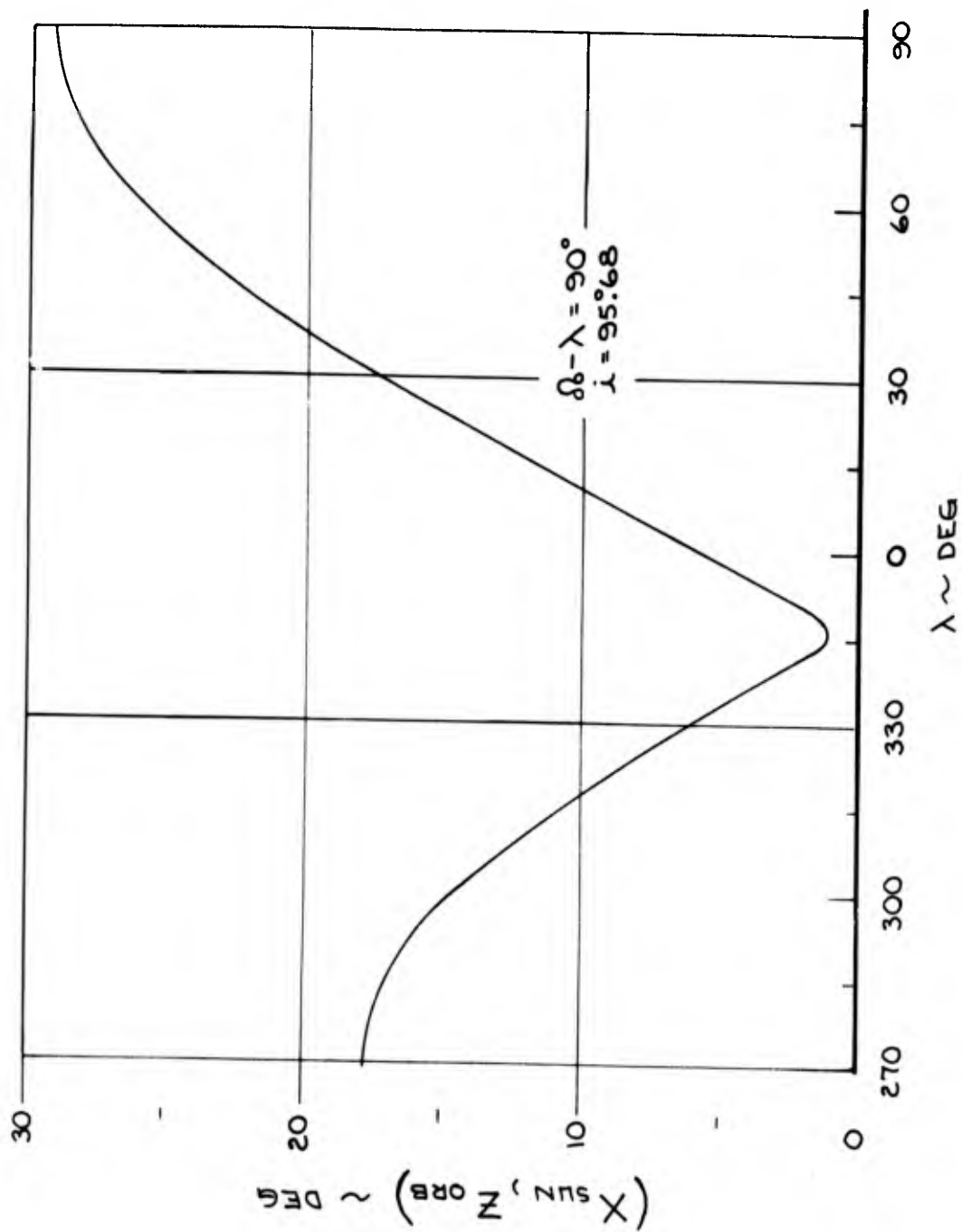
Figure 11. The Angle Between the Sun Line and the Normal to the Orbit Plane versus Celestial Longitude

5. OTHER ORIENTATIONS, $\Omega - \lambda = K$

A noneclipsed band of altitudes between 751.9 n mi and 1796.6 n mi has been found at $\Omega - \lambda = 90°$ and $\lambda = 90°$, the most restrictive time of year. Similar altitude bands should exist for sun-synchronous orbits at $\lambda = 90°$ and values of $\Omega - \lambda$ near 90°. The feasibility of these bands may be visualized by selecting an orbit which has an altitude (for example 1300 n mi) that is well within the discovered band. Picture the cylindrical shadow with the orbit around it at the summer solstice. Now imagine a rotation of the orbit in either direction about the earth's polar axis; the Ω is changing. The entire orbit remains in sunlight until it becomes tangent to the shadow. The value of Ω and $\Omega - \lambda$ at the point of tangency may be analytically determined.

Equation (11) can produce an equation which defines the tangency condition by the same logic that produced Equation (22) from Equation (14). If $\lambda = 90°$ is substituted into this tangency equation, the result is

$$\cos^2\phi' = \left(\sin \epsilon \sin i + \cos \epsilon \cos i \cos \Omega\right)^2 + \left(\cos \epsilon \sin \Omega\right)^2 \tag{34}$$

The difference between Equations (22) and (34) is that Equation (22) allows arbitrary λ but is restricted to $\Omega - \lambda = 90°$ whereas Equation (34) allows arbitrary $\Omega - \lambda$ but is restricted to $\lambda = 90°$. Equation (34) may be solved for $\cos \Omega$ after a considerable amount of algebraic manipulation. Therefore,

$$\cos \Omega = \frac{\sin \epsilon \cos i - \sin \phi'}{\cos \epsilon \sin i} = \frac{\sin \epsilon \cos i - \dfrac{R}{R+h}}{\cos \epsilon \sin i} \tag{35}$$

Equations (35) and (13) were used to produce the egg-shaped curve in Figure 12 which presents h versus $\Omega - \lambda$ for $\lambda = 90°$. Any point inside the egg defines a noneclipsed orbit whereas any point outside the egg defines an orbit
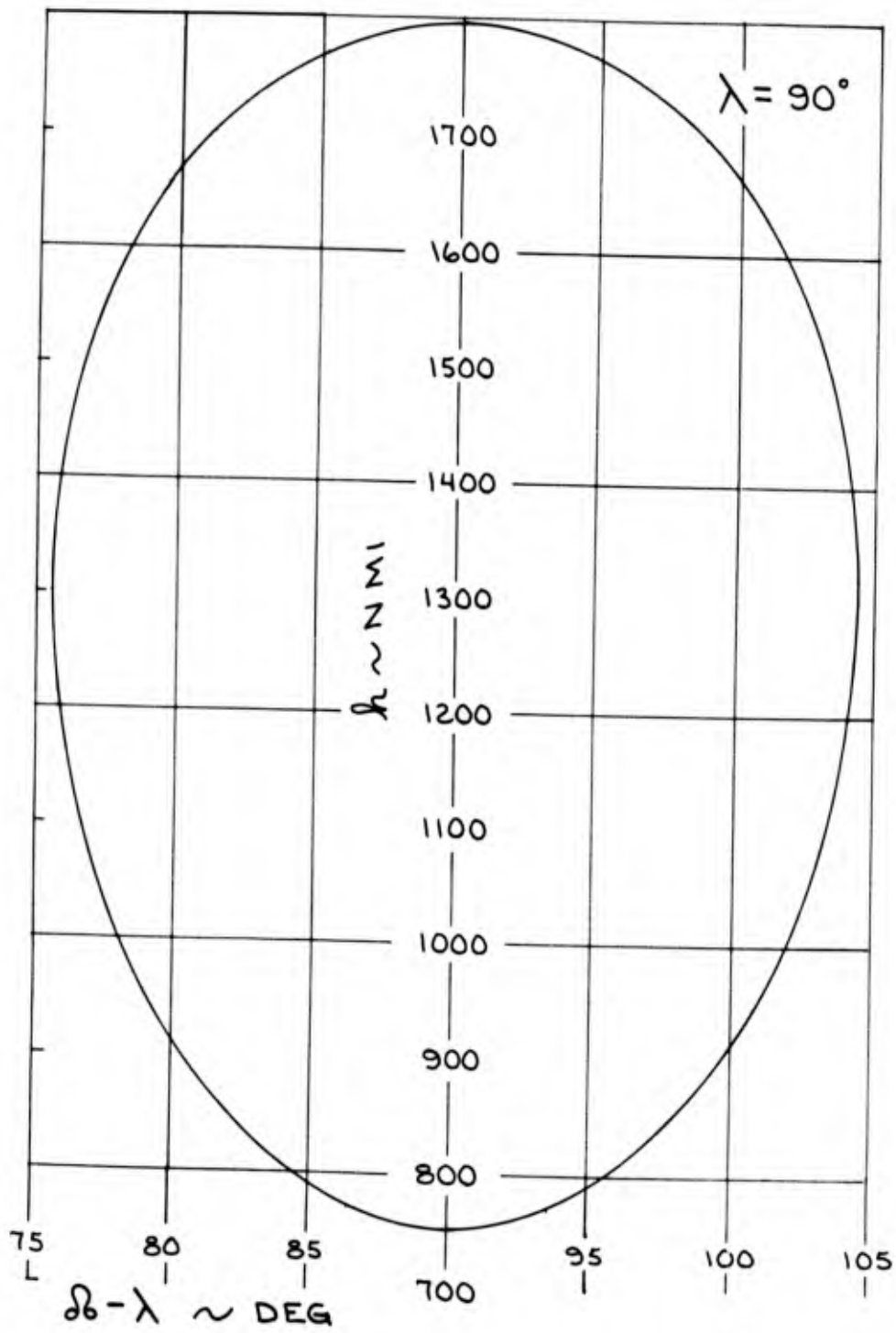
Figure 12. Noneclipsing Window

-30-

which has a nonzero eclipse fraction. The egg is symmetrical about $\Omega - \lambda = 90°$ for which h = 751.9 n mi and h = 1796.6 n mi. As $\Omega - \lambda$ departs from 90° the noneclipsed altitude band decreases until at $\Omega - \lambda = 75°.6$ and $104°.4$ the band reduces to a single point at h = 1300 n mi.

Equations similar to Equation (35) may be derived for $\lambda = 0°$, 180° and 270°. For $\lambda = 270°$,

$$\cos \Omega = \frac{\sin \epsilon \cos i + \dfrac{R}{R + h}}{\cos \epsilon \sin i} \tag{36}$$

For $\lambda = 0°$ and $\lambda = 180°$,

$$\sin \Omega = \frac{\dfrac{R}{R + h}}{\sin i} \tag{37}$$

Noneclipsing windows for $\lambda = 90°$, 270° and for 0° and 180° are shown in Figure 13. As expected the windows for $\lambda = 270°$ and for $\lambda = 0°$ and 180° are larger than the window for $\lambda = 90°$. At $\Omega - \lambda = 90°$ and $\lambda = 270°$, h = 154.0 n mi and 3207.9 n mi. At $\Omega - \lambda = 90°$ and $\lambda = 0°$ and 180°, h = 17.6 n mi and 2900.9 n mi. The curves yield the following kind of information. A satellite in a sun-synchronous orbit at h = 2800 n mi and $\Omega - \lambda = 65°$ will be eclipsed for part of each day during a six month period centered on the summer solstice. Note that although the summer solstice is the most restrictive time of year, the winter solstice is not always the least restrictive time of year because of the crossings of the $\lambda = 270°$, and 0° and 180° curves at approximately $\Omega - \lambda = 59°$ and 121°. For $59° \leq \Omega - \lambda \leq 121°$ and h < 600 n mi, $\lambda = 0°$ and 180° is less restrictive than $\lambda = 270°$. This situation is aptly demonstrated in Figure 9 which reveals that f for $\lambda = 0°$ is always less than f for $\lambda = 270°$ except in those cases when both values equal zero or 0.500.
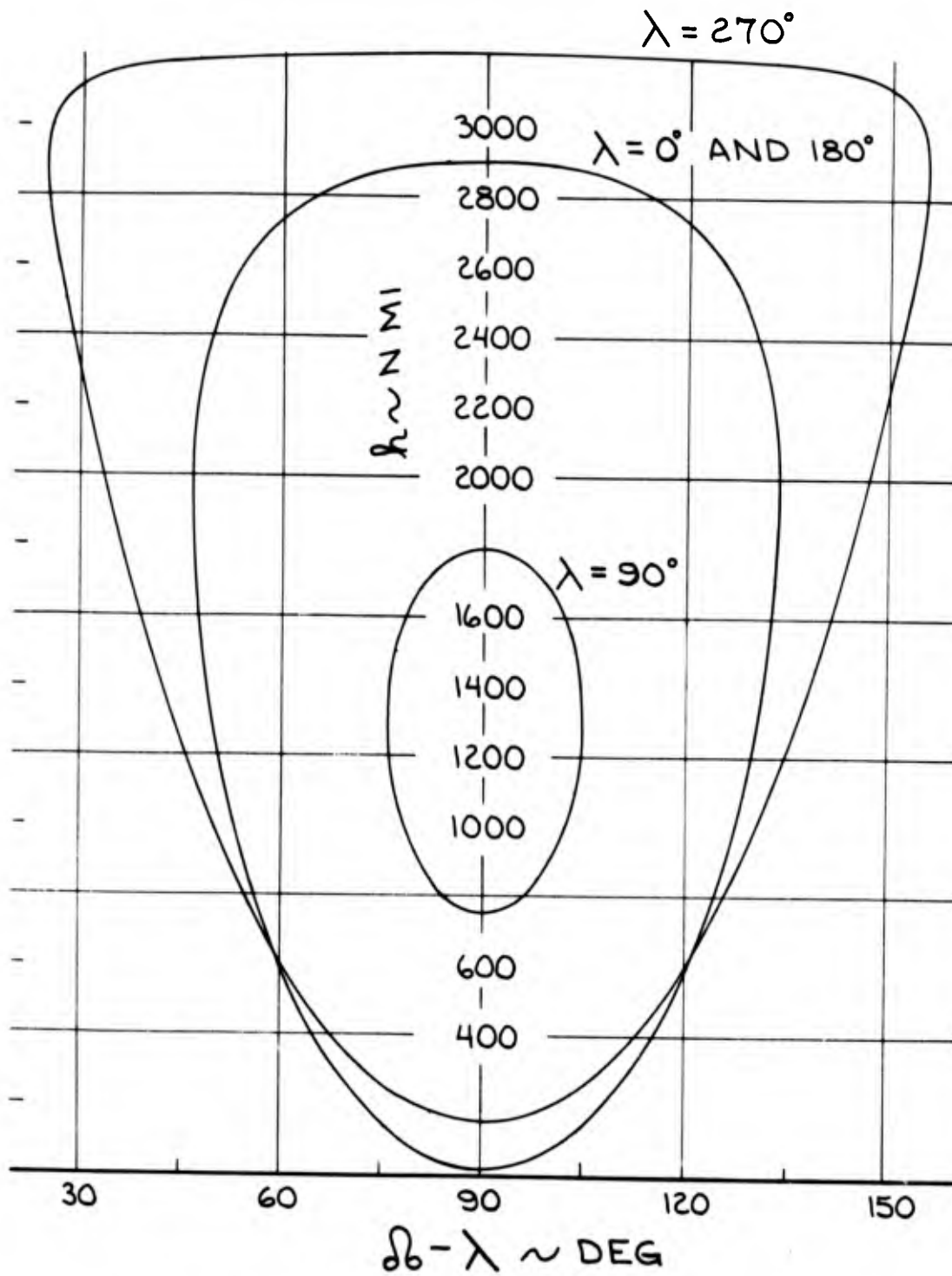
Figure 13. More Noneclipsing Windows

To this point in the analysis the search for orbits has been restricted to a search for noneclipsed orbits or orbits which have minimum average eclipse fractions. Orbits which have maximum average eclipse fractions are interesting if for no other reason than to determine an upper bound. Sun-synchronous noon-midnight ($\Omega - \lambda = 0$) orbits appear to be in this category. As indicated in Figure 5 these orbits are eclipsed for part of each day of the year. Eclipse fraction (f) for these orbits, as a function of λ for various values of h is displayed in Figure 14. Since these curves are mirror images about $\lambda = 0°$ and $\lambda = 180°$ only the $0 \leq \lambda \leq 180°$ region is presented. Note that the value of $\bar{f}$ for each value of h is greater than the $\bar{f}$ of Figure 9 or 10 for the corresponding h, except for h = 0 n mi and h = 3225.3 n mi (an equatorial orbit). The f vs λ histories for these two altitudes are identical for $\Omega - \lambda = 0°$ and $\Omega - \lambda = 90°$, therefore their values of $\bar{f}$ are identical.

Maximum values of f for all h occur at $\lambda = 0°$ and $180°$. The physical reason for this is that at the vernal and autumnal equinoxes these orbits pass through the center of the cylindrical shadow. The values of λ which correspond to minimum values of f for constant h may be analytically determined as follows. The angle between X_{sun} and Z_{orb} is again expected to be a minimum. When $\Omega - \lambda = 0$, Ω may be eliminated from Equation (30) so

$$\cos\left(X_{sun}, Z_{orb}\right) = \sin \lambda \left[\cos \lambda \sin i \left(1 - \cos \epsilon\right) + \cos i \sin \epsilon\right] \qquad (38)$$

Again the partial derivative of (X_{sun}, Z_{orb}) with respect to λ will be set equal to zero and solved for the optimum value of λ,

$$\frac{\partial\left(X_{sun}, Z_{orb}\right)}{\partial \lambda} = \frac{\left(\sin^2\lambda - \cos^2\lambda\right)\sin i \left(1 - \cos \epsilon\right) - \cos \lambda \cos i \sin \epsilon}{\sin\left(X_{sun}, Z_{orb}\right)} = 0 \qquad (39)$$
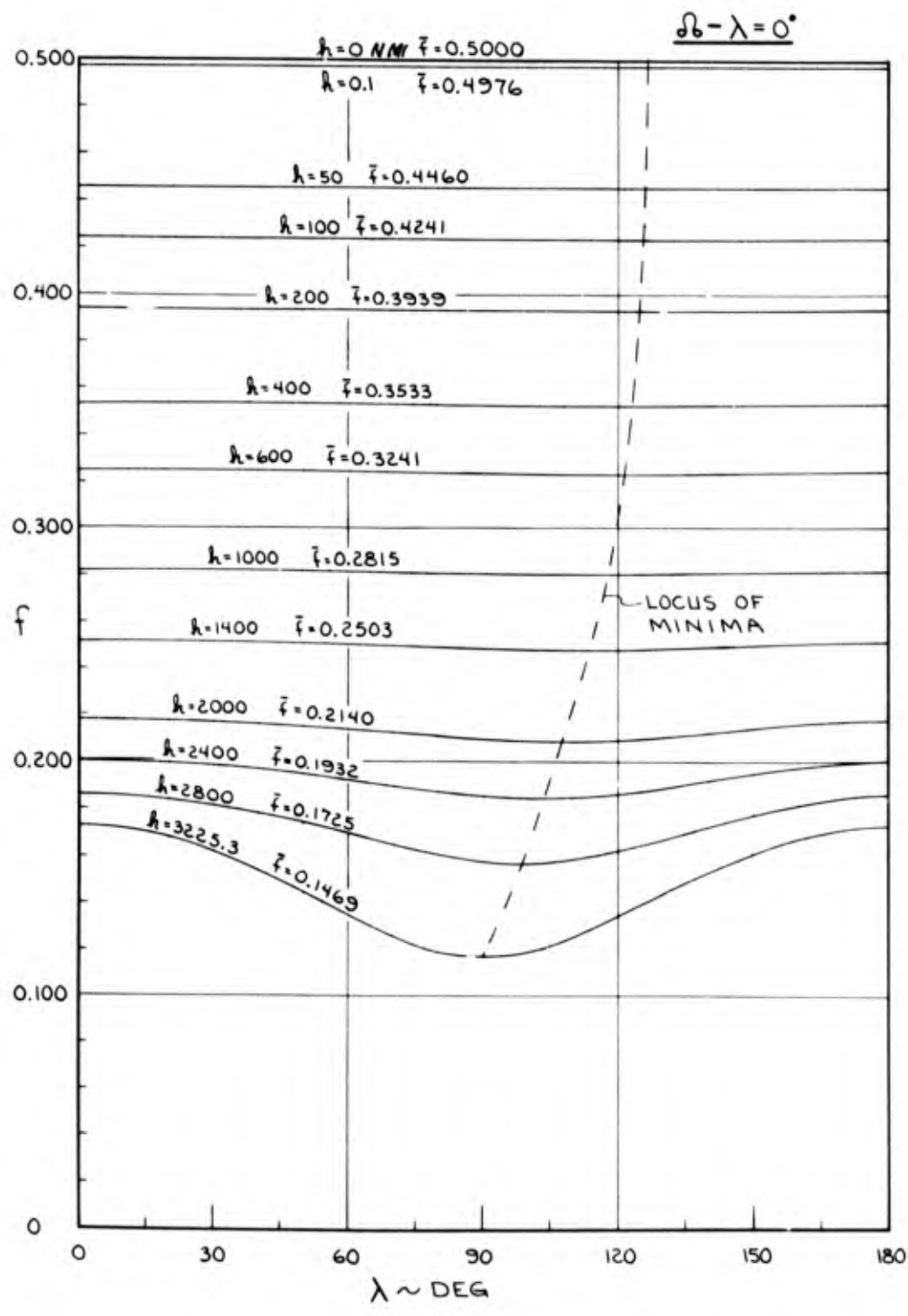
Figure 14.   Eclipse Fraction versus Celestial
Longitude for Various Altitudes

-34-

The solution for λ_{opt} is

$$\cos \lambda_{opt} = \frac{-\cos i \sin \epsilon - \sqrt{\cos^2 i \sin^2 \epsilon + 8 \sin^2 i (1 - \cos \epsilon)^2}}{4 \sin i (1 - \cos \epsilon)} \tag{40}$$

Solutions of Equation (40) produced the dashed line of Figure 14 which defines the locus of minimum f.

Figures 9 and 10 for $\Omega - \lambda = 90°$ and Figure 14 for $\Omega - \lambda = 0°$ note values of $\bar{f}$ for various altitudes. Figure 15 presents $\bar{f}$ versus $\Omega - \lambda$ for those altitudes. The curves are symmetrical about $\Omega - \lambda = 0°$, $90°$, $180°$ and $270°$. Maximum values of $\bar{f}$ occur at $\Omega - \lambda = 0°$ and $180°$ while minimum values of $\bar{f}$ occur at $\lambda = 90°$ and $270°$. Values of $\bar{f}$ for h = 0 and h = 3225.3 n mi are seen to be constant, i.e., independent of $\Omega - \lambda$. The noneclipsing window of Figure 12 is shown, in a different perspective, along the $\bar{f} = 0$ line of Figure 15. The curves for h = 751.9 n mi and h = 1796.6 n mi are both tangent to $\bar{f} = 0$ at $\Omega - \lambda = 90°$, indicating the altitude extent of the window. The $\Omega - \lambda$ extent of the window is indicated, approximately, by the h = 1400 n mi curve.

Figure 15.   Average Eclipse Fraction versus the Difference Between
Node and Celestial Longitude for Various Altitudes
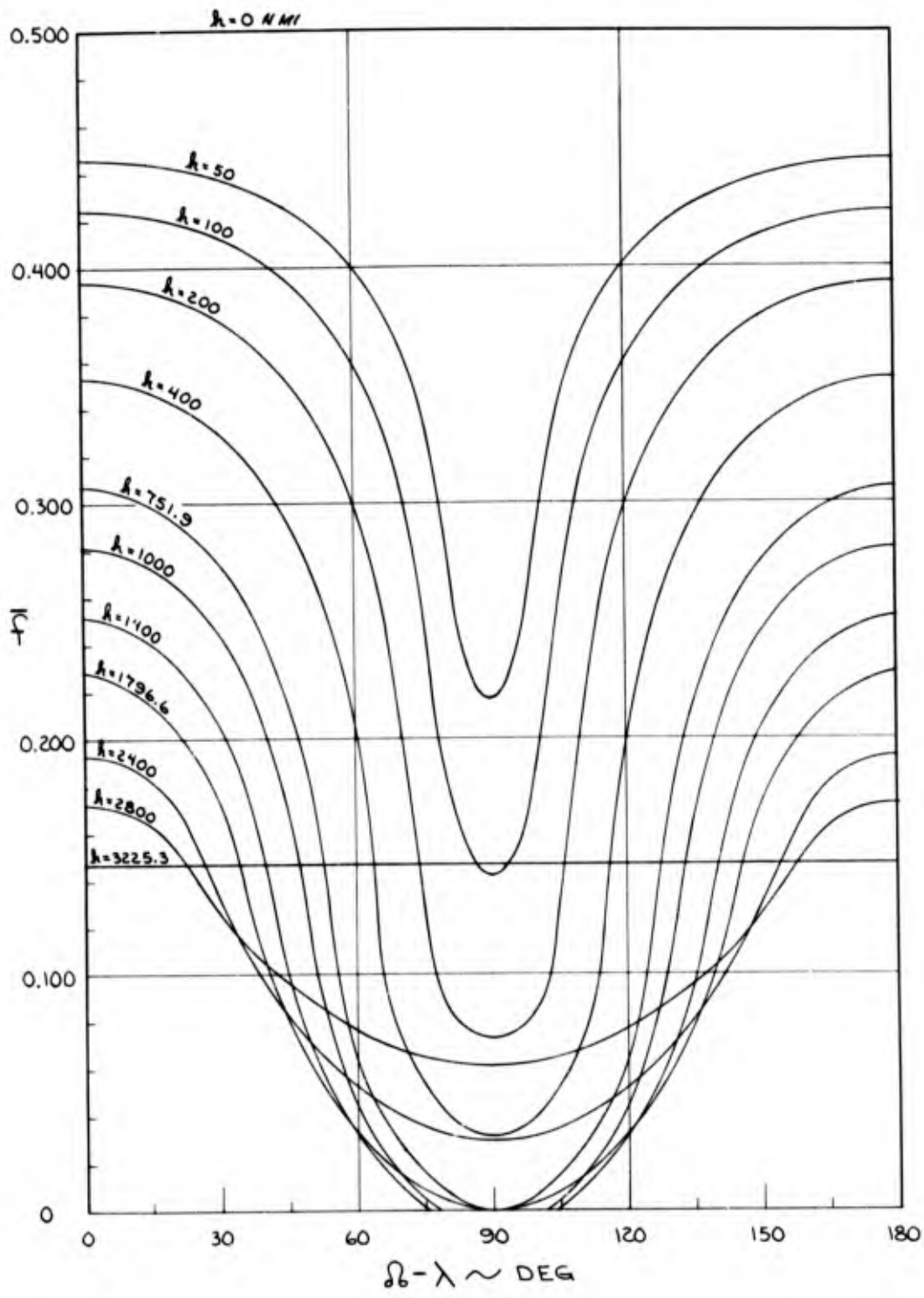
6. COMPARISONS WITH NON-SUN-SYNCHRONOUS ORBITS

Sun-synchronous orbits with a $\Omega - \lambda = 90°$ orientation have been shown to possess small eclipse fractions. In fact $\bar{f} = 0$ for $751.9 \leq h \leq 1796.6$ n mi. A comparative question naturally arises. For a given altitude, is the $\bar{f}$ for the best sun-synchronous orbit less than the $\bar{f}$'s for all non-sun-synchronous orbits? If so, by how much? The locus of all non-sun-synchronous orbits at a given altitude is a horizontal line in Figure 4 if the region $0 \leq i < 90°$ is included. The sun-synchronous orbit is only one point on this line.

A convincing plausibility argument may be made for the $\bar{f} = 0$ altitude region. Any non-sun-synchronous orbit in this altitude region will possess a nodal regression rate $\dot{\Omega}$ not equal to $\dot{\lambda}$. Thus, during a sufficiently long period of time, $\Omega - \lambda$ will assume all possible values, regardless of the initial value. One of those values is zero; at zero, eclipsing must occur, even at the summer solstice. Thus, $\bar{f}$ can not equal zero, and the sun-synchronous, $\Omega - \lambda = 90°$ orbits are better than any non-sun-synchronous orbit in the $751.9 \leq h \leq 1796.6$ n mi region.

Convincing arguments for any hypothesis are more difficult to make about the $0 \leq h \leq 751.9$ n mi and $1796.6 \leq h \leq 3225.3$ n mi regions. The machine program previously mentioned is able to compute eclipse fractions for any orbit, sun-synchronous or not. Only h, i, $\Omega_{initial}$, $\lambda_{initial}$, and λ_{final} need be given. Care must be taken in choosing the interval, $\lambda_{initial} - \lambda_{final}$, so that a true value for $\bar{f}$ will result. A true value is one which averages over all possible orientations of Ω and λ. Thus, the interval must be cyclic in both Ω and λ. For example, a two year interval is required for an orbit having $\dot{\Omega} = 1/2$ deg/deg of λ. Another complicating factor is that the difference between the initial values of Ω and λ is an additional parameter. For different values of $\Omega_{initial}$, two orbits with the same h, i, $\dot{\Omega}$ and $\lambda_{initial}$ will sample the shadow differently and obtain different values of $\bar{f}$. The factors just

mentioned make it impossible to exhaustively compute all possible non-sun-synchronous orbit parameter combinations. However, a representative subset has been calculated.

Figure 16 presents $\bar{f}$ as a function of h for polar, equatorial and sun-synchronous orbits (both $\Omega - \lambda = 90°$ and $\Omega - \lambda = 0°$). These curves and their intersections are very interesting. The fact that polar orbits possess smaller $\bar{f}$'s than the sun-synchronous, $\Omega - \lambda = 90°$ orbits in the region, $2745 < h \leq 3225.3$ n mi, is immediately obvious. This altitude region applies to the lower, $(\Omega - \lambda)_{initial} = 90°$, $270°$, of the two polar curves. The differences between the two polar curves reflect the effects of different values for $(\Omega - \lambda)_{initial}$. Polar curves for all possible values of $(\Omega - \lambda)_{initial}$ lie between the two polar curves presented in Figure 16.

At this point in the analysis many machine runs utilizing various combinations of h, i and $(\Omega - \lambda)_{initial}$ were made. The results of these runs were quite revealing. None of the resultant $\bar{f}$'s fell below the polar, $(\Omega - \lambda)_{initial} = 90°$, $270°$ curve. At any given value of h, $\bar{f}$ typically displayed the following behavior as a function of i. As i increased from zero, $\bar{f}$ would decrease from its equatorial value. As i approached $90°$, equaled $90°$ and increased toward $180°$, $\bar{f}$ would approach the polar, $(\Omega - \lambda)_{initial} = 90°$ curve, touch it and then increase again toward the equatorial curve. This behavior is graphically presented in Figure 17 for h = 2400 n mi. When values of $(\Omega - \lambda)_{initial}$ other than $90°$ were tested, $\bar{f}$ would approach, touch and move away from the polar curve which possessed the corresponding value of $(\Omega - \lambda)_{initial}$.

Questions concerning the behavior of $\bar{f}$ in the vicinity of the inclination corresponding to a sun-synchronous orbit naturally arise. The results of the machine runs revealed that $\bar{f}$ at the sun-synchronous inclination is apparently a singular point. As i increases from $90°$ to $180°$, $\bar{f}$ increases smoothly from a minimum at i = $90°$ to a maximum at i = $180°$ except for a singular point at the sun-synchronous inclination.

-38-

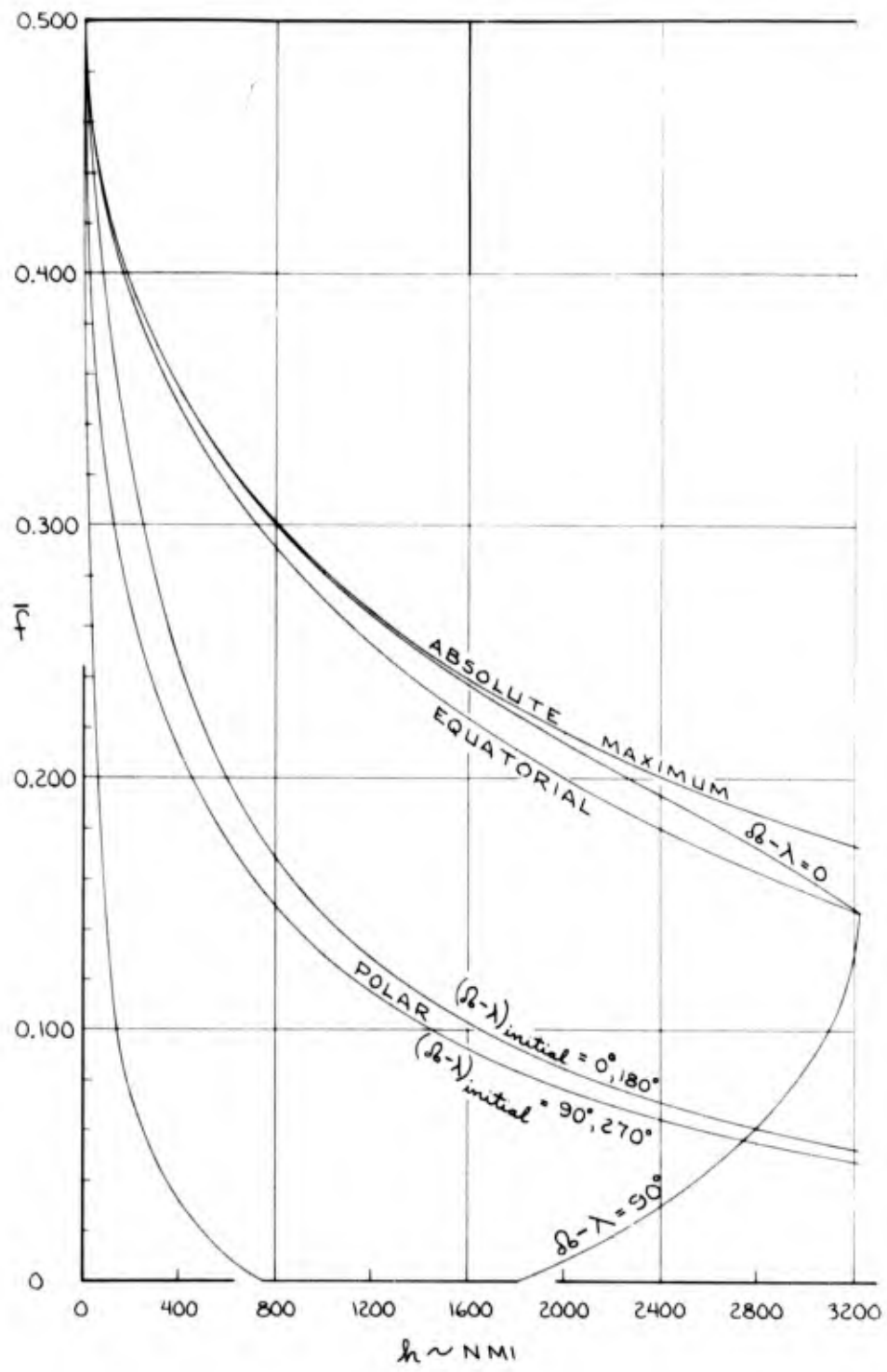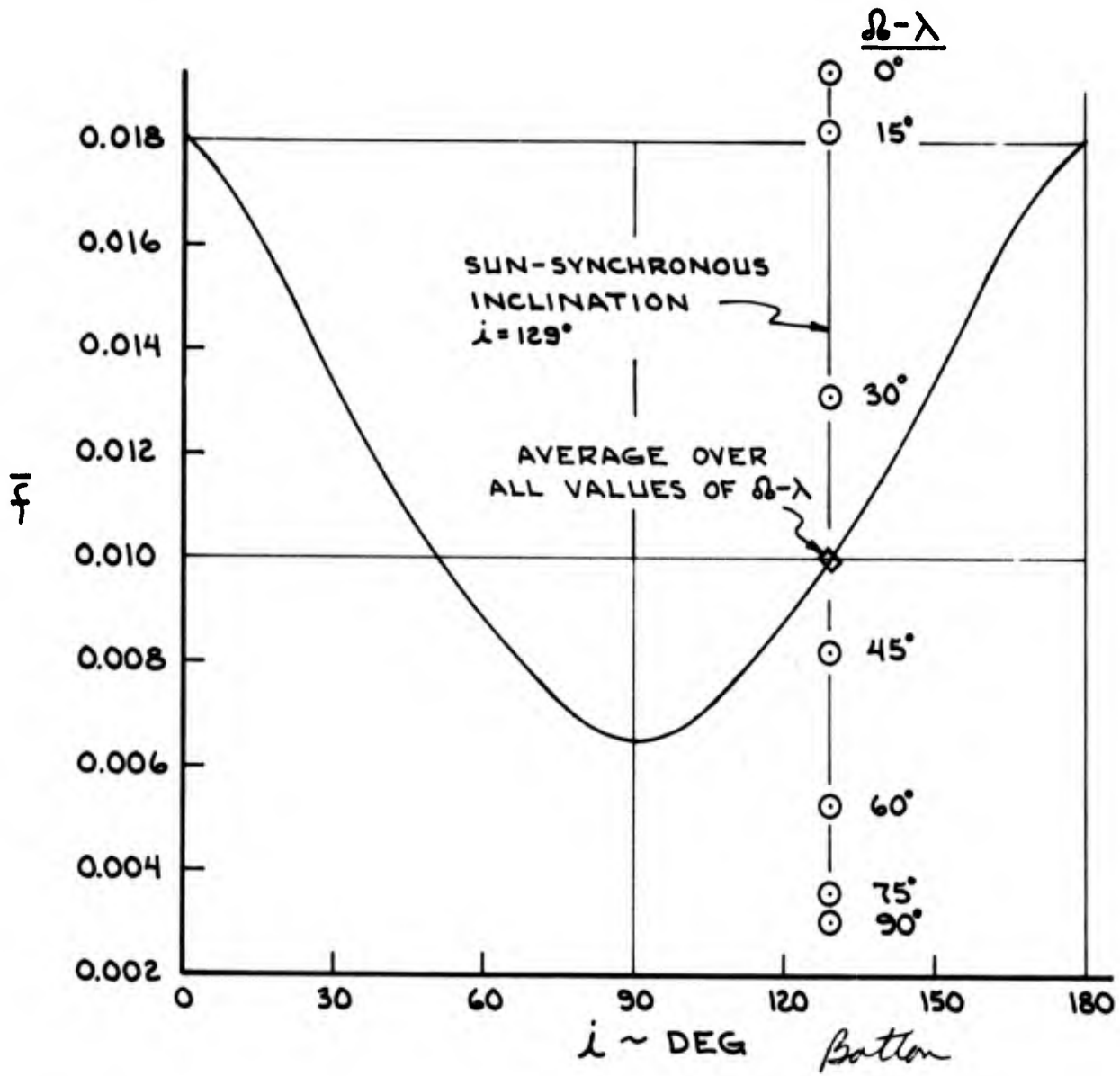Figure 16. Average Eclipse Fraction versus Altitude for Various Classes of Orbits

Figure 17.   Average Eclipse Fraction versus
Inclination for h = 2400 n mi

As Figure 16 indicates, the singular point value of $\bar{f}$ will lie on the vertical line, corresponding to the given h, between the $\Omega - \lambda = 0°$ and $\Omega - \lambda = 90°$ curves. The point on this line segment which $\bar{f}$ assumes is determined by the assumed value of $\Omega - \lambda$. This variation of $\bar{f}$ with $\Omega - \lambda$ for a given h was depicted earlier in Figure 15. This behavior is also shown in Figure 17 for h = 2400 n mi. Figures 15 and 17 reveal that $\bar{f}$ for h = 2400 n mi possesses a maximum value of 0.193 at $\Omega - \lambda = 0°$. As $\Omega - \lambda$ increases, $\bar{f}$ decreases until a minimum value of 0.030 is obtained at $\Omega - \lambda = 90°$. As $\Omega - \lambda$ continues to increase, $\bar{f}$ increases to a maximum value of 0.193 at $\Omega - \lambda = 180°$. An average value of $\bar{f}$, obtained by integrating over all values of $\Omega - \lambda$, was found to equal 0.099. This point does fit on the smooth curve of $\bar{f}$ vs i shown on Figure 17. Therefore, $\bar{f}$ does increase smoothly from a minimum at i = 90° to a maximum at i = 180° if an average value of $\bar{f}$ (over all $\Omega - \lambda$) is assumed at the sun-synchronous inclination.

Thus, our search for minimum values of $\bar{f}$ has led to the following conclusions: the locus of minimum $\bar{f}$ for non-sun-synchronous orbits is the polar, $(\Omega - \lambda)_{initial} = 90°, 270°$ curve; the locus of minimum $\bar{f}$ for sun-synchronous orbits is the $\Omega - \lambda = 90°$ curve. As Figure 16 shows, the combination locus follows the sun-synchronous, $\Omega - \lambda = 90°$ curve to h = 2745 n mi and then transfers to the polar, $(\Omega - \lambda)_{initial} = 90°, 270°$ curve between h = 2745 n mi and h = 3225.3 n mi.

The $\Omega - \lambda = 0°$ and the absolute maximum curves of Figure 16 are also interesting. The $\Omega - \lambda = 0°$ curve is the locus of previously described noon-midnight, sun-synchronous orbits. The absolute maximum curve describes an upper limit for $\bar{f}$ as a function of altitude. This limit was calculated assuming that the satellite passes through the deepest part of the shadow (i.e., that the orbit plane contains the axis of the cylindrical shadow) on every revolution. The equation for the maximum curve is $\bar{f}_{max} = \frac{1}{\pi} \sin^{-1}[R/(R + h)]$. Although this limit is not practical, since no satellite orbit will always pass through the deepest shadow, it does serve as a reference by which to gauge the eclipse fractions of real orbits. Note that the sun-synchronous, $\Omega - \lambda = 0°$

-41-

curve lies near the absolute maximum, especially in the low altitude regime. The $\Omega - \lambda = 0°$ curve always lies above the equatorial curve except at $h = 0$ n mi and $h = 3225.3$ n mi where the two curves intersect.

In brief summary, all sun-synchronous orbits are represented by points which lie on, or between, the $\Omega - \lambda = 0°$ and $\Omega - \lambda = 90°$ curves of Figure 16 while all non-sun-synchronous orbits are represented by points which lie on, or between, the equatorial and polar, $(\Omega - \lambda)_{initial} = 90°$ curves.

7. PERTURBATION EFFECTS ON SUN-SYNCHRONOUS ORBITS AND VELOCITY REQUIREMENTS FOR COMPENSATION

7.1 ATMOSPHERIC DRAG PERTURBATION

Atmospheric drag causes a satellite to decay (lose altitude). With small deviations the orbit remains circular and the inclination remains constant. As can be deduced from Figure 4, the orbit moves vertically downward from the initial altitude, h_o. As the satellite decays, $\dot{\Omega}$ increases. Thus, f is affected by both a decreasing h and an increasing $\Omega - \lambda$. Approximate analytical expressions for both h and $\Omega - \lambda$, as functions of time (t), may be obtained.

Following the analysis of Billik (Reference 2) an exponential atmosphere will be assumed:

$$\rho = \bar{\rho}e^{-\beta h} \tag{41}$$

where ρ is the atmospheric density (lb $\sec^2/\text{ft}^4$) at altitude h (ft) and $\bar{\rho}$(lb $\sec^2/\text{ft}^4$) and β(1/ft) are constants to be selected for the purpose of fitting an exponential atmosphere to the actual atmosphere in a given altitude region.

For $h \ll R$, Billik has derived an expression involving h, t and known constants

$$\left(\frac{t}{W/C_D A}\right) g \sqrt{\mu R}\ \beta\bar{\rho} + e^{\beta h} = e^{\beta h_o} \tag{42}$$

where $W/C_D A$ is the ballistic coefficient involving: W, the satellite weight (lb), C_D, the satellite drag coefficient (dimensionless), and A,

the area (ft^2) corresponding to C_D; and where g is the acceleration (ft/sec^2) due to gravity; and where μ is the earth's gravitational constant (ft^3/sec^2). Equation (42) may be solved for h,

$$h = \frac{1}{\beta} \ln\left[-B\left(\frac{t}{W/C_D A}\right) + e^{\beta h_o}\right] \tag{43}$$

where

$$B = \beta \bar{\rho} g \sqrt{\mu R} = \text{constant.}$$

As $W/C_D A \to \infty$, $h \to h_o$ as it should.

An equation for $\Omega - \lambda$ in terms of t and known constants will now be derived.

$$\Omega - \lambda = \int (\dot{\Omega} - \dot{\lambda}) \, dt + K \text{ (constant)} \tag{44}$$

Since the orbit is initially sun-synchronous, $\dot{\lambda} = \dot{\Omega}$ for $h = h_o$ and $i = i_o$ in Equation (13). As the satellite decays, $\dot{\Omega}$ remains the same as given in Equation (13) except that $h = h$ and $i = i_o$,

$$\Omega - \lambda = K - 9.9608 \cos i_o \int\left[\left(\frac{R}{R+h}\right)^{3.5} - \left(\frac{R}{R+h_o}\right)^{3.5}\right] dt \tag{45}$$

Assuming $h \ll R$,

$$\Omega - \lambda = K - 9.9608 \cos i_o \int\left[-3.5\left(\frac{h - h_o}{R}\right)\right] dt \tag{46}$$

The integral of $h \, dt$ must now be determined. Using h from Equation (43),

$$\int h \, dt = \frac{1}{\beta} \int \ln\left[-B\left(\frac{t}{W/C_D A}\right) + e^{\beta h_o}\right] dt \tag{47}$$

-44-

Let

$$Z = \left[-B\left(\frac{t}{W/C_D A}\right) + e^{\beta h_o} \right] \quad \text{so that } dZ = \frac{-B}{W/C_D A}\, dt \ .$$

Substituting into Equation (47),

$$\int h\, dt = \frac{W/C_D A}{\beta B} \int -\ln Z\, dZ = -\frac{W/C_D A}{\beta B}\left[Z(\ln Z - 1) \right] \tag{48}$$

By substituting Equation (48), Z and B into Equation (46) and rearranging,

$$(\Omega - \lambda) - K = -\frac{(3.5)(9.9608)(W/C_D A)\cos i_o}{R}$$

$$\times \left[\left\{ -\frac{1}{\beta}\left(\frac{t}{W/C_D A}\right) + \frac{1}{(86400)\rho_o \beta^2 g \sqrt{\mu R}} \right\} \left\{ \ln\left[-(86400)\beta\bar{\rho} g \sqrt{\mu R}\left(\frac{t}{W/C_D A}\right) \right. \right. \right.$$

$$\left. \left. \left. + \frac{\bar{\rho}}{\rho_o} \right] - 1 \right\} + h_o\left(\frac{t}{W/C_D A}\right) \right] \tag{49}$$

The factor (86400) allows t to be measured in days. The constant K may be determined from an evaluation of Equation (49) at t = 0 when $h = h_o$ and $(\Omega - \lambda) = (\Omega - \lambda)_{t=0}$.

$$K = (\Omega - \lambda)_{t=0} + \frac{(3.5)(9.9608)(W/C_D A)\cos i_o}{R}\left[\frac{\beta h_o - 1}{(86400)\rho_o \beta^2 g \sqrt{\mu R}} \right] \tag{50}$$

Substituting K into Equation (49),

$$\frac{(\Omega - \lambda) - (\Omega - \lambda)_{t=0}}{W/C_D A} = - \frac{(3.5)(9.9608)\cos i_o}{R}$$

$$\times \left[\left\{ \frac{1}{(86400)\rho_o \beta^2 g \sqrt{\mu R}} - \frac{1}{\beta}\left(\frac{t}{W/C_D A}\right) \right\} \right.$$

$$\times \left\{ \ln\left[\frac{\bar{\rho}}{\rho_o} - (86400)\beta\bar{\rho}g\sqrt{\mu R}\left(\frac{t}{W/C_D A}\right)\right] - 1 \right\}$$

$$\left. - \left\{ \frac{\beta h_o - 1}{(86400)\rho_o \beta^2 g \sqrt{\mu R}} \right\} + h_o \left(\frac{t}{W/C_D A}\right) \right] \qquad (51)$$

For purposes of discussion it will be assumed that the 1959 ARDC Model
Atmosphere (Reference 3) is an adequate simulation to the actual atmosphere.
Figure 18 presents ρ versus h for this model between h = 100 n mi and
h = 300 n mi. In order to obtain an exponential match in this region, $\bar{\rho}$ and β
will be determined by substituting values of ρ and h at 140 and 250 n mi
into Equation (41),

$$2.006 \times 10^{-13} = \bar{\rho}e^{-140\beta}$$

$$7.030 \times 10^{-15} = \bar{\rho}e^{-250\beta}$$

Solving this set of equations for $\bar{\rho}$ and β,

$$\bar{\rho} = 1.428 \times 10^{-11} \frac{\text{lb sec}^2}{\text{ft}^4}$$

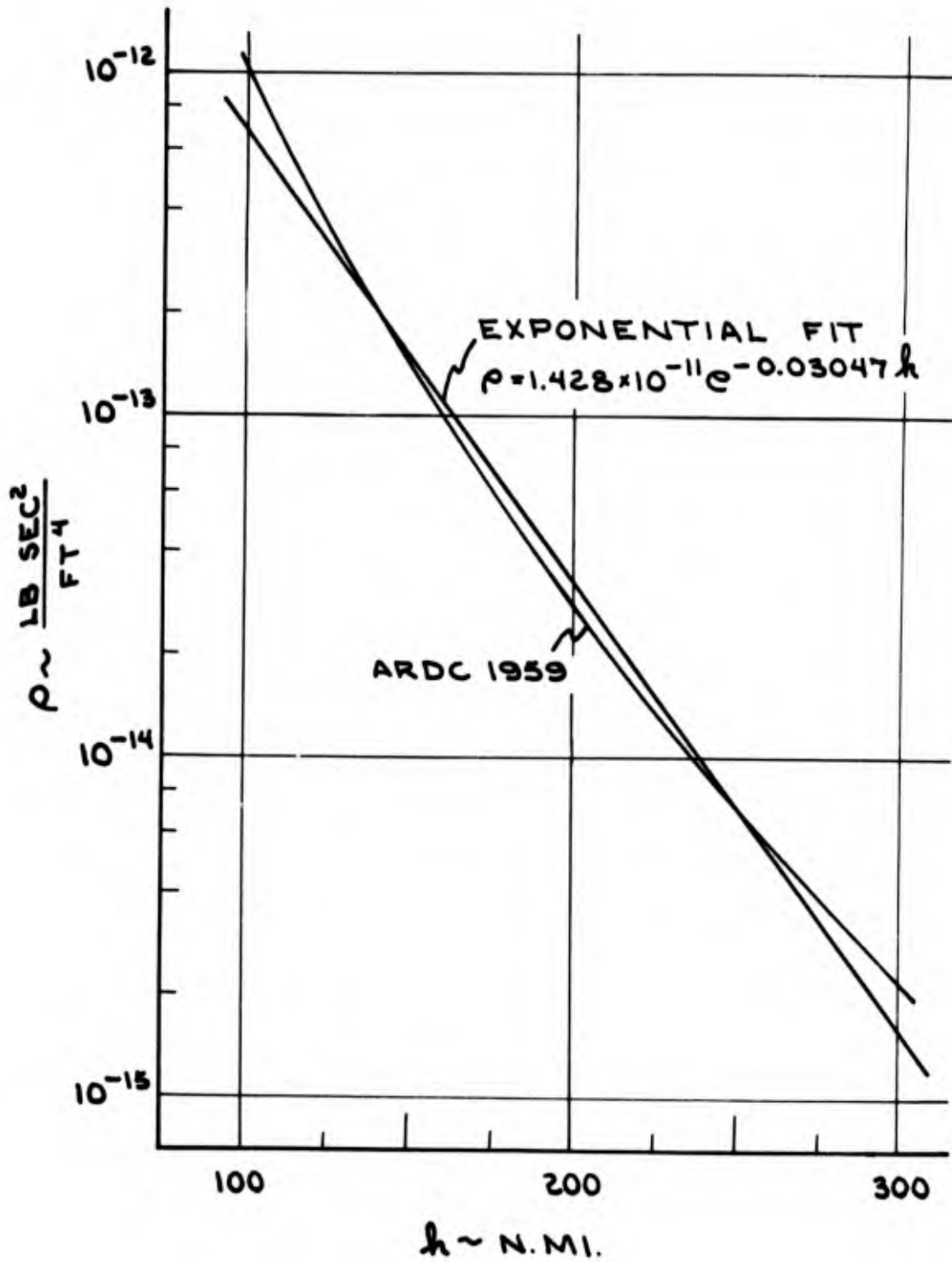$$\beta = 0.03047/\text{n mi} = 5.015 \times 10^{-6}/\text{ft}$$

Figure 18. Atmospheric Density as a Function of Altitude

-47-

Substituting $\bar{\rho}$ and β into Equation (41),

$$\rho = 1.428 \times 10^{-11} e^{-0.03047\,h} \tag{52}$$

Results from Equation (52) are also presented in Figure 18. The exponential fit matches the ARDC 1959 Model reasonably well between 100 and 300 n mi.

When all of the various constants are substituted into Equation (51),

$$\frac{(\Omega - \lambda) - (\Omega - \lambda)_{t=0}}{W/C_D A} = -1.0123 \times 10^{-2} \cos i_o$$

$$\times \left[\left\{ \left(\frac{4.858 \times 10^{-12}}{\rho_o} - 32.82 \left(\frac{t}{W/C_D A} \right) \right) \right. \right.$$

$$\times \left\{ \ln \left[\frac{1.428 \times 10^{-11}}{\rho_o} - 96.48 \left(\frac{t}{W/C_D A} \right) \right] - 1 \right\}$$

$$\left. - \left\{ \frac{4.858 \times 10^{-12}(0.03047\,h_o - 1)}{\rho_o} \right\} + h_o \left(\frac{t}{W/C_D A} \right) \right] \tag{53}$$

Note that $\dfrac{(\Omega - \lambda) - (\Omega - \lambda)_{t=0}}{W/C_D A}$ is only a function of initial conditions (h_o, ρ_o and i_o) and $\left(\dfrac{t}{W/C_D A} \right)$. Equations (51) and (53) were satisfactorily checked for the case, $W/C_D A \to \infty$; $(\Omega - \lambda) - (\Omega - \lambda)_{t=0} \to 0$ as it should. Figure 19 presents $\dfrac{(\Omega - \lambda) - (\Omega - \lambda)_{t=0}}{W/C_D A}$ versus $\left(\dfrac{t}{W/C_D A} \right)$ for three decay histories: (1) from $h_o = 200$ n mi to $h = 100$ n mi; (2) from $h_o = 250$ n mi to $h = 100$ n mi; (3) from $h_o = 300$ n mi to $h = 100$ n mi. Intermediate altitudes are noted on the curves.

As an example, consider the effects of decay from $h_o = 200$ n mi to $h = 100$ n mi. From Figure 19 $\dfrac{(\Omega - \lambda) - (\Omega - \lambda)_{t=0}}{W/C_D A} = 0.14 \dfrac{\deg}{\mathrm{lb/ft}^2}$ and $\left(\dfrac{t}{W/C_D A} \right) = 4.14 \dfrac{\mathrm{days}}{\mathrm{lb/ft}^2}$. If $W/C_D A = 50 \dfrac{\mathrm{lb}}{\mathrm{ft}^2}$ is assumed, $(\Omega - \lambda) - (\Omega - \lambda)_{t=0} = 7.0°$ and $t = 207$ days
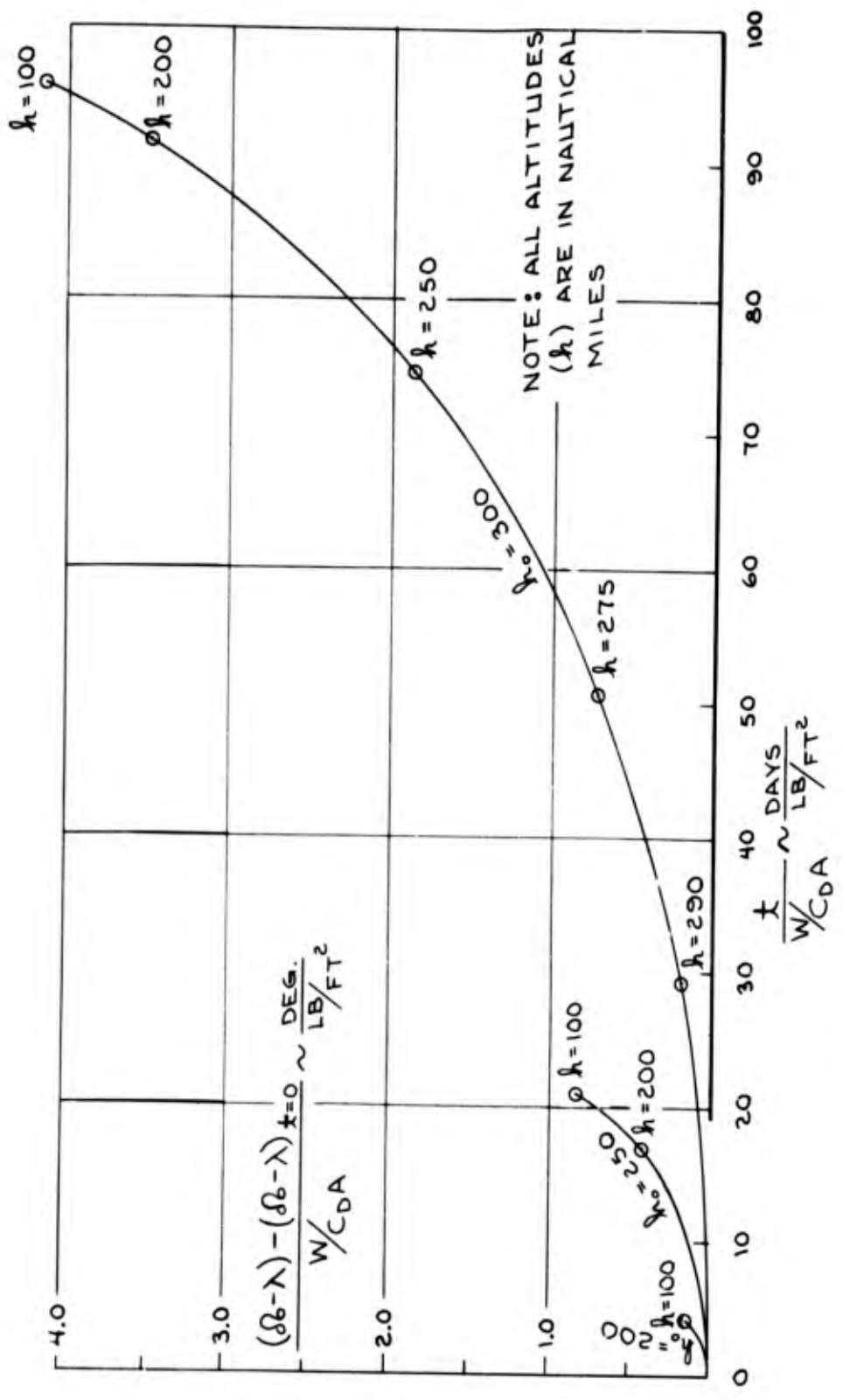
Figure 19. Effect of Altitude Decay on $(\Omega - \lambda)$ as a Function of Time for Three Initial Altitudes

or 204° of λ. The effects of this decay on f are displayed in Figure 20 for $(\Omega - \lambda)_{t=0} = 90°$. The solid curves for h = 200 n mi and h = 100 n mi represent f histories for ($\Omega - \lambda = 90°$) sun-synchronous orbits which are not perturbed by the atmosphere. The long dashed curve describes the locus of points at h = 100 n mi after decay from h_o = 200 n mi. The two short dashed curves represent typical f histories during decay: one starts at $\lambda = 60°$ and ends at $\lambda = 264°$; the other starts at $\lambda = 320°$ and ends at $\lambda = 164°$. These histories begin at the sun-synchronous h = 200 n mi curve and end at the h = 100 n mi locus after decay. Consider first the f history which ends at $\lambda = 264°$. At this point f = 0.220, all of which is due to decay since f = 0 for h = 200 n mi. The fraction, f = 0.220, may be considered the sum of two parts: one due to decreasing h; the other due to increasing $\Omega - \lambda$. From the h = 100 n mi curve, decreasing h accounts for f = 0.202 while increasing $\Omega - \lambda$ accounts for the remainder, f = 0.018. Next consider the f history which ends at $\lambda = 164°$. At this point f = 0.090, all of which is due to decay. Furthermore, it is all due to increasing $\Omega - \lambda$ since f = 0 for h = 100 n mi.

If the eclipse fractions due to decay are prohibitively detrimental to the satellite system, orbit sustaining is necessary. Bruce (Reference 4) has determined orbit sustaining requirements for two methods of thrust application. The first method is simply a continuous application of thrust equal to drag. The second method consists of altitude gaining Hohmann transfers interspersed with altitude decays due to drag. Thrust is applied for only short periods of time; in fact, impulsive applications are assumed. In this method the altitude is allowed to vary an amount Δh whose upper limit is the desired altitude.

Equation (5) of Reference 4 in combination with the familiar rocket equation provides the velocity requirements for continuous thrust orbit sustaining:

$$\Delta V = g_o I_{SP} \ln \left[\frac{1}{1 - \left(\frac{t}{W/C_D A}\right)\left(\frac{q}{I_{SP}}\right)} \right] \tag{54}$$
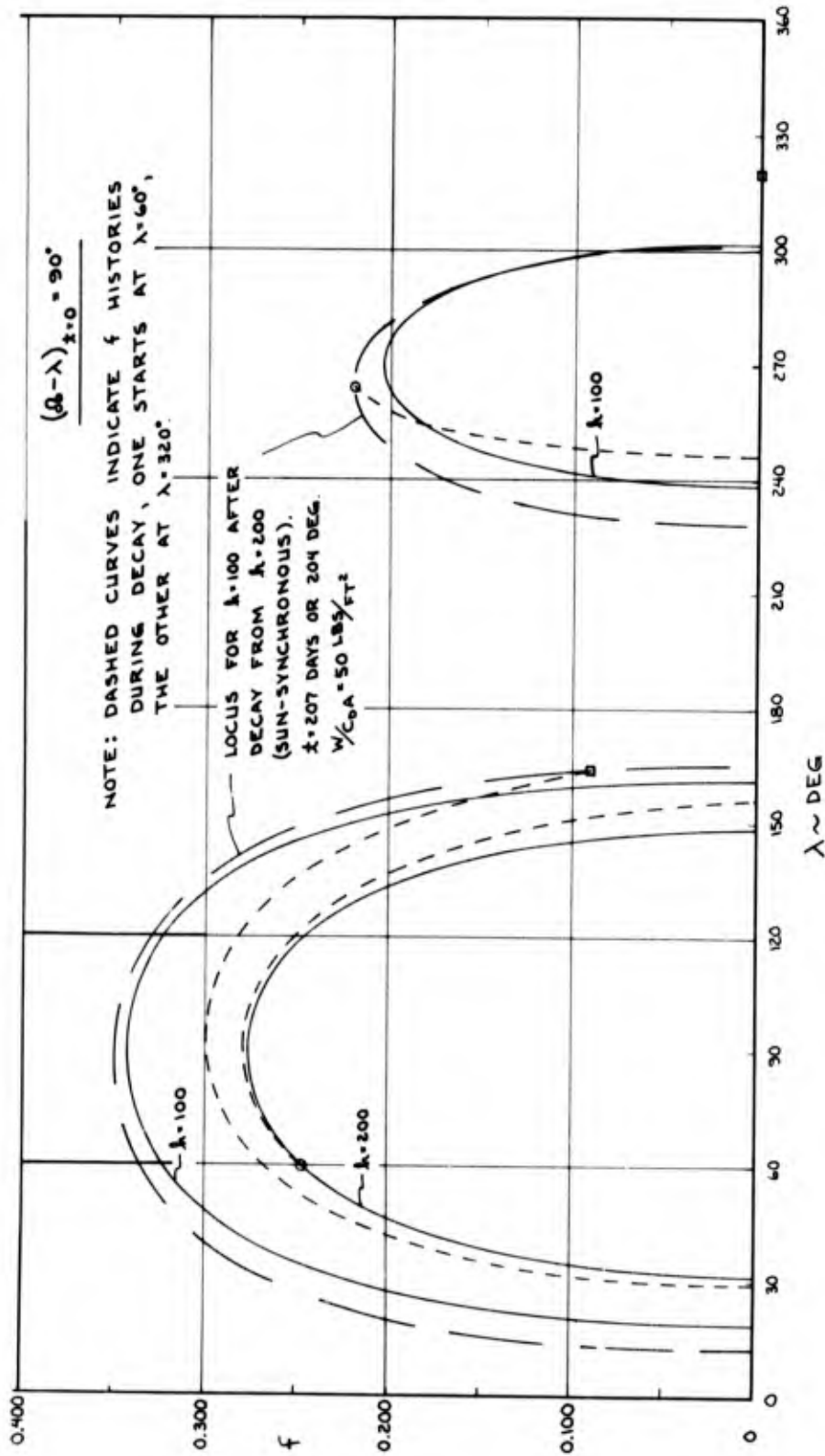
-50-

Figure 20. Effect of Altitude Decay on Eclipse Fraction as a Function of Celestial Longitude

where

g_o = the acceleration (ft/sec^2) due to gravity at the altitude of the test stand where I_{SP} is measured (g_o is required for conversion between mass and weight)

I_{SP} = the specific impulse (sec) of the rocket engine

t = the time (sec) in orbit

q = the dynamic pressure (lb/ft^2) defined by $q \triangleq \frac{1}{2} \rho V^2$

V = the satellite orbit velocity (ft/sec)

Given I_{SP} and h, from which ρ and V may be determined, ΔV is solely a function of $[t/(W/C_D A)]$. This functional dependence is presented in Figure 21 for various combinations of I_{SP} and h. In addition, one curve corresponding to the second method, Hohmann transfers and altitude decays, is presented. Returning to the previous example where h = 200 n mi and $W/C_D A$ = 50 lb/ft^2, the continuous thrust velocity requirements for a year $\left(\frac{t}{W/C_D A} = 7.3 \frac{days}{lb/ft^2} \right)$ for I_{SP} = 1000 sec are 79 ft/sec.

7.2 SOLAR AND LUNAR GRAVITATIONAL PERTURBATIONS

The perturbative effects of the gravitational attraction of the sun and moon will be examined in this section. These perturbative effects have been investigated by Moe (Reference 5) who begins her analysis with Lagrange's Planetary Equations. A lucid derivation and description of Lagrange's Planetary Equations exist in Moulton's An Introduction To Celestial Mechanics (Reference 6).* These equations describe the time rates of change of the orbital elements of a satellite as a function of the elements, the radial distance (r) the true anomaly (v) and the components of the perturbative acceleration. Moe averages these equations by integrating the derivatives of the elements over one revolution of the satellite and thereby obtains the change in each element per orbital revolution. Constant values for the elements are assumed for each revolution.
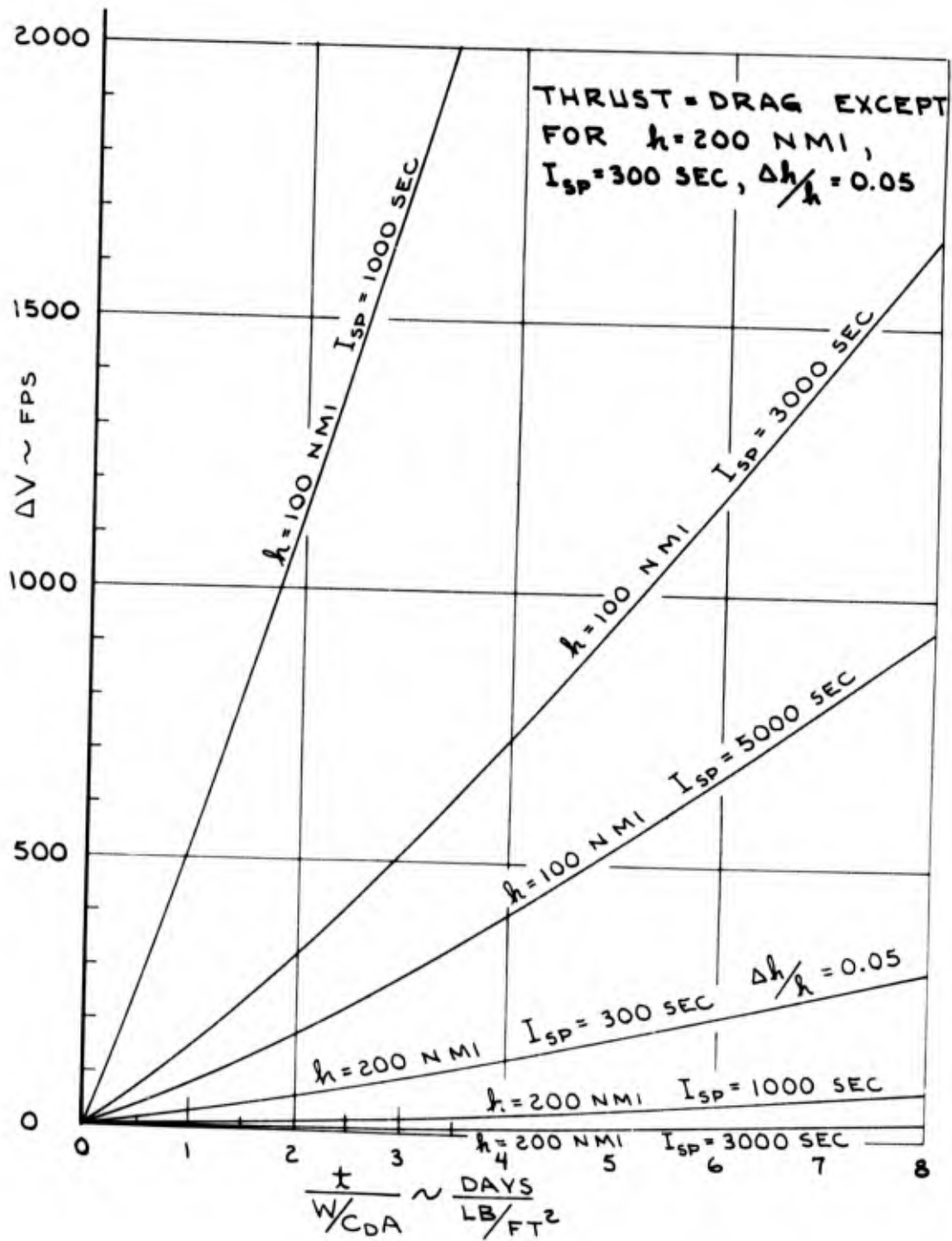
-52-

Figure 21.   Velocity Requirements for Orbit Sustaining

When the unperturbed orbit is circular, Moe's equations reduce to

$$\Delta a = 0 \tag{55a}$$

$$\Delta e = 0 \tag{55b}$$

$$\Delta i' = \frac{-6K_d \pi \sin \gamma \cos \gamma \sin i'}{n^2} \tag{55c}$$

$$\Delta \Omega' = \frac{-6K_d \pi \sin^2 \gamma \cos i'}{n^2} \tag{55d}$$

where

$$K_d = \mu_d / 2 a_d^3$$

μ_d = the gravitational constant (ft^3/sec^2) for the perturbing body

n = the satellite's mean angular motion (rad/sec)

The symbols a_d, γ, i' and Ω' are defined in Figure 22.

Equations (55a) and (55b) predict no secular changes in a or e due to the gravitational attraction of extraterrestrial bodies. However, i' and Ω', which are referenced to the plane of the perturbing body rather than to the equatorial plane, do vary according to Equation (55c) and Equation (55d), respectively.

When the sun is considered to be the perturbing body, the geometry of the problem is described by Figure 23. Trigonometric relations which may be obtained from this figure are

$$\cos i' = \cos i \cos \epsilon + \sin i \sin \epsilon \cos \Omega \tag{56}$$

$$\sin(\lambda + \gamma) = \sin \Omega \frac{\sin i}{\sin i'} \tag{57}$$

-54-
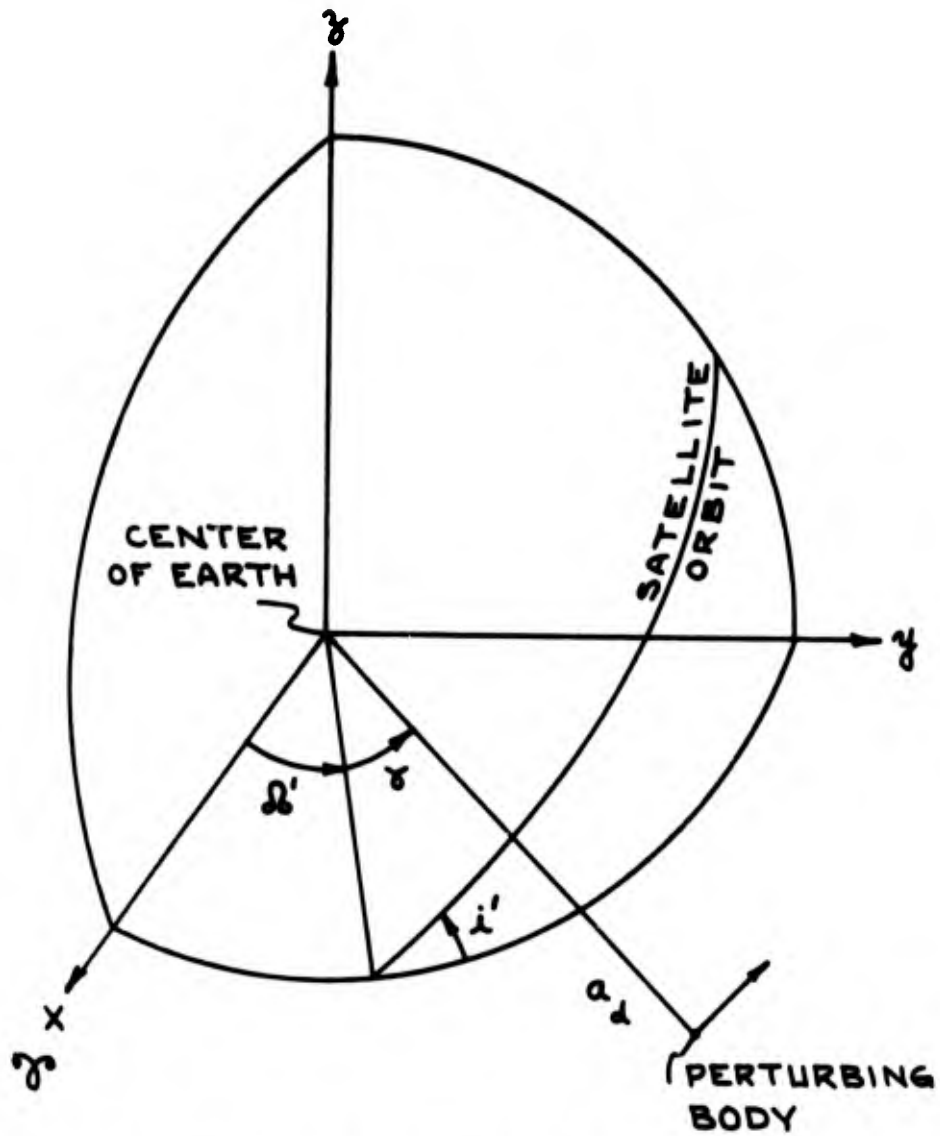
THE xy PLANE IS THE
ORBIT PLANE OF THE
PERTURBING BODY

Figure 22.   Notation for Solar-Lunar Perturbations
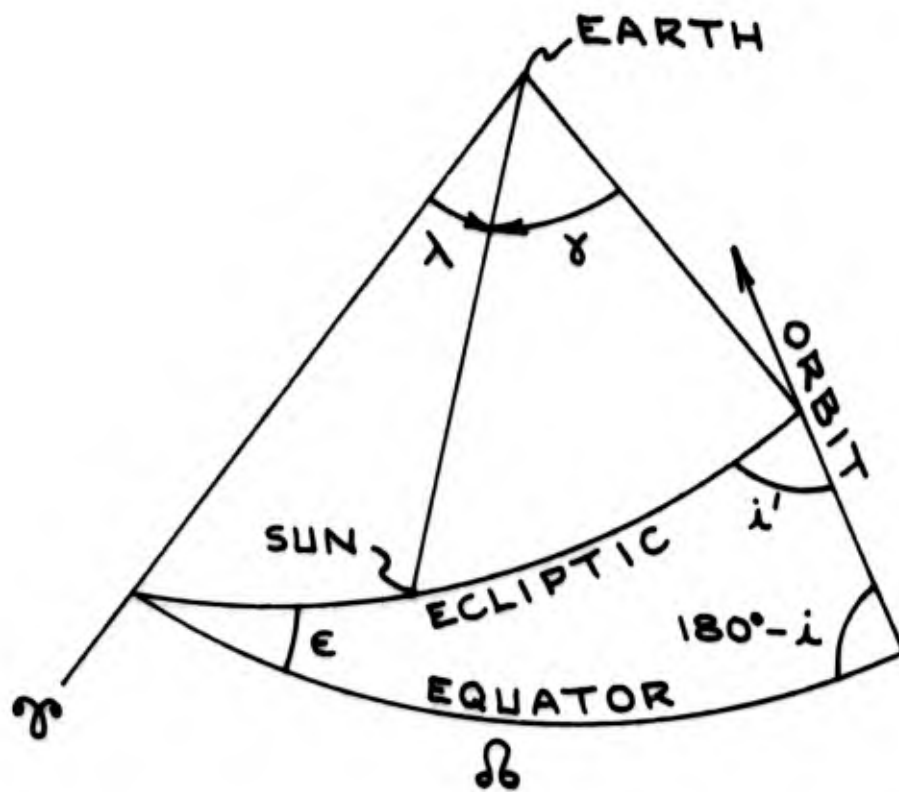
Figure 23. Geometry of Solar Perturbations

If $\Omega - \lambda$ = constant and if i is given, then Equation (56) may be solved for i' as a function of λ. Equation (57) may then be solved for γ as a function of λ. Assuming $\Omega - \lambda = 90°$ and a sun-synchronous orbit inclined at $150°$ (h = 2960 n mi), these equations have been solved for i' and γ and the functions (sin γ cos γ sin i') and (sin$^2\gamma$ cos i') are presented in Figures 24 and 25, respectively. Figure 24 shows that the integrated average value of (sin γ cos γ sin i') during the period of one year is zero. Therefore, the sun's effect on orbit inclination averages to zero after every year of satellite life. The variation during any year is small. The integrated effect during the three month period between $\lambda = 0°$ and $\lambda = 90°$ is only 0.006 degrees of inclination change.

From Figure 25 it can be concluded that the average value of (sin$^2\gamma$ cos i') during one year is -0.555. Substituting this value into Equation (55d) yields $\Delta\Omega' = 0.122$ deg/yr.

When the moon is considered to be the perturbing body, an additional averaging process may be incorporated. Since the variation of i' during one revolution of the moon in its orbit is small, the functions involving γ may be integrated over one revolution of the moon. These integrations are

$$\frac{1}{2\pi} \int_0^{2\pi} \sin \gamma \cos \gamma \, d\gamma = 0 \quad \text{and} \quad \frac{1}{2\pi} \int_0^{2\pi} \sin^2 \gamma \, d\gamma = \frac{1}{2}$$

Thus, the moon's effect on orbit inclination averages to zero after every month of satellite life.

The function (sin$^2\gamma$ cos i') is presented in Figure 26 as a function of λ. The integrated average value of (sin$^2\gamma$ cos i') from Figure 26 is -0.396 which, when substituted into Equation (55d), yields $\Delta\Omega' = 0.192$ deg/yr.
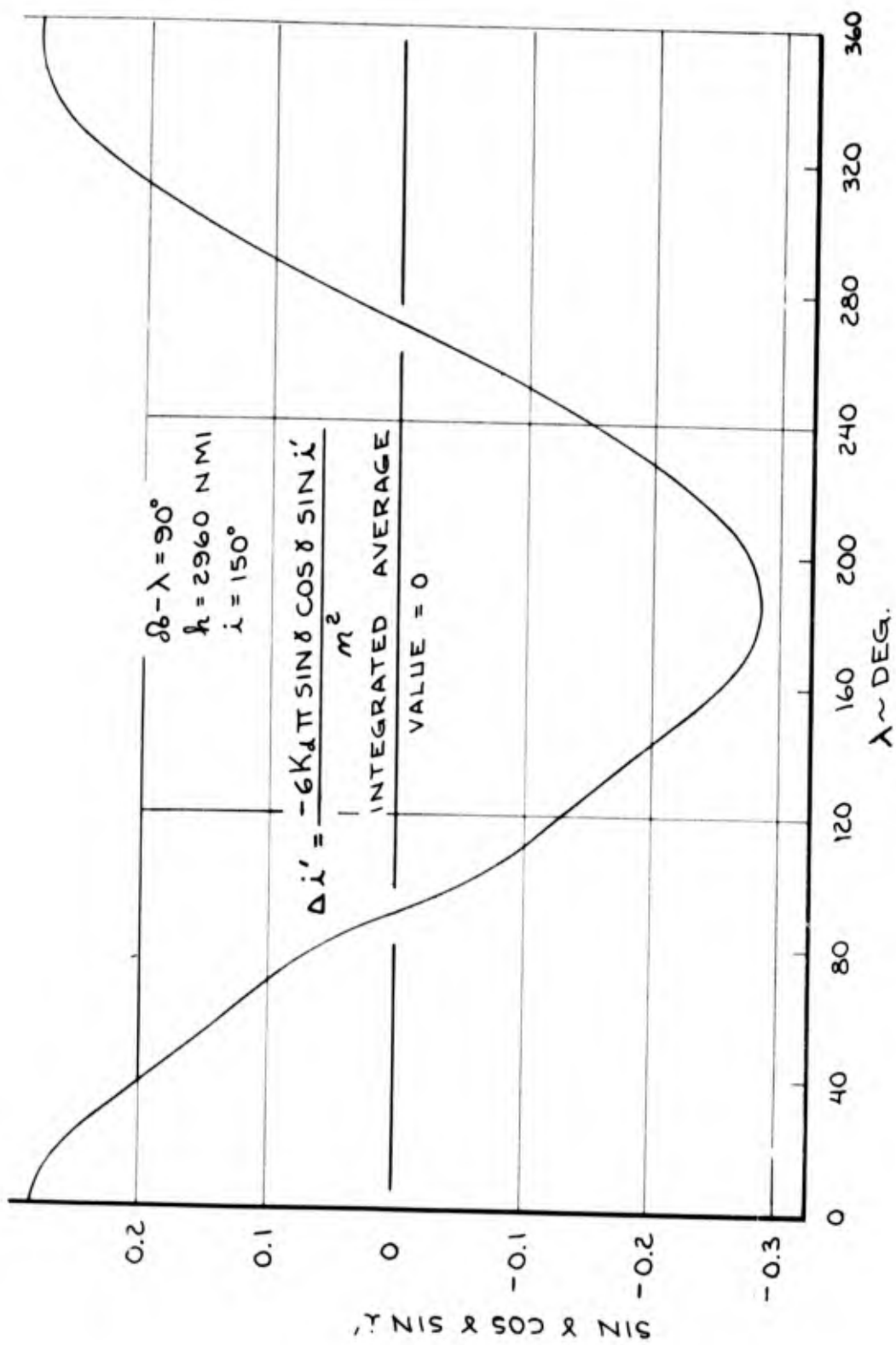
-57-

Figure 24. The Function $(\sin \gamma \cos \gamma \sin i')$ for the Sun versus Celestial Longitude
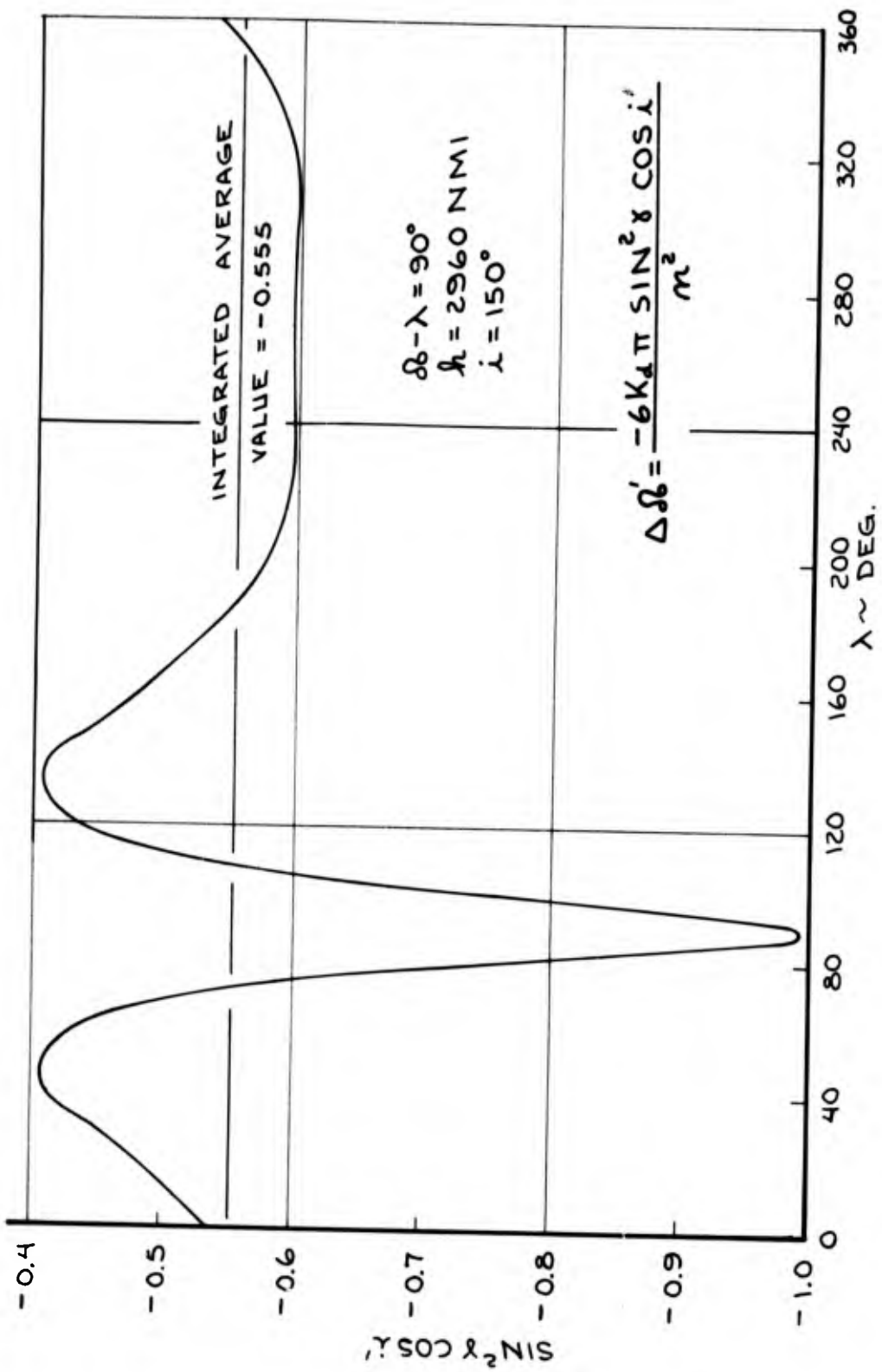
Figure 25. The Function $(\sin^2 \gamma \cos i')$ for the Sun versus Celestial Longitude
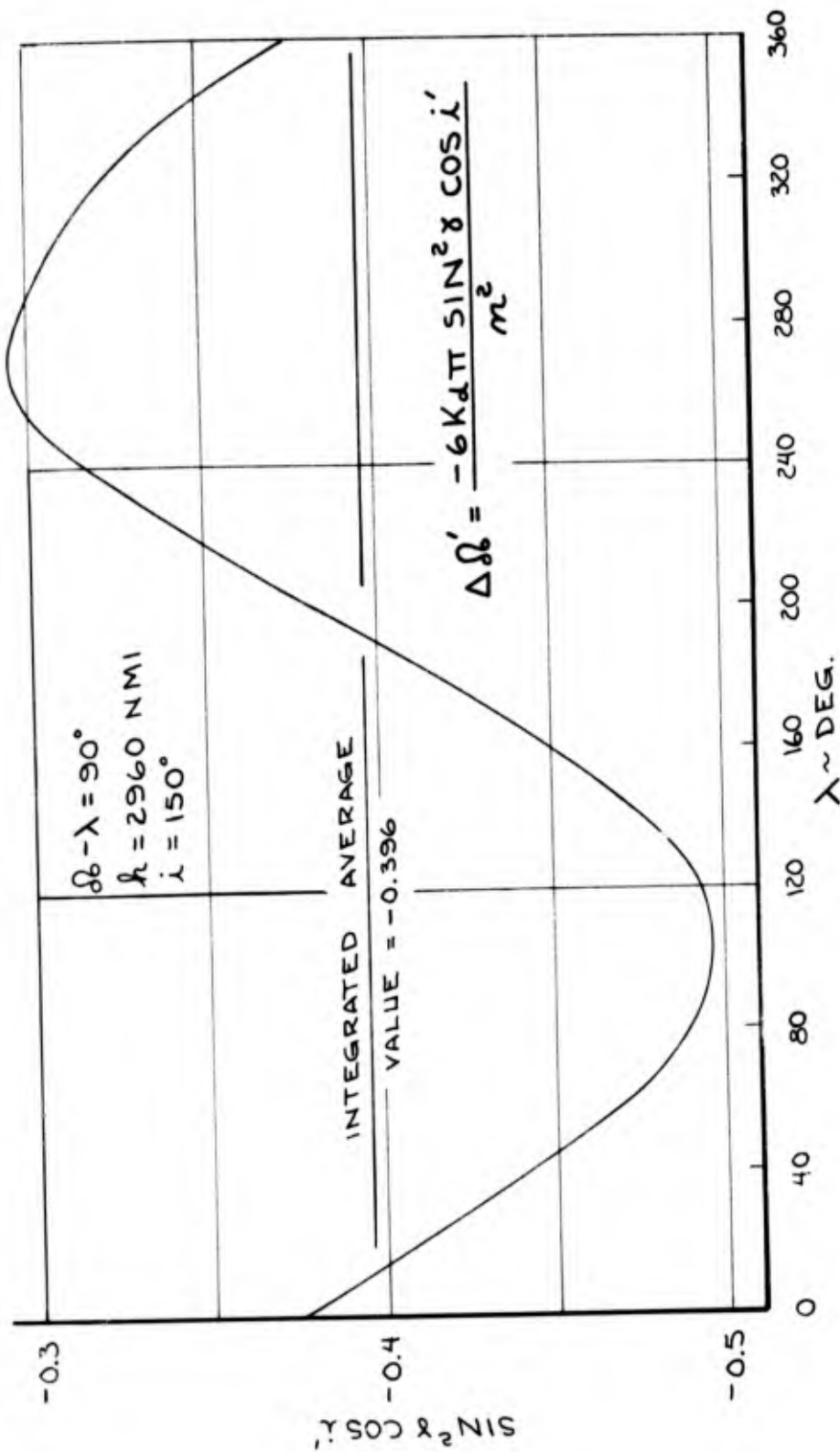
Figure 26. The Function $(\sin^2 \gamma \cos i')$ for the Moon versus Celestial Longitude

The combined perturbation on the node by the sun and moon is approximately
0.122 + 0.192 = 0.314 deg/yr. This increment accumulates year after year
but since the operational lifetime of most satellites is no more than a few
years, the accumulation will not be much more than a degree. Since the
effect of this accumulation on the eclipse fraction is insignificant, no velocity
compensation determinations will be made.

8. OTHER EFFECTS

8.1 INJECTION ERRORS

Satellite injection errors in h and i will produce deviations in $\dot{\Omega}$ from the sun-synchronous rate. The deviation in $\dot{\Omega}$ may be expressed

$$\Delta\dot{\Omega} = \frac{\partial\dot{\Omega}}{\partial i} \Delta i + \frac{\partial\dot{\Omega}}{\partial h} \Delta h \tag{58}$$

The partial derivatives are obtained by differentiating Equation (13),

$$\frac{\partial\dot{\Omega}}{\partial i} = +9.9608\left(\frac{R}{R+h}\right)^{3.5} \sin i = -\dot{\Omega} \tan i \tag{59}$$

$$\frac{\partial\dot{\Omega}}{\partial h} = -\frac{3.5\,\dot{\Omega}}{R+h} \tag{60}$$

Equations (59) and (60) are graphically presented in Figures 27 and 28, respectively.

In order to ascertain the effects of injection errors, consider the following example. Assume the nominal orbit to be sun-synchronous at h = 400 n mi and i = 98.°36. From Figures 27 and 28, $\Delta\dot{\Omega}$ = 0.1175 Δi - 0.000 898 Δh. If Δi = +0.°1, $\Delta\dot{\Omega}$ = +0.01175 deg/day or if Δh = +10 n mi, $\Delta\dot{\Omega}$ = -0.00898 deg/day. Since $\Delta\dot{\Omega}$ is a constant, unless there are changes in h and/or i, the difference between Ω and λ will increase or decrease linearly with time; Figure 29 depicts $(\Omega - \lambda) - (\Omega - \lambda)_{t=0}$ as a function of time for the following injection errors: Δh(n mi) = +10, +20, +30, -10, -20 and -30; Δi(deg) = +0.1, +0.2, +0.3, -0.1, -0.2 and -0.3. Figures 30 and 31 depict the same parameters for the same injection errors but for altitudes of 1400 n mi and 2400 n mi, respectively. Because $\partial\dot{\Omega}/\partial i$ decreases more rapidly with increasing h than does $\partial\dot{\Omega}/\partial h$, the injection error, Δi = ±0.°3 , which produces the greatest deviations in $(\Omega - \lambda) - (\Omega - \lambda)_{t=0}$ at h = 400 n mi, is replaced by Δh = ±30 n mi at both h = 1400 n mi and h = 2400 n mi.
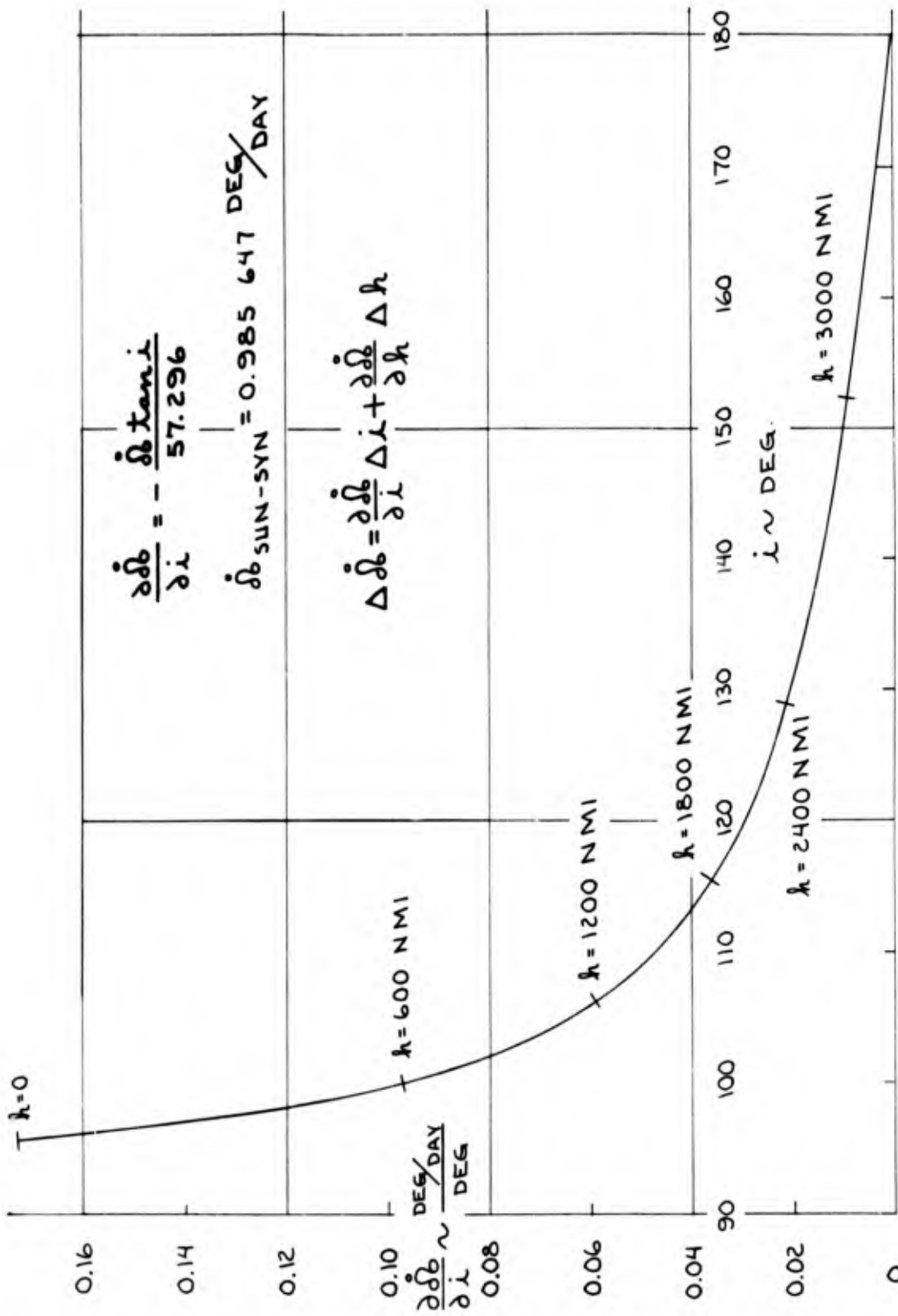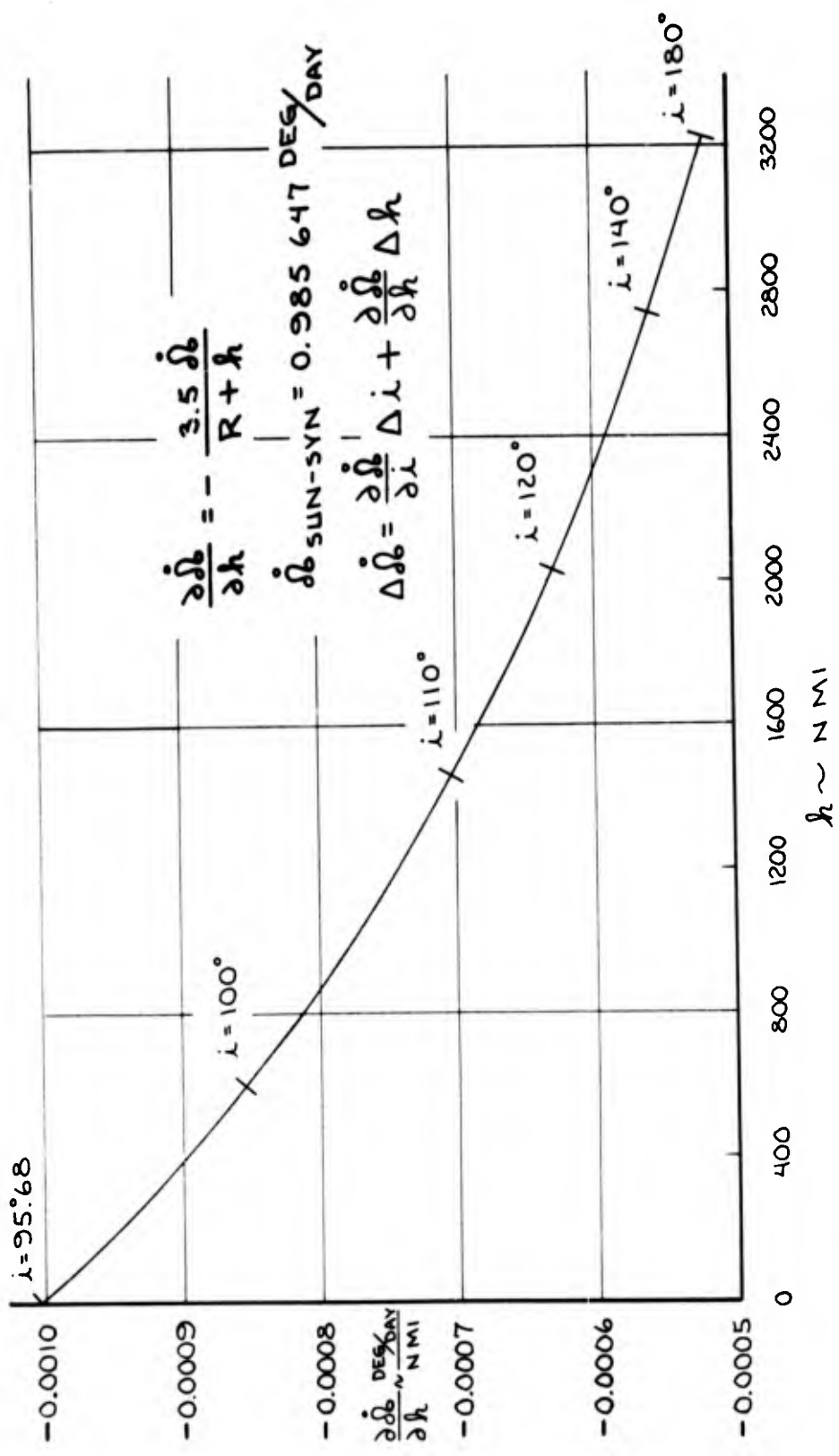
Figure 27. Inclination Error Coefficient
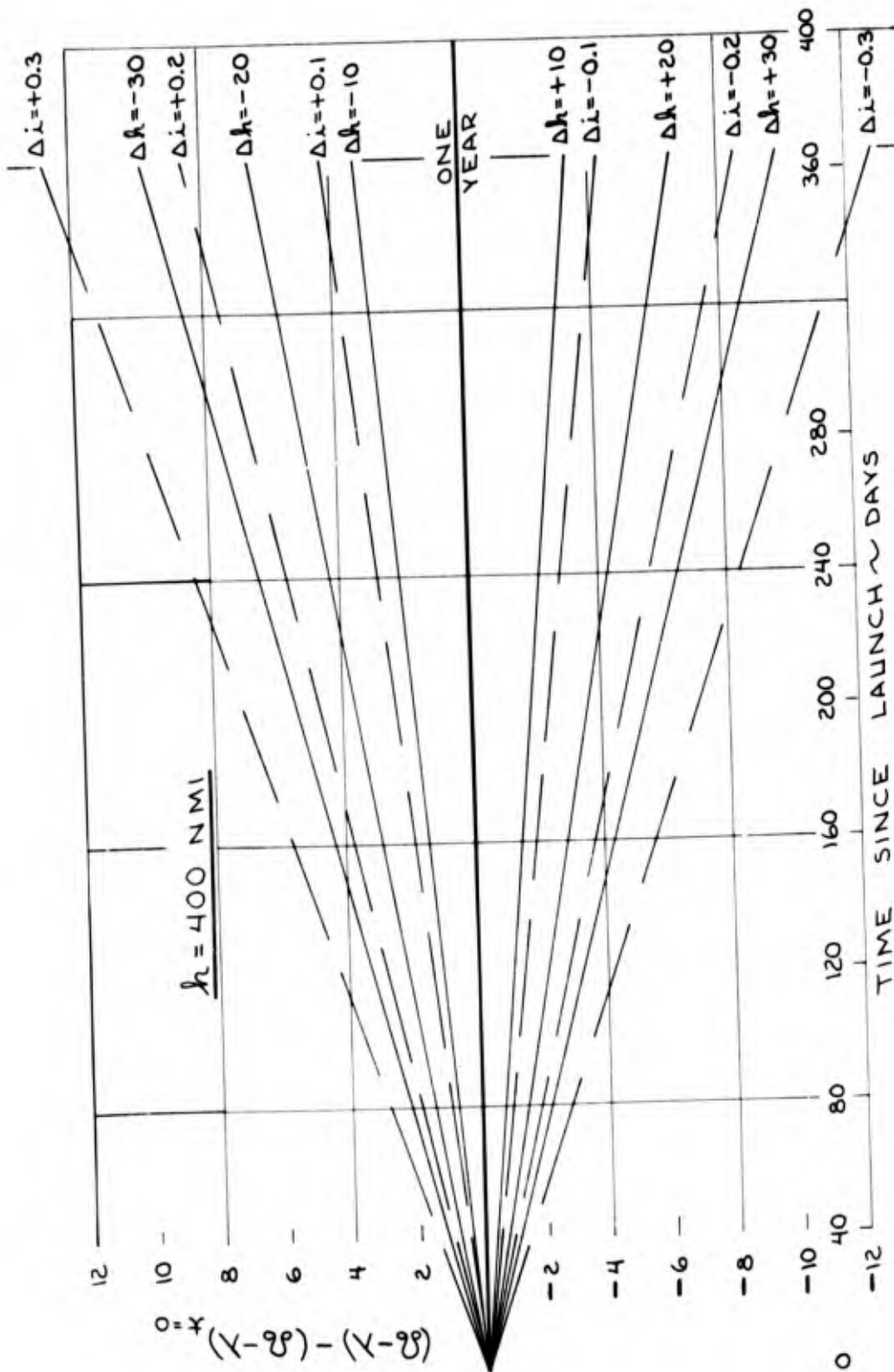
Figure 28   Altitude Error Coefficient

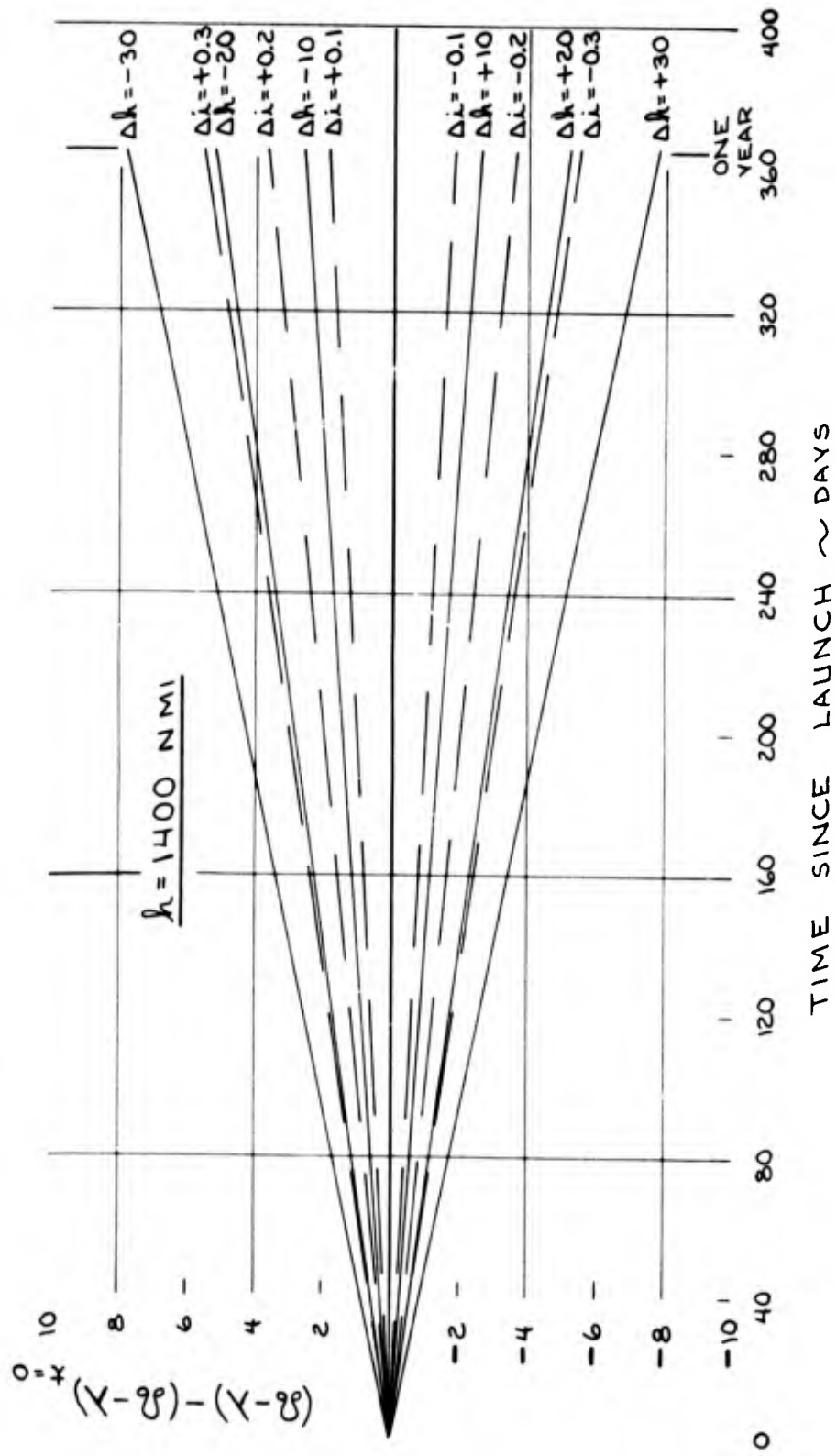Figure 29. Effect of Injection Errors on $(\Omega - \lambda)$ as a Function of Time

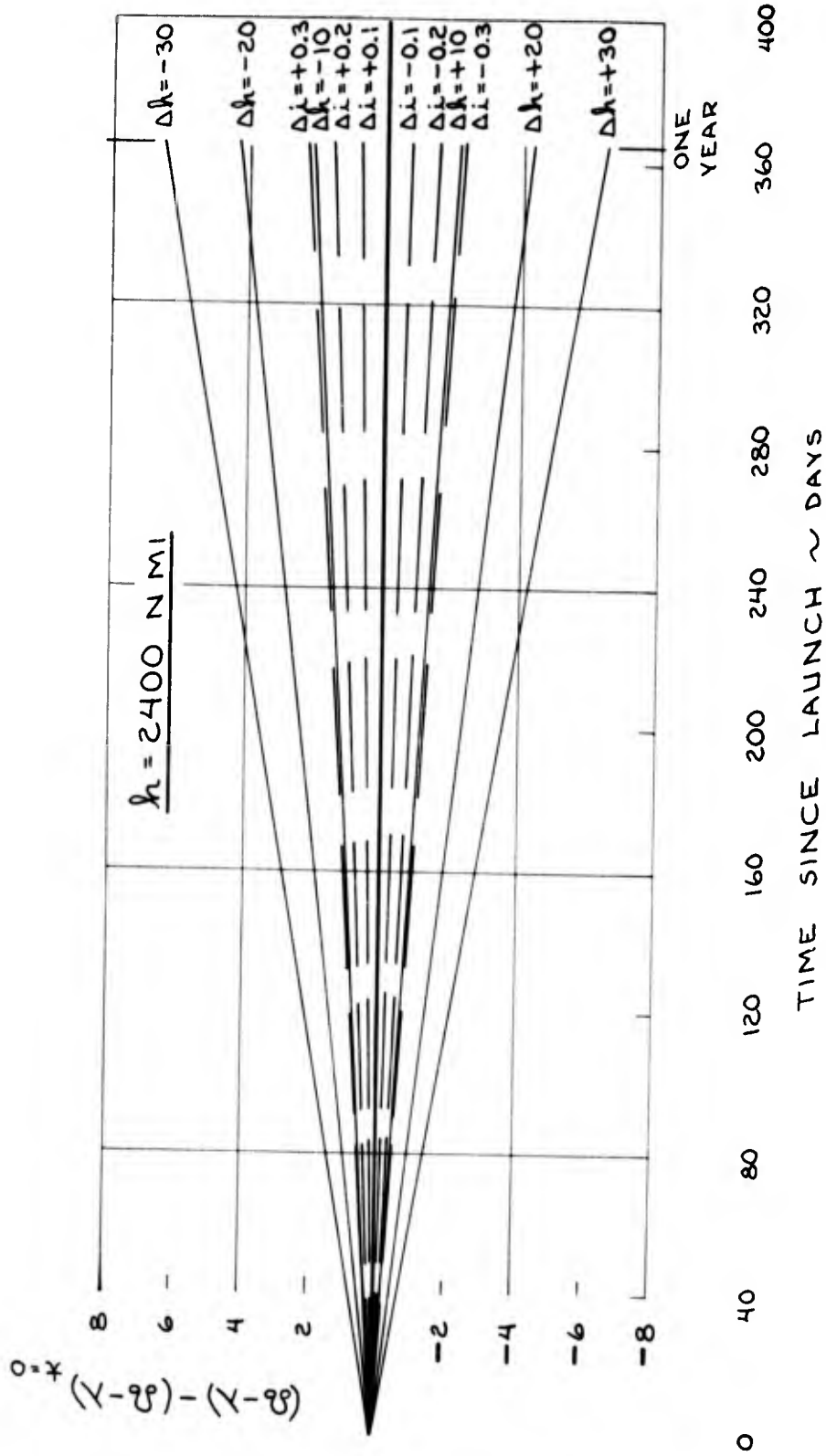Figure 30. Effect of Injection Errors on $(\Omega - \lambda)$ as a Function of Time

Figure 31. Effect of Injection Errors on $(\Omega - \lambda)$ as a Function of Time

The effect of injection errors on the eclipse fraction may be illustrated by the following three examples. In each example $(\Omega - \lambda)_{t=0} = 90°$ and combined injection errors of $\Delta h = -30$ n mi and $\Delta i = +0.°3$ will be assumed. The f versus λ history for the first example, h = 400 n mi, is presented in Figure 32. At $\lambda = 90°$ (t = 0), f for the misinjected orbit is 0.200 while f for the nominal orbit is 0.181. At $\lambda = 450°$, one year later, f for the misinjected orbit is 0.263. The relatively large difference between 0.263 and 0.200 is due to the deviation in $\Omega - \lambda$ after one year. From Figure 29 this deviation is seen to be 9.°8 for $\Delta h = -30$ n mi and 12.°8 for $\Delta i = +0.°3$ for a total of 22.°6.

For the second example, h = 1400 n mi, f = 0 for the first year for both the nominal and misinjected orbits. Since $\Omega - \lambda = 90° + 7.°8 + 5.°5 = 103.°3$ (from Figure 30) for the misinjected orbit after one year, both orbits remain entirely within the noneclipsing window of Figure 12.

The f versus λ history for the third example, h = 2400 n mi, is shown in Figure 33. At $\lambda = 90°$ (t = 0), f for the misinjected orbit is 0.1391 while f for the nominal orbit is 0.1353. One year later f for the misinjected orbit is 0.1424. The relatively small difference between 0.1424 and 0.1391 is due to the deviation in $\Omega - \lambda$ which (from Figure 31) is found to be 8.°8.

8.2   OBLATE GEOMETRY OF THE EARTH

In the analysis to this point the earth has been assumed spherical in shape with radius equal to the equatorial radius of the oblate earth, i.e. $R = R_E = 3443.93$ n mi. The oblate geometry and the spherical geometry at the summer solstice are pictured in Figure 34. Note that the orbit radius r which is tangent to the oblate earth shadow is less than the corresponding r for the spherical earth shadow. But note also that the earth's radius R is less than R_E. The effect of both decreasing and increasing the altitude for tangency appears to be a net decrease. If this is true the noneclipsing window of Figure 12 will increase in size.
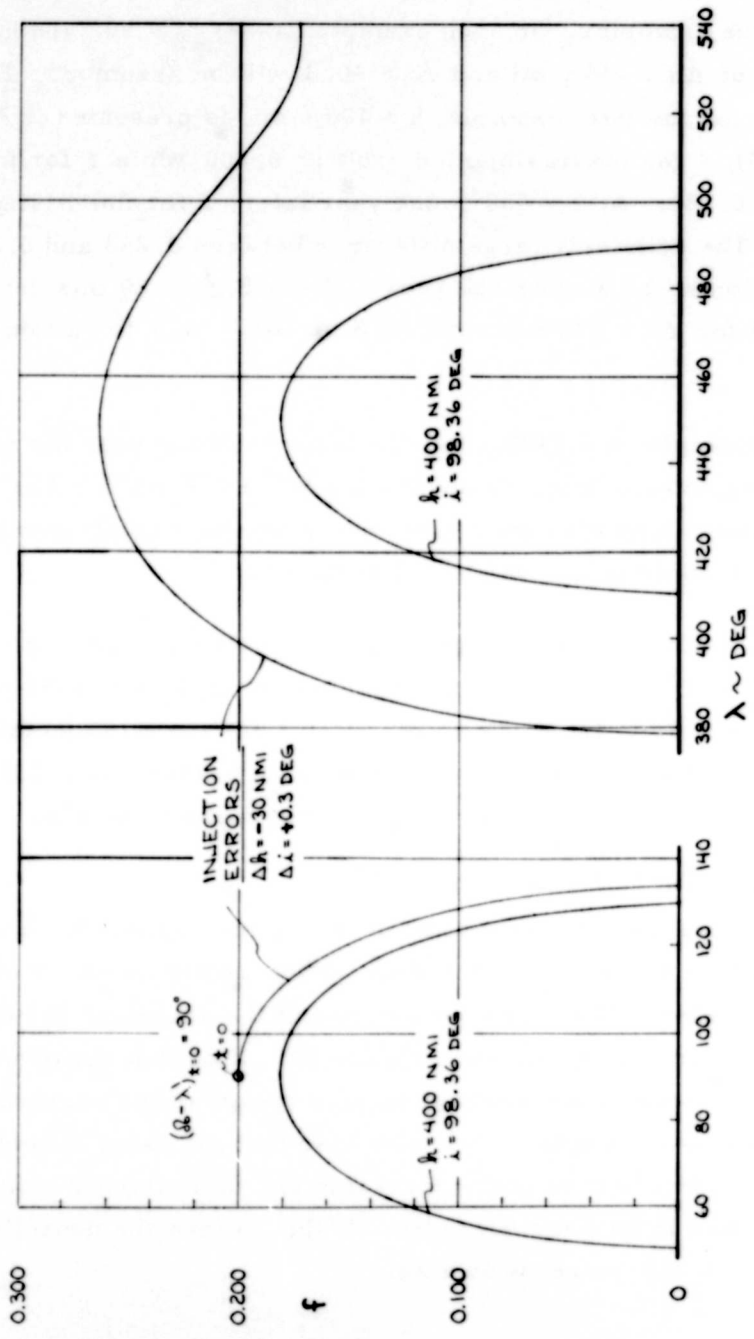
Figure 32. Effect of Injection Errors on Eclipse Fraction
as a Function of Celestial Longitude
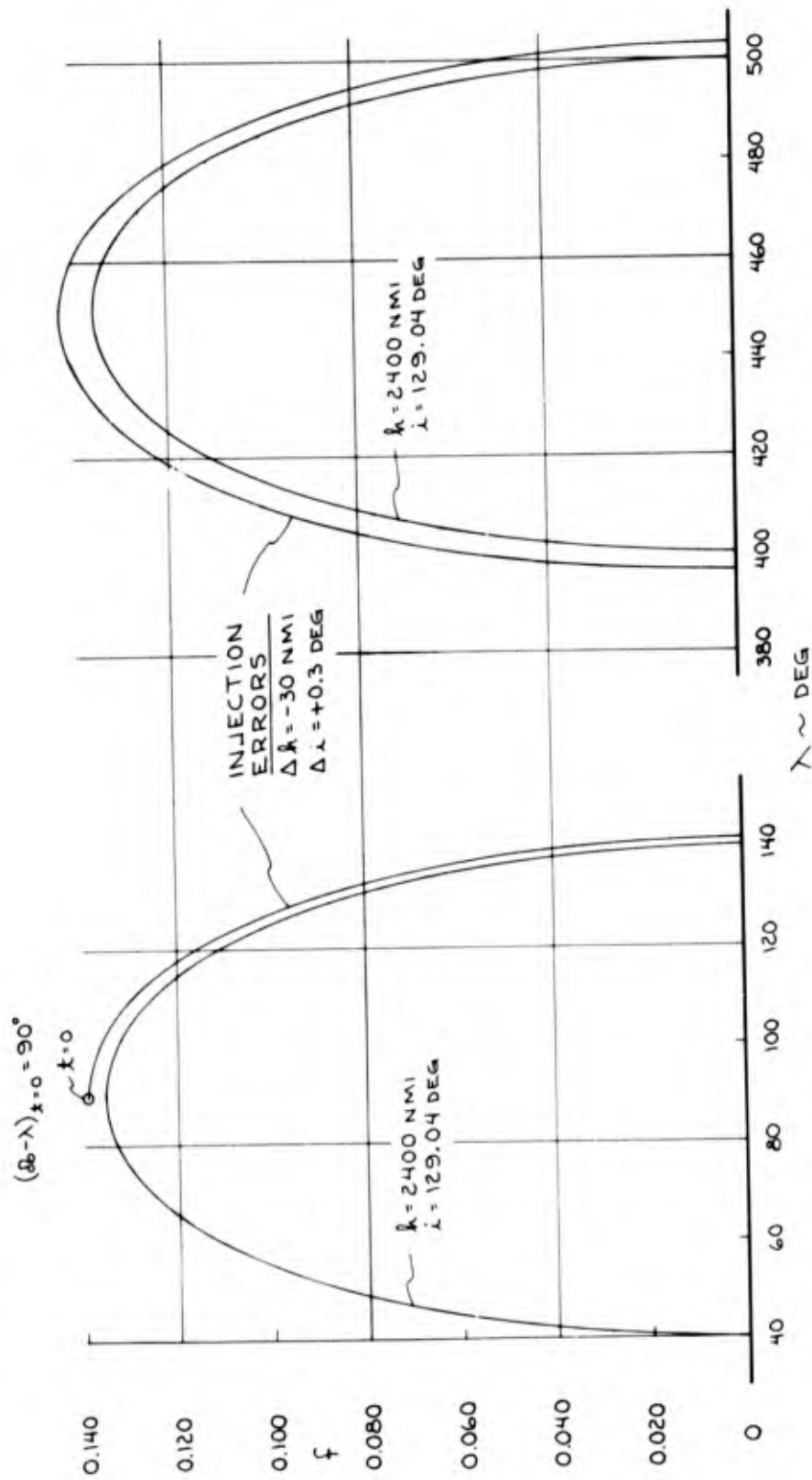
Figure 33. Effect of Injection Errors on Eclipse Fraction as a Function of Celestial Longitude

-71-

SUMMER SOLSTICE
$\lambda = 90°$
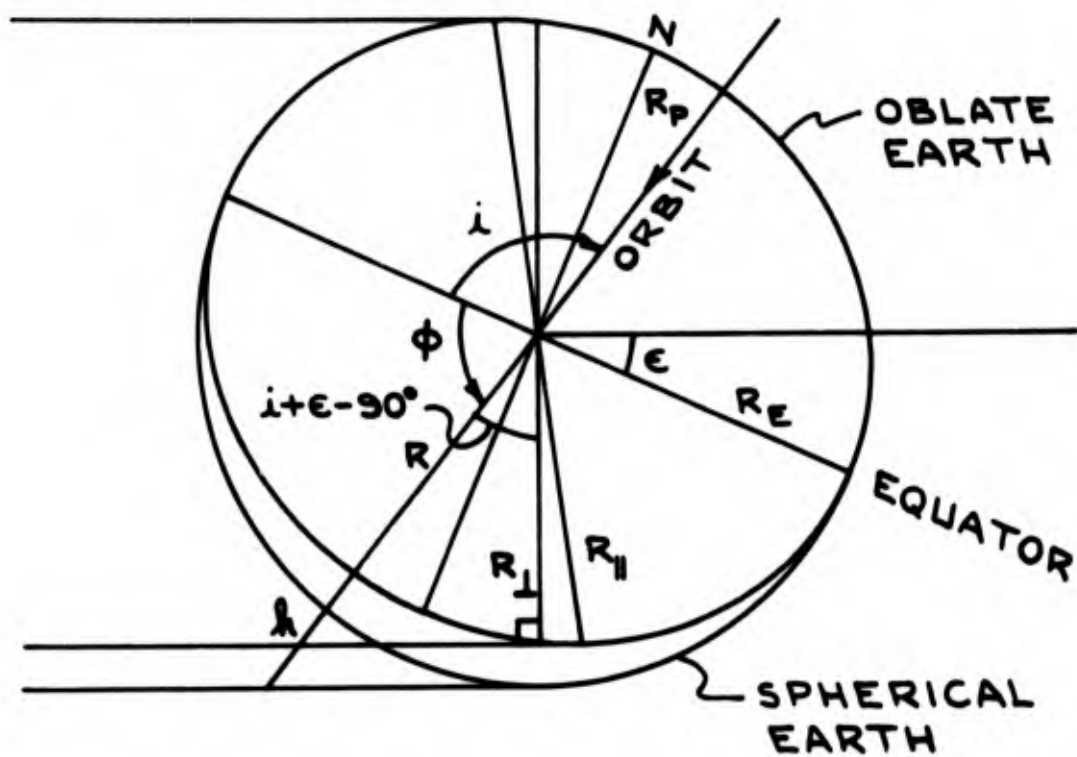
Figure 34. Oblate Earth Geometry

The unfamiliar symbols of Figure 34 are defined as follows. The radius of the oblate earth (R) is given by

$$R = R_E(1 - f \sin^2 \phi) \tag{61}$$

where

    f = the flattening defined by

$$f \triangleq \frac{R_E - R_P}{R_E} = \frac{11.545 \text{ n mi}}{3443.93 \text{ n mi}} = \frac{1}{298.30}$$

    R_P = the polar radius of the oblate earth

    ϕ = latitude

Equation (61) describes an ellipse. The radius $R_\perp$ is the perpendicular distance in the plane of Figure 34 from the earth's cei   to the boundary of the shadow. The radius $R_{||}$ is the radius of the earth at the point where the slope of the earth's surface is parallel to the sun line.

When the oblate geometry is considered, the nodal regression rate must be determined from the generalized form of Equation (13)

$$\dot{\Omega} = -9.960\ 795 \left(\frac{R_E}{\bar{r}} \right)^{3.5} \cos i \tag{62}$$

where $\bar{r}$ is an average orbit radius. Since the orbits are assumed to remain circular, $\bar{r} = r = R + h =$ constant. From Figure 34,

$$\sin(i + \epsilon) = \frac{R_\perp}{R + h} = \frac{R_\perp}{\bar{r}} \tag{63}$$

Equation (63) cannot be substituted into Equation (62) until $R_\perp$ has been described in terms of R_E.

The slope of an ellipse is dy/dx where $y = R \sin \phi$ and $x = R \cos \phi$,

$$\frac{dy}{dx} = \frac{R \cos \phi \, d\phi - 2 f R_E \sin^2 \phi \cos \phi \, d\phi}{-R \sin \phi \, d\phi - 2 f R_E \sin \phi \cos^2 \phi \, d\phi} \tag{64}$$

Substituting for R from Equation (61) and canceling,

$$\frac{dy}{dx} = - \frac{\cos \phi - 3f \sin^2 \phi \cos \phi}{\sin \phi - f \sin^3 \phi + 2f \sin \phi \cos^2 \phi} \tag{65}$$

The latitude corresponding to $R_\perp$ is $\phi = -90° + \epsilon = -66°56$ for which $dy/dx = 0.43074$ and $\tan^{-1} dy/dx = 23°30$. It will now be assumed that the angle between $R_\perp$ and $R_{||}$ is the difference in the arc tangents of their slopes (i.e., $23°44 - 23°30 = 0°14$). Thus, the ϕ corresponding to $R_{||}$ is $-66°56 + 0°14 = -66°42$ and

$$R_\perp = R_{||} \cos 0°14 = R_E \left[1 - f \sin^2 (-66°42) \right] \cos 0°14 = 0.99718 \, R_E \tag{66}$$

Substituting Equation (66) into Equation (63),

$$\sin(i + \epsilon) = \frac{0.99718 \, R_E}{\bar{r}}$$

or

$$\frac{R_E}{\bar{r}} = 1.00282 \sin(i + \epsilon) \tag{67}$$

Substituting Equation (67) into Equation (62) where $\dot{\Omega} = \dot{\lambda} = 0.985\ 647$ deg/day

$$\sin^{3.5}(i + \epsilon) \cos i = -0.097\ 980\ 9 \tag{68}$$

-74-

Equation (68) yields double roots, $i = 101°.17$ and $i = 115°.76$, which correspond to $h = 740.2$ n mi and $h = 1821.6$ n mi, respectively. Thus, as Figure 35 indicates, the oblate geometry of the earth does slightly increase the non-eclipsing window.

8.3 ATMOSPHERIC REFRACTION

The sun's rays which pass near the surface of the earth are influenced by atmospheric refraction. The amount of refraction depends on the density of the atmosphere through which the rays pass and on the altitude (angular elevation above the horizon) of the sun. Since the rays are bent toward the regions of greater density, the sun's rays which are on the horizon will curve around the earth's surface and illuminate a portion of the region which was formerly thought to be eclipsed. This effect is depicted in Figure 36. Russell, et al, (Reference 7) state that under average atmospheric conditions sunlight on the horizon will bend approximately 35 min of the arc relative to an observer on the earth's surface. The refraction relative to an observer behind the earth and beyond the atmosphere will be twice this amount, or approximately 70 min of arc.

The radius R' (see Figure 36) is perpendicular to the light ray which has been bent 70 min $= 1°.17$ after passing through the atmosphere near the earth's surface. The latitude (ϕ) corresponding to R' is $\phi = -66°.42 - 1°.17 = -67°.59$ (see Section 8.2, OBLATE GEOMETRY) and

$$R' = R_E\left[1 - f\sin^2(-67°.59)\right] = 0.997\ 14\ R_E \qquad (69)$$

For $\phi = -67°.59$, dy/dx from Equation (65) is 0.40977 and $\tan^{-1}$ dy/dx $= 22°.28$. Thus, $\psi = 67°.59 + 22°.28 = 89°.87$ and $\alpha = 180° - (i + \epsilon - 1°.16)$. From the law of sines,

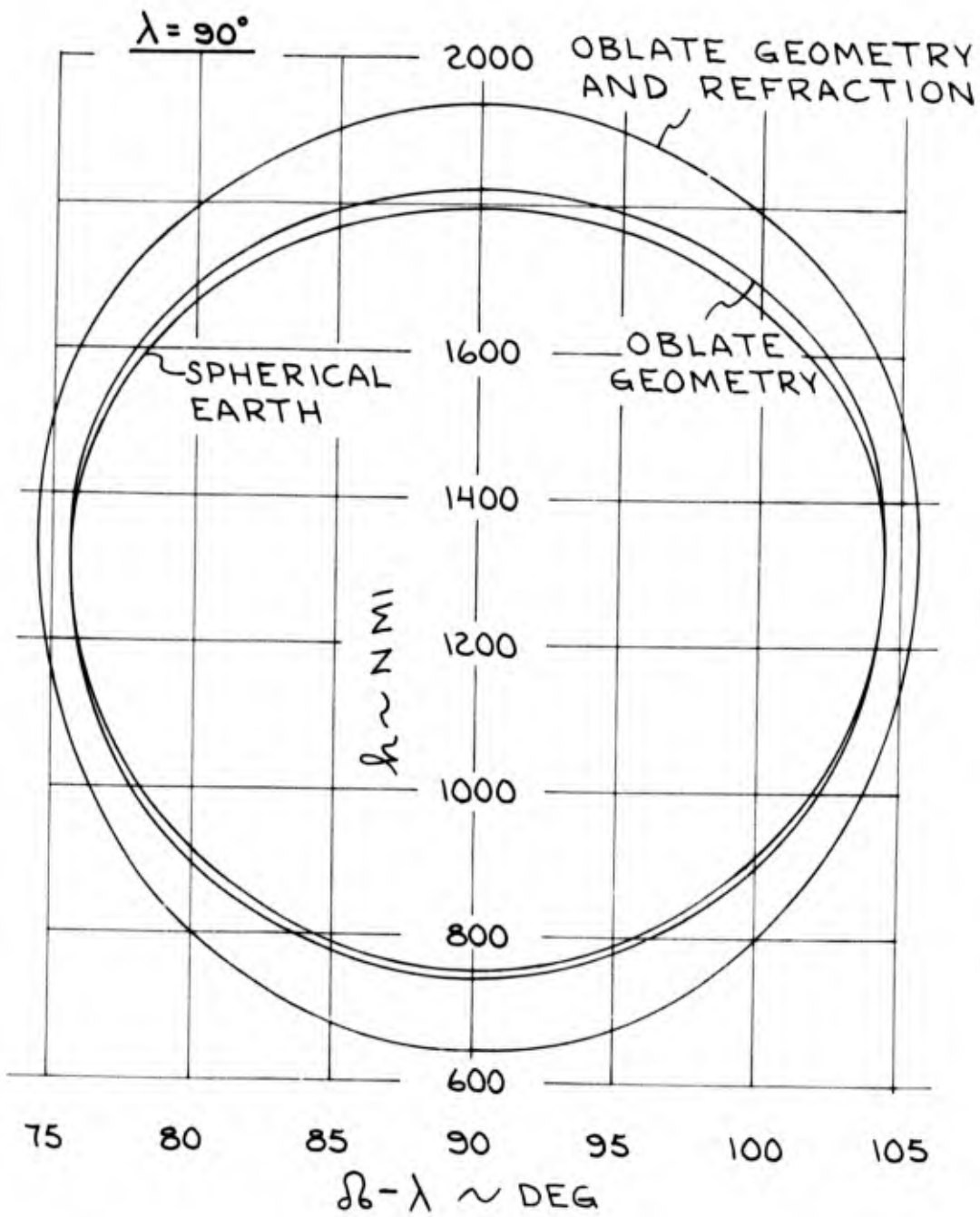$$\frac{\bar{r}}{\sin\psi} = \frac{R'}{\sin\alpha} \qquad (70)$$

Figure 35.   Oblate Earth Geometry and Atmospheric Refraction
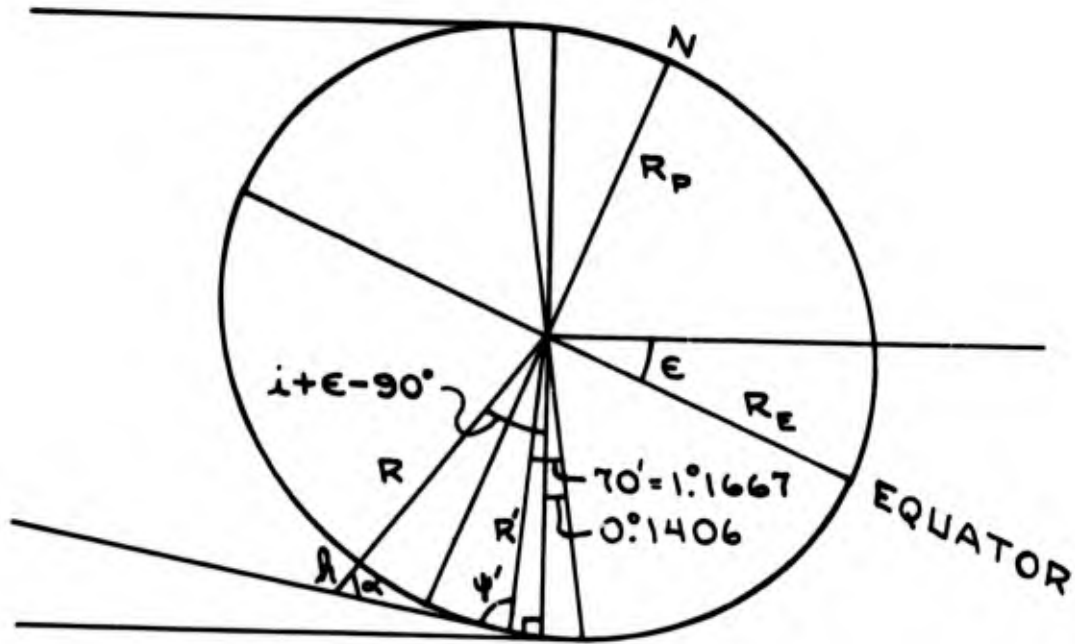Effects on the Noneclipsing Window

SUMMER SOLSTICE
$\lambda = 90°$

Figure 36. Atmospheric Refraction

By substituting R', ψ and α into Equation (70),

$$\frac{R_E}{\bar{r}} = 1.002\ 88 \left[0.99979\ \sin(i + \epsilon) - 0.02028\ \cos(i + \epsilon)\right] \tag{71}$$

By substituting Equation (71) into Equation (62) where $\dot{\Omega} - \dot{\lambda} = 0.985\ 647$ deg/day,

$$\left[0.99979\ \sin(i + \epsilon) - 0.02028\ \cos(i + \epsilon)\right]^{3.5} \cos i = -0.097\ 963\ 1 \tag{72}$$

Equation (72) yields double roots ($i = 100\overset{\circ}{.}26$ and $i = 117\overset{\circ}{.}99$) which correspond to $h = 640.8$ n mi and $h = 1938.0$ n mi, respectively.

As these solutions indicate, atmospheric refraction increases the size of the noneclipsing window. Figure 35 presents the noneclipsing window for combined oblate geometry and refraction.

8.4 ECCENTRICITY OF THE EARTH'S ORBIT

The analysis, to this point, has assumed that $\dot{\lambda}$, the rate of revolution of the earth about the sun, is constant and equal to the mean rate, 0.985 647 deg/day. Actually, the eccentricity, $e = 0.0167$, of the earth's orbit causes $\dot{\lambda}$ to vary sinusoidally about the mean rate. This variation will cause λ to vary sinusoidally about the value given by the mean rate, $\lambda = \dot{\lambda}_{mean}t$.

When referenced to perihelion, the variation in λ from that given by the mean rate is the same as the difference between true anomaly (v) and mean anomaly (M). This difference is given by Moulton (Reference 6) as,

$$v - M = 2e\ \sin M + \frac{5}{4}\ e^2 \sin 2M + 0(e^3) \tag{73}$$

Equation (73) is graphically presented in Figure 37 (the short-dashed line) as a function of time for 1963 and 1964. Note that the variation is zero at every perihelion ($M = 0$) and aphelion ($M = 180°$) and reaches a maximum of
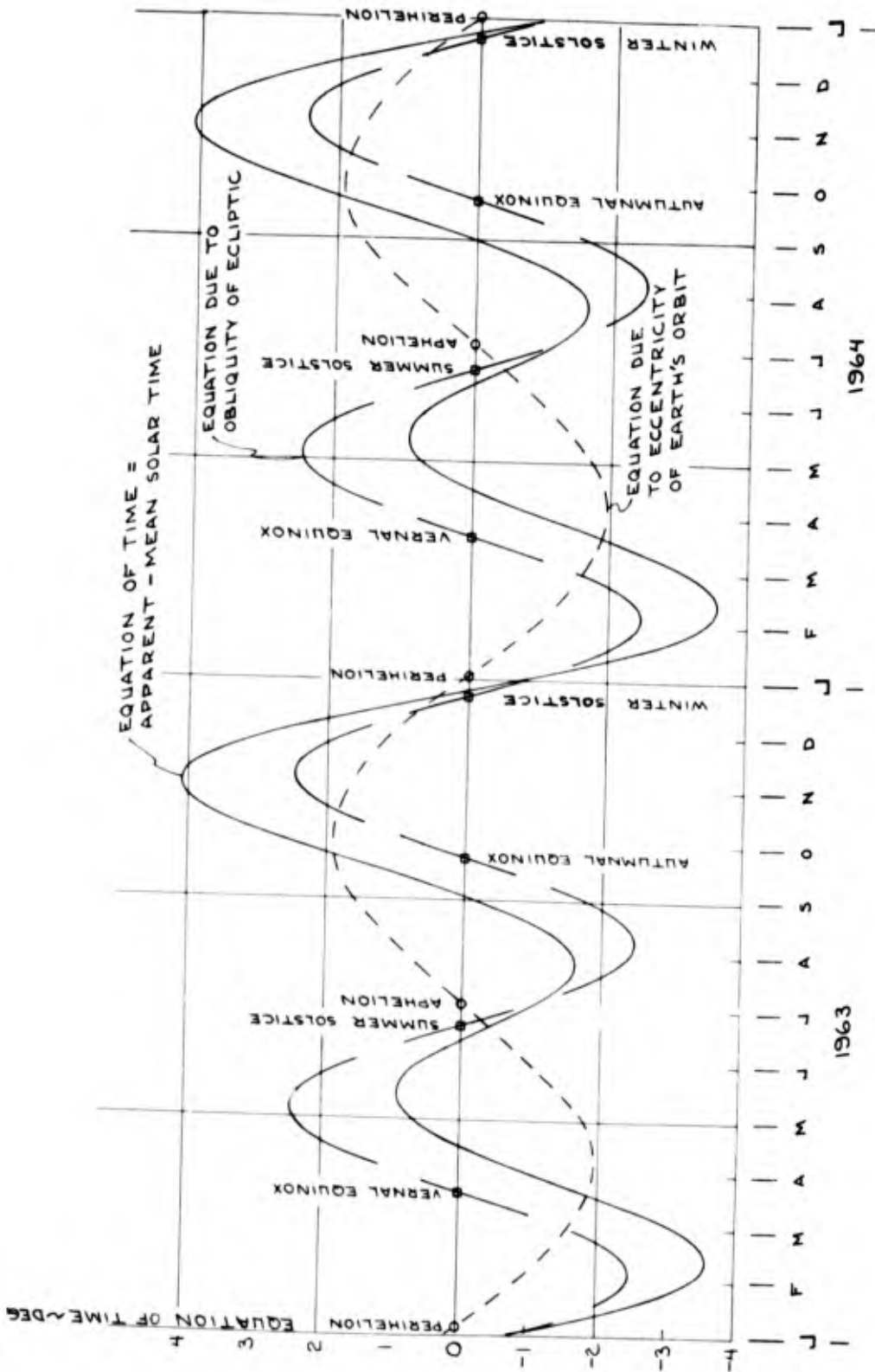
-78-

Figure 37. Variation in Celestial Longitude Due to the Eccentricity of the Earth's Orbit and the Obliquity of the Ecliptic

almost 2° early in April and about the first of October. The effect of this variation, even at its maximum, on the eclipse fraction is small.

The nodal-sun orientations which were schematically depicted in Figure 5 neglected both the eccentricity of the earth's orbit and the obliquity of the ecliptic, ϵ = 23°4441. However, the analysis of this paper has always considered the obliquity of the ecliptic. The effect of the obliquity of the ecliptic on the difference between apparent and mean solar time is shown for comparative purposes in Figure 37 by the long-dashed line. Note that the variation in λ due to ϵ is zero at the equinoxes and solstices and reaches a maximum of about 2°5 in the early portions of Februrary, May, August and November.

The combined effects of earth's orbit eccentricity and obliquity of the ecliptic produce the equation of time which is the difference between apparent and mean solar time. The equation of time is represented in Figure 37 by the solid line. The equation of time is zero four times a year; the middle of April, the middle of June, the first of September and the end of December. A maximum of about 4° is reached near the first of November.

8.5   ELLIPTICAL ORBITS

The analysis, to this point, has considered only circular orbits. The effects of orbit eccentricity, especially in the range $0 < e \leq 0.1$, on eclipse fractions are certainly of interest. Cunningham (Reference 8) presents eclipse fractions for elliptical satellite orbits. His technical note tabulates eclipse fraction as a function of perigee altitude, apogee altitude, δ (the angle between the orbit plane and the solar vector) and β (the angle between the line of apsides and the projection of the solar vector onto the orbit plane).

Table 1 presents eclipse fractions from Reference 8 as a function of β for two values of eccentricity ($e \approx 0.1$ and $e \approx 0.4$) and two values of δ ($\delta = 20°$ and $\delta = 50°$). Also noted are perigee altitude, apogee altitude, $\bar{h}$ (the average altitude) and f_{ave} (the eclipsed fraction averaged over all values of β). Another

-80-

Table 1. Eclipse Fractions for Elliptical Orbits

$e \approx 0.1$ $\bar{h} = 900$ km
$h_P = 200$ km, $h_A = 1600$ km

$e \approx 0.4$ $\bar{h} = 4600$ km
$h_P = 200$ km, $h_A = 9000$ km

$f_{circle} = 0.329$	$\delta = 20°$		$f_{circle} = 0.166$	$\delta = 20°$
$\beta = 0°$	$f = 0.352$		$\beta = 0°$	0.182
20°	0.352		20°	0.190
40°	0.350		40°	0.198
60°	0.347		60°	0.196
80°	0.342		80°	0.187
$f_{ave} = 0.334$ 100°	0.335		$f_{ave} = 0.169$ 100°	0.172
120°	0.325		120°	0.156
140°	0.317		140°	0.143
160°	0.311		160°	0.135
180°	0.309		180°	0.133

$f_{circle} = 0.230$	$\delta = 50°$		$f_{circle} = 0$	$\delta = 50°$
$\beta = 0°$	0.153		$\beta = 0°$	0.000
20°	0.165		20°	0.000
40°	0.192		40°	0.000
60°	0.222		60°	0.000
80°	0.246		80°	0.000
$f_{ave} = 0.229$ 100°	0.260		$f_{ave} = 0.041$ 100°	0.000
120°	0.264		120°	0.099
140°	0.263		140°	0.103
160°	0.262		160°	0.103
180°	0.261		180°	0.103

parameter f_{circle} (the eclipse fraction corresponding to a circular orbit at altitude $\bar{h}$ and to the appropriate δ) is presented for comparison with f_{ave}. For the four cases examined in Table 1, the values of f_{circle} are nearly equal to their corresponding values of f_{ave}. In addition, except for the high e, high δ case the dispersions in f from the average are not large. Thus, the additional complexity of elliptical orbits (two more parameters) and the relatively small differences in f values between circular orbits and elliptical orbits of moderate eccentricity are deemed sufficient reasons for not separately considering elliptical orbits.

8.6 EFFECTS OF MINOR SIGNIFICANCE

Effects due to a sun not at infinity which would produce umbra-penumbra cones whose elements would deviate from a cylinder by approximately 16 minutes of arc and effects due to the oblate potential of the earth which could produce deviations from a circular orbit as large as ±0.9 n mi were judged to be of minor significance to the eclipse fraction and, thus, were not fully investigated.

-82-

9. COMPARISONS WITH OTHER AUTHORS

In the past other authors have investigated eclipse fractions for earth satellites. It is the intent of this section to compare the analyses and results of these authors with the analysis and results of this paper.

Patterson (Reference 9) was perhaps the first to publish a method for calculating the percentage time which a satellite in a circular orbit spends in sunlight (1 - eclipse fraction). This time is determined as a function of h, i and two earth-sun-orbit orientation angles. A spherical earth and a cylindrical shadow are assumed. Pierce, in a subsequent paper (Reference 10) expresses Patterson's equations in terms of h, i, Ω, α (right ascension of the sun) and δ (declination of the sun) in order to present a convenient graphical method for determining the eclipse fraction.

Cunningham (Reference 8) adds complexity and value to his paper by examining elliptical orbits. His technical note tabulates eclipse fraction as a function of perigee altitude, apogee altitude and two orientation angles, δ and β. Section 8.5 of this paper compares Cunningham's elliptical orbit eclipse fractions with circular orbit eclipse fractions for corresponding values of $\bar{h}$ (average altitude).

Escobal (Reference 11) derives equations which yield eclipse times for elliptical orbits. In addition, umbra and penumbra deviations from the basic cylindrical shadow are developed. He also presents a correction for the geometrical flattening of the earth although the analysis is restricted to Keplerian orbits.

The four papers briefly described above have some common characteristics. They all obtain equations, with varying degrees of sophistication, for the eclipse fraction. Escobal's development is the most sophisticated. Two of the authors present eclipse fraction (Pierce graphically and Cunningham tabularly) as a function of altitude, inclination and orientation angles. None

of the authors, except Patterson, and he with only one example, describe
an eclipse fraction time history for a given orbit. Any point on such a time
history for a circular orbit may, of course, be determined from any of the
four papers. In fact various points on Figures 9 and 10 of this report were
checked with results from Pierce and Cunningham and the agreement was
very good. Since the authors were point oriented rather than orbit oriented,
none of them considered sun-synchronism and/or orbit perturbations.

Murrell (Reference 12) does describe a few eclipse time histories. However,
he restricts his investigation to circular, _equatorial_ orbits. Since all of
Murrell's time histories are at altitudes above those considered in this paper,
two machine runs at h = 8000 statute miles and h = 22,300 statute miles (24-
hour orbit) were made for comparative purposes. The computer program
described in Section 2 was used. Complete agreement with his results was
found.

Since eclipse fractions at higher altitudes are probably of general interest,
Figure 38 presents $\bar{f}$ versus h to h = 21,000 n mi. Curves for equatorial
orbits, polar, $(\Omega - \lambda)_{initial} = 90°$ orbits and $\bar{f}_{max}$ are displayed.

Hanson and Fairweather (Reference 13) consider satellite eclipsing and
examine the possibility of noneclipsed sun-synchronous orbits. They cor-
rectly determine in a manner similar to Section 4 of this report the most
critical time of year to be the summer solstice. However, their criteria
for noneclipsing (displayed in Figure 8 of Reference 13) are apparently in-
correct. They display the sun-synchronous orbit inclination versus the
"minimum" orbit inclination which is obtained from $R/(R + h) = \sin(i_{min} + \epsilon)$.
They then claim that the noneclipsed orbits are those for which $i_{min} > i_{sun-syn}$.
This procedure is valid but their figure indicates a noneclipsed region which
is far too large. Their difficulty may stem from the fact that $i_{sun-syn}$ is
incorrectly found to lie between 0° and 90° and/or the fact that i_{min} is found
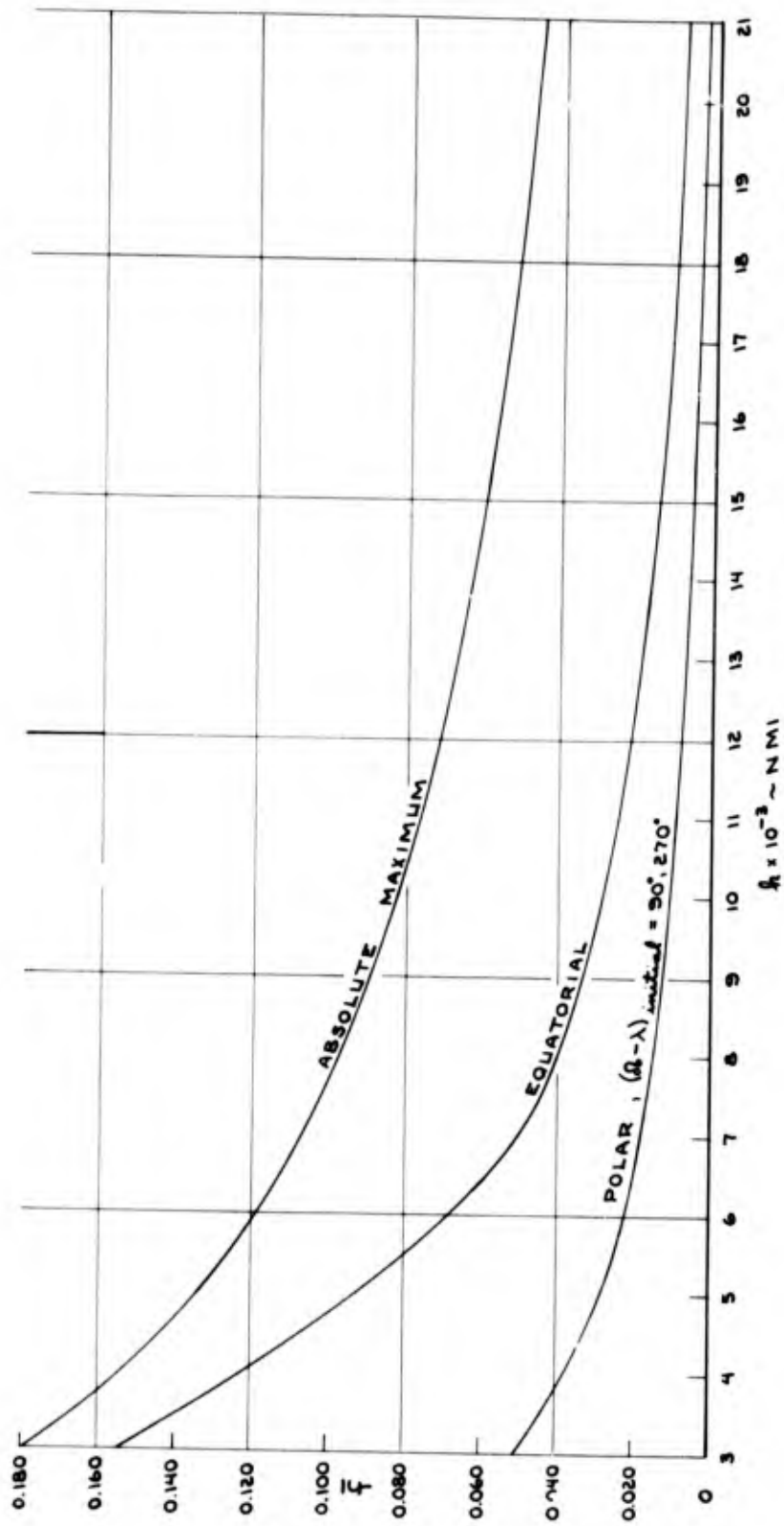to be "negative". Figure 39 of this report correctly displays their criteria.

-84-

Figure 38. Average Eclipse Fraction versus Altitude for Various Classes of Orbits

Figure 39.   Noneclipsing Criteria
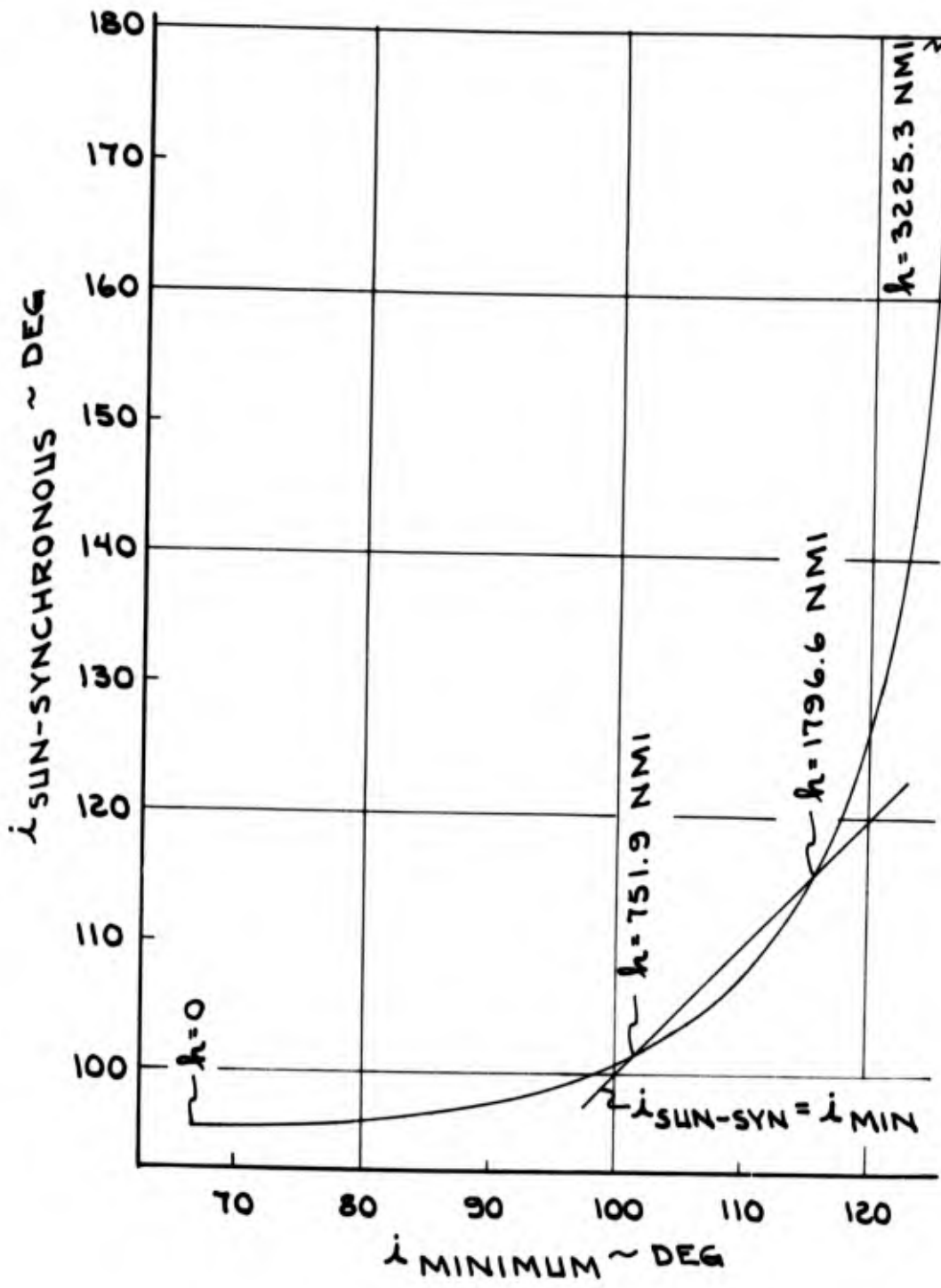
-86-

The region for which $i_{min} > i_{sun-syn}$ is correctly bounded by the points, $i = 101°.39$, $h = 751.9$ n mi and $i = 115°.47$, $h = 1796.6$ n mi, which were previously found in Section 4. Hanson and Fairweather do not consider non-sun-synchronous orbits, orbit perturbations, injection errors, oblate earth geometry, atmospheric refraction, etc. in their investigation.

REFERENCES

1. W. R. Bandeen, Earth Oblateness and Relative Sun Motion Considerations in the Determination of an Ideal Orbit for the Nimbus Meteorological Satellite, NASA TN D-1045, Goddard Space Flight Center, Greenbelt, Maryland (July 1961).

2. B. H. Billik. "Survey of Current Literature on Satellite Lifetimes," ARS Journal 32 (11), 1641-1650, (November 1962).

3. R. A. Minzner, K. S. W. Champion and H. L. Pond, "The ARDC Model Atmosphere, 1959," Air Force Surveys in Geophysics 115, AFCRC-TR-59-267, Air Force Cambridge Research Center, Air Research and Development Commission, USAF, Bedford, Massachusetts (August 1959).

4. R. W. Bruce, "Satellite Orbit Sustaining Techniques," ARS Journal 31 (9), 1237-1241 (September 1961).

5. M. M. Moe, "Solar-Lunar Perturbations of the Orbit of an Earth Satellite," ARS Journal 30 (5), 485-487 (May 1960).

6. F. R. Moulton, An Introduction to Celestial Mechanics, The Macmillian Co., New York (1914).

7. H. N. Russell, R. S. Dugan and J. Q. Stewart, Astronomy, I, The Solar System, Ginn and Company, Boston (1945).

8. F. G. Cunningham, Calculation of the Eclipse Factor for Elliptical Satellite Orbits, NASA TN D-1347, Goddard Space Flight Center, Greenbelt, Maryland (June 1962).

9. G. B. Patterson, "Graphical Method for Prediction of Time in Sunlight for a Circular Orbit," ARS Journal 31 (3), 441-442 (March 1961).

10. D. Pierce, "A Rapid Method for Determining the Percentage of a Circular Orbit in the Shadow of the Earth," The Journal of the Astronautical Sciences IX (3), (Fall 1962).

11. P. R. Escobal, "Orbital Entrance and Exit From the Shadow of the Earth," ARS Journal 32 (12), 1939-1941 (December 1962).

12. M. D. Murrell, "Time Per Orbit That Earth Satellites in Equatorial Orbits are in Earth's Shadow," Journal of the British Interplanetary Society 19 (2), 41-44 (March-April 1963).

13. J. N. Hanson, and S. H. Fairweather, "Nodal Rotation for Continuous Exposure of an Earth Satellite to the Sun," ARS Journal 31 (5), 640-645 (May 1961).

DISTRIBUTION

Internal

E.	Levin		D. R. S.	McColl
N. L.	Anderson		J. E.	Michaels
J. M.	Baker		A. H.	Milstead
B. L.	Beskind		M.	Nakamura
H.	Bernstein		J. M.	Nilles
B. H.	Billik		H. W.	Nordyke
R. W.	Bruce		F. M.	Perkins
C. K.	Cretcher		J. E.	Pierson
S.	Evans, Jr.		C. M.	Price
R. J.	Farrar		D. E.	Regan
T. P.	Gabbard		R. S.	Robins
E. A.	Goldberg		H. L.	Roth
R. C.	Gore		I. B.	Russak
A.	Grossman		C. W.	Sarture
A. S.	Gutman		R. W.	Slocum, Jr.
P. T.	Guttman		D. R.	Speece
N. S.	Hall		L. T.	Tedeschi
H. E.	Hogfors		J. C.	Travis
H. K.	Karrenberg		C. J.	Wang
A. S.	Lawin		D.	Willens
E.	Loft		AOCRC	
R. D.	Lüders			

External

Capt D. L. DeBus (SSD)
Lt Col E. D. Harney (SSD)